DISSERTATION FOR THE DEGREE OF DOCTOR OF PHILOSOPHY (PHD)

Neutrophil and Macrophage Interactions with Ferryl Hemoglobin Mediate Oxidative Inflammation and Arterial Wall Remodeling in Abdominal Aortic Aneurysm

by Yuchao Ding

Supervisor: József Balla, MD, PhD, DSc, MHAS

UNIVERSITY OF DEBRECEN

DOCTORAL SCHOOL OF MEDICAL SCIENCES

DEBRECEN, 2026

Table of contents

Abbreviations

Abdominal aortic aneurysm (AAA)

Analysis of variance (ANOVA)

Angiotensin-converting-enzyme inhibitor (ACE inhibitor)

Angiotensin II (AngII)

Apolipoprotein E deficient ($ApoE^{-/-}$)

Carbon dioxide (CO_2)

Carboxypeptidase M (CPM)

C-C motif chemokine ligand (CCL)

Chronic obstructive pulmonary disease (COPD)

Cluster of differentiation 163 (CD163)

Complementary DNA (cDNA)

Coronary artery bypass surgery (CABG)

Cysteine (CYS)

Differentially expressed genes (DEGs)

Dulbecco's Modified Eagle Medium (DMEM)

Endothelial cells (ECs)

Endovascular aneurysm repair (EVAR)

Enzyme-linked immunosorbent assay (ELISA)

Extracellular matrix (ECM)

False discovery rate (FDR)

Fetal bovine serum (FBS)

Gene ontology (GO)

Hank's Balanced Salt Solution (HBSS+)

Hematoxylin-eosin (H&E)

Heme oxygenase-1 (HO-1/ HMOX1)

Hemoglobin (Hb)

Hemoglobin subunit alpha 1 (HBA1)

Hemoglobin subunit beta (HBB)

High-fat diet (HFD)

Horseradish peroxidase (HRP)

Human aortic endothelial cells (HAoECs)

Human aortic smooth muscle cells (HAoSMCs)

Immunohistochemical (IHC)

Immunoprecipitation (IP)

Intercellular adhesion molecule 1 (ICAM1)

Interleukin-1 beta (IL1β)

Interleukin-6 (IL6)

Lactotransferrin (LTF)

Macrophages (MACs)

Matrix metalloproteinases (MMPs)

Myeloperoxidase (MPO)

Naphthol AS-D (NASD)

Neutrophils (NEUs)

Neutrophil elastase (NE)

Neutrophil extracellular traps (NETs)

NOD-, LRR- and pyrin domain-containing protein 3 (NLRP3)

Noninsulin-dependent diabetes mellitus (NIDDM)

Peptidyl arginine deiminase 4 (PAD4)

Phorbol 12-myristate 13-acetate (PMA)

Phosphate buffered saline (PBS)

polymerase chain reaction (PCR)

Polymorphonuclear leukocyte (PMN)

Principal component analysis (PCA)

Reactive oxygen species (ROS)

RNA sequencing (RNA-seq)

Ribosomal RNA (rRNA)

Singular value decomposition (SVD)

Small interfering RNA (siRNA)

Smooth muscle cells (SMCs)

Standard chow diet (STD)

Standard deviation (SD)

Standard error of the mean (SEM)

Systolic blood pressure (SBP)

Tin protoporphyrin IX (SnPP)

Tumor necrosis factor α (TNFα)

Vascular smooth muscle cells (VSMCs)

Verhoeff-Van Gieson (EVG)

Volume pressure recording (VPR)

3,3′,5,5′-tetramethylbenzidine (TMB)

List of Figures

List of Supplemental Figures

List of Tables

1 Introduction

1.1 Overview of abdominal aortic aneurysm

Abdominal aortic aneurysm (AAA) is a large-vessel disease characterized by localized or diffuse dilation of the abdominal aorta due to pathological changes or damage to the aortic wall, which can lead to rupture and pose a life-threatening risk to patients if severe (1-4). The formation of an aortic aneurysm is a long-term, asymptomatic, and permanent dilation process of the artery that may result in patient death upon rupture (5). As there are currently no targeted pharmacological treatments for AAA, surgical intervention and endovascular aortic repair remain the primary therapeutic options; however, the persistently high mortality and disability rates remain insurmountable bottlenecks for these treatment modalities (6-10). Therefore, elucidating the disease progression of AAA is critical for promoting subsequent targeted drug screening and treatment.

1.2 Epidemiology of abdominal aortic aneurysm

1.2.1 Long-term trends

Since the early 20th century, the incidence of AAA has continued to rise, which is closely associated with large-scale epidemiological screening and cohort follow-up studies conducted in various countries. Two surveys conducted in the United States in 1988 and 2000 revealed that the incidence of AAA among adults increased from 54.6 per 100,000 in 1988 to 74.4 per 100,000 in 2000 (11). Similarly, in Sweden, the

incidence among men aged 60-69 years increased from 16 per 100,000 in 1986 to 56 per 100,000 in 2004, with rates rising to 117 per 100,000 in men aged 70-79 years (12). With the ongoing trends of global population aging, improvements in living standards, and changes in dietary patterns, the incidence of AAA is projected to continue increasing annually (13).

1.2.2 Geographic distribution

The prevalence of AAA varies significantly across different geographic regions, with a much higher incidence in European and American populations than in Asian and African populations (Table 1). For example, a large-scale screening program launched in the United States in 2010, which included 3.1 million participants aged 50 to 84, estimated the prevalence of AAA at 1.4%. A similar screening program conducted in Brazil in 2004, targeting individuals aged 50 and older, yielded a prevalence of 4.6%. Two independent screening studies published in Denmark in 2010 reported corresponding prevalence rates of 3.0% and 4.0%, respectively.

The United Kingdom implemented a series of screening programs for AAA in 2002, 2007, and 2012, and its AAA prevalence has consistently ranked among the highest compared with other European countries. Australia also completed three large-scale screening surveys in 1995, 2004, and 2016, with detected AAA prevalence rates of 7.6%, 7.2%, and 6.6%, respectively. In contrast, a screening study conducted in Japan in 2000 found a local AAA prevalence of only 0.3%, a figure significantly lower than the prevalence in Caucasian populations in Europe and the Americas.

A comprehensive comparison of these research data confirms that the prevalence of AAA is significantly lower in Asia (represented by South Korea, Japan, and China Hong Kong) than in the Americas (the United States and Brazil), Europe (Denmark and the United Kingdom), and Australia.

Table 1. Geographic distribution of abdominal aortic aneurysm in selected epidemiological studies

Author	*Country*	*Year*	*Sample Size*	*Study Population*	*Prevalence (%)*
Americas					
K. Craig Kent (14)	*USA*	*2010*	*3.10 million*	*50-84 years*	*1.4*
Pedro P.-L. (15)	*Brazil*	*2004*	*12,000*	*>50 years (men)*	*4.6*
Europe					
Grondal Nikola (16)	*Denmark*	*2010*	*25,000*	*65-74 years (men)*	*3.0*
Viborg Lindholt (17)	*Denmark*	*2010*	*4,900*	*64-73 years*	*4.0*
Lindholt J.S. (18)	*Denmark*	*2017*	*18,700*	*65-74 years (men)*	*5.1*
Lindholt J.S. (19)	*Denmark*	*2019*	*10,500*	*65-74 years (men)*	*5.1*
H.A. Ashton (20)	*UK*	*2002*	*27,100*	*65-74 years (men)*	*4.9*
Ashton H.A. (21)	*UK*	*2007*	*6,000*	*65-80 years (men)*	*2.8*
Thompson S.G. (22)	*UK*	*2012*	*67,800*	*65-74 years (men)*	*4.9*
Svensjo S. (23)	*Sweden*	*2011*	*22,200*	*65 years (men)*	*2.2*
Wanhainen A. (24)	*Sweden*	*2016*	*302,900*	*65 years (men)*	*1.5*
Ricardo C.-F. (25)	*Portugal*	*2019*	*7,000*	*>65 years (men)*	*2.1*
Salvador-G.B. (26)	*Spain*	*2016*	*6,000*	*65-74 years (men)*	*2.3*
Gianfagna F. (27)	*Italy*	*2018*	*3,700*	*65-75 years (men)*	*1.9*

Author	*Country*	*Year*	*Sample Size*	*Study Population*	*Prevalence (%)*
Dereziński T.L. (28)	*Poland*	*2017*	*9,000*	*≥65 years (men)*	*9.3*
Australia					
R.A.P. Scott	*Australia*	*1995*	*5,400*	*65-80 years*	*7.6*
Norman P.E.	*Australia*	*2004*	*41,000*	*65-83 years (men)*	*7.2*
Mccaul K.A. (29)	*Australia*	*2016*	*9,000*	*64-74 years (men)*	*6.6*
Asia					
Se Hoon Oh (30)	*Korea*	*2010*	*6,200*	*>60 years*	*0.4*
Koichi Adachi (31)	*Japan*	*2000*	*1,600*	*>60 years (men)*	*0.3*
W.K. Cheng (32)	*China Hong Kong*	*2003*	*100,000*	*≥65 years (men)*	*0.1*

1.2.3 Population distribution

1.2.3.1 Age

AAA has a significantly higher incidence in the elderly population, particularly among individuals over 65 years of age, who are considered a high-risk group. In developed Western countries, the average age of AAA patients is approximately 70 years, with a lower incidence in those under 50 years of age. AAA rupture in individuals under 65 is extremely rare, and women typically develop AAA approximately 10 years later than men (33). Studies have shown that AAA accounts for approximately 1% of all deaths in men over 65 (34).

1.2.3.2 Gender

AAA exhibits marked gender differences, with numerous studies confirming a higher prevalence in men, who are approximately five times more likely to develop AAA than women (35). Additionally, the average age at diagnosis of female AAA patients is approximately 10 years higher than that of male patients (36). However, the growth and rupture rates of AAA relative to aneurysm diameter appear similar between men and women (37).

1.3 Etiology of abdominal aortic aneurysm

It is generally believed that the formation of AAA results from the combined effects of genetic, environmental, and biochemical factors. Factors such as a family history of AAA, genetic defects affecting collagen and elastin, increased protease activity, or reduced inhibitory activity may all increase the risk of developing AAA. However, the precise pathogenesis of AAA remains unclear.

1.3.1 Susceptibility genes

To date, although there have been numerous scattered reports on changes in the expression of single genes related to AAA, systematic studies on the expression profiles of these gene changes have not received sufficient attention. Since Schena M et al. (38, 39) first studied gene expression profiling using microarray technology in 1995, microarrays have become a rapid and effective method for investigating the differential expression of pathogenic genes.

The aortic wall is rich in collagen, primarily composed of type I and type III collagen. Studies have reported significant qualitative alterations in collagen during the formation of AAA. Known genetic alterations in collagen associated with AAA include several mutations in type III collagen. One example is a substitution at position 619, where glycine is replaced by arginine, which makes type III collagen more prone to degradation. Another is a mutation in the AvaII allele located at the 3′ end of the type III collagen gene, which has been associated with an increased prevalence of AAA. In addition, a mutation at position 531 detected by AluI results in a threonine substitution (AluI-Thr variant). However, these findings remain controversial, and the relationship between these mutations and the occurrence, development, and rupture of AAA has not been definitively established (39-44).

Contemporary research indicates that dysregulation of multiple gene subpopulations is involved in the occurrence, development, and eventual rupture of AAA. Differentially expressed genes associated with apoptosis, membrane receptor signaling, cytoskeleton dynamics, and protein translation are significantly correlated with phenotypic changes in vascular smooth muscle cells (VSMCs) and the remodeling of extracellular matrix (ECM) components (including collagen and elastin) during AAA pathogenesis. Further exploration of the functional characteristics and regulatory networks of these gene clusters will provide crucial insights into the potential pathogenic mechanisms of AAA.

1.3.2 Pathology

The development and progression of AAA constitute an extremely complex pathological cascade. Although the cellular and molecular mechanisms controlling this disease are not fully elucidated, its histopathological features have been comprehensively described. Key histopathological features of AAA include persistent inflammatory cell infiltration, senescence and apoptosis of VSMCs, endothelial cells (ECs) shedding, endothelial dysfunction, and ECM degradation.

AAA is widely considered an inflammation-driven vascular disease, exhibiting a strong inflammatory response throughout its pathogenesis and progression. Pathological analysis and imaging studies of clinical AAA specimens and experimental animal models have shown that the progression of AAA occurs concurrently with significant inflammatory cell infiltration within the aortic adventitia (45). Infiltrating inflammatory cells include neutrophils, macrophages, mast cells, natural killer cells, dendritic cells, B lymphocytes, and T lymphocytes; increasing evidence confirms that several of these cell subsets actively contribute to the pathogenesis of AAA (46, 47).

ECM remodeling and inflammatory response are two closely intertwined processes that together constitute the pathophysiological features of aortic AAA. Pathological manifestations of ECM remodeling include the destruction and degradation of the elastic media, as well as extensive collagen deposition within the aortic wall. Inflammatory cells infiltrating the aortic wall can secrete matrix metalloproteinases (MMPs), a class of enzymes that play a crucial role in mediating elastic mediate membrane degradation. Furthermore, ECs, VSMCs, and fibroblasts all possess the

ability to synthesize and secrete various proteolytic enzymes. These proteases, acting in conjunction with aortic wall degradation products, can serve as important biomarkers for assessing AAA progression.

1.4 Current clinical treatment status of abdominal aortic aneurysm

1.4.1 Surgical treatment

Surgery is currently the primary treatment method for large-diameter AAAs, aiming to prevent rupture-related mortality. The long-term survival rate after endovascular aneurysm repair (EVAR) largely depends on preoperative risk factors. The perioperative mortality rate associated with EVAR varies considerably in the surgical literature, reported to range from 1% to 4% (48, 49). Major complications after EVAR include endoleaks, graft migration, kinking, graft occlusion, and infection, with incidences ranging from 0.5% to 5.0%. Studies have indicated that a larger preoperative AAA diameter is associated with higher rates of postoperative endoleaks, graft migration, and other complications.

1.4.2 Pharmacological treatment

Currently, there are no targeted pharmacological therapies available to inhibit AAA expansion in clinical practice. However, with the deepening understanding of the mechanisms underlying AAA formation and progression, and with continuous improvements in experimental animal models of AAA, a solid foundation has been laid for the future development of drugs targeting AAA.

Some studies have found that inhibiting vascular wall inflammation, suppressing the phenotypic switching of smooth muscle cells (SMCs), and preventing the formation of neovascularization and vasa vasorum can exert inhibitory effects on AAA (6, 50). Therefore, current drug development targets mainly include the inhibition of inflammatory responses, protease activity, oxidative effects, and the enhancement of ECM protein synthesis.

1.5 The role of neutrophils and neutrophil extracellular traps in abdominal aortic aneurysm

Neutrophils, as the most abundant circulating leukocytes, are among the earliest immune cells recruited to sites of vascular injury and inflammation (51, 52), playing a pivotal role in the initiation and progression of AAA. One of the unique mechanisms by which neutrophils contribute to vascular inflammation is through the formation of neutrophil extracellular traps (NETs) (53-55). NETs are extracellular reticular structures composed of decondensed chromatin decorated with histones and granular proteins, including neutrophil elastase and myeloperoxidase, released via a process known as NETosis (56-59).

Accumulating evidence suggests that neutrophil-derived proteolytic enzymes, including neutrophil elastase (NE) and proteinase-3, exert dual pathological effects: they not only directly degrade ECM components within the aortic wall but also promote the formation of NETs, thereby accelerating the pathogenesis of AAA (60-62). The released NETs can function as a scaffold to recruit and concentrate inflammatory mediators and proteases, amplifying local inflammatory responses in the aortic wall

and further accelerating ECM breakdown, a core histopathological hallmark of AAA (63, 64).

Moreover, NETs intensify vascular inflammatory damage by inducing apoptotic or necrotic death of ECs and VSMCs. This cellular injury impairs the structural integrity of the aortic wall, leading to progressive aortic dilation and aneurysm enlargement (65-67). Notably, histones contained within NETs exhibit potent cytotoxicity, which can directly trigger necrosis or apoptosis of ECs and VSMCs; this process further compromises aortic wall stability and facilitates the infiltration of additional inflammatory cells (68).

Interestingly, interventions targeting NET formation have been shown to reduce the infiltration of macrophages and neutrophils in the aneurysmal wall, underscoring the pivotal role of NETs in coordinating immune cell recruitment and activation throughout AAA progression (62, 69, 70). In experimental AAA models, pharmacological inhibition or genetic deletion of key mediators of NETosis, such as peptidyl arginine deiminase 4 (PAD4), has been verified to alleviate aneurysm formation and progression (71, 72). These findings imply that targeting the NET formation pathway could represent a promising therapeutic strategy to suppress inflammation-mediated aortic wall degeneration and curb aneurysm growth (73).

In addition, recent research has revealed that NETs can interact with platelets and the coagulation cascade, inducing the formation of intraluminal thrombus within aneurysmal lesions. Thrombus formation may further lead to hypoxia in the aortic wall, which in turn enhances the secretion of proteases and reactive oxygen species by

infiltrating neutrophils (62, 70, 74). This vicious cycle encompassing NET formation, persistent inflammation, and intraluminal thrombosis underpins the pathophysiological complexity of AAA, while also shedding light on the specific mechanisms through which neutrophils and NETs drive disease progression (75).

1.6 The role of macrophages in abdominal aortic aneurysm

AAA is increasingly acknowledged as a chronic inflammatory disorder of the vascular wall, distinguished by progressive ECM degradation, depletion of vascular smooth muscle cells, and structural impairment that ultimately elevates the risk of aortic rupture. Among the proteolytic enzymes involved in this pathological process, MMPs, especially MMP-9, exert a central regulatory function. MMP-9 is highly expressed in aneurysmal tissues; such expression is particularly prominent in areas of elastic fiber breakdown and at sites of vascular rupture, where this enzyme is primarily synthesized and secreted by infiltrating macrophages (76, 77). These findings highlight MMP-9 as a key mediator of ECM destruction and vascular wall destabilization throughout the progression of AAA.

AAA is widely categorized as an “inflammatory aneurysm” on account of the pronounced infiltration of immune cells, including lymphocytes, neutrophils, and macrophages, into the diseased aortic wall. Among these infiltrating cell populations, macrophages play an especially critical role: they not only trigger and amplify inflammatory cascades in the early stages of disease development but also contribute to vascular wall rupture in the advanced phases of pathology (78). Upon activation,

macrophages secrete a spectrum of pro-inflammatory mediators, including cytokines (e.g., interleukin-1 beta (IL1β), interleukin-6 (IL6), tumor necrosis factor α (TNFα)), chemokines (e.g., C-C Motif Chemokine Ligand 2 (CCL2)), proteases (MMP-2, MMP-9, cathepsins), and reactive oxygen species. These bioactive substances collectively drive ECM degradation, smooth muscle cell apoptosis, and neovascularization within the aortic wall.

Notably, macrophages display substantial functional plasticity, with both pro-inflammatory (M1-like) and tissue-remodeling (M2-like) phenotypes detected in AAA lesions. An imbalance that favors the expansion of destructive, pro-inflammatory macrophage subsets sustains chronic inflammation and accelerates the structural weakening of the aortic wall. Given their pivotal role in multiple stages of the disease process, macrophages are now recognized as a core cellular driver of AAA pathogenesis and a promising target for therapeutic intervention. Strategies aimed at modulating macrophage recruitment, activation, and polarization are being increasingly explored as potential approaches to decelerate aneurysm growth and reduce the risk of life-threatening rupture.

1.7 Hemoglobin oxidation

Intramural hemorrhage represents a hallmark pathological feature during the progression of AAA (79, 80). It is now well established that the accumulation of intramural erythrocytes and hemoglobin (Hb) within the aneurysmal wall exacerbates local oxidative stress and inflammatory responses, thus accelerating aortic wall

structural impairment and aneurysm dilation. Neutrophils and macrophages possess a robust capacity to oxidize Hb efficiently (81, 82). Specifically, when metHb (Fe^{3+}) reacts with peroxides, this redox reaction triggers the generation of reactive globin radicals and ferryl (Fe^{4+}) heme species (83). This process proceeds within a timeframe of mere seconds, resulting in the oxidation of heme moieties into their ferryl form while simultaneously inducing the formation of protein-derived radicals on globin chains (83, 84). Such rapid redox conversion underscores the highly pro-oxidative microenvironment within the aneurysmal wall, which further aggravates ECM degradation and SMCs apoptosis, the core histopathological hallmarks of AAA.

Advanced spectrophotometric techniques enable the capture of spectral fingerprints of transient ferrylHb species, thereby facilitating quantitative evaluation of heme-iron oxidative states within the aneurysmal wall (85). Application of this analytical approach to human complicated atherosclerotic plaques demonstrated that 55% of the total Hb pool in these lesions exists as ferrylHb, 39% as metHb, and a mere 1.4% as oxyHb (82). This distinctive distribution pattern highlights the predominance of oxidized Hb forms in vascular lesions, implying their potential role in sustaining oxidative stress and inflammatory reactions throughout AAA pathogenesis.

Sustained ferryl iron and globin centered protein radicals, generated via the redox cycling of metHb with peroxides, have been verified to mediate lipid peroxidation and endothelial functional impairment (86). Furthermore, the interaction between oxidized Hb derivatives and inflammatory cells (including neutrophils and macrophages) fosters a pro-inflammatory microenvironment within the aneurysmal wall, which in turn

promotes further immune cell recruitment and amplifies the inflammatory cascade (87, 88). FerrylHb has also been reported to induce ECs death and upregulate the expression of adhesion molecules, thereby facilitating leukocyte adhesion and transmigration into the vascular wall (89).

Recent investigations have revealed that oxidative modification of Hb within the aneurysmal wall not only augments oxidative stress but also modulates the immunogenicity of Hb derived peptides, potentially triggering autoimmune responses targeting vascular components (82, 90-92). This pathological mechanism may further accelerate the degradation of structural proteins in the aortic wall, thereby promoting aneurysm expansion and rupture. Additionally, the presence of intraluminal thrombus, which is enriched with trapped erythrocytes and Hb, serves as a continuous reservoir of oxidative and proteolytic mediators within the aneurysm sac, contributing to pathological remodeling of the aortic wall (82, 92).

Collectively, these findings indicate that Hb oxidation and the subsequent formation of ferrylHb and globin radicals within the aneurysmal wall constitute critical mechanisms bridging intramural hemorrhage to oxidative stress, inflammation, and vascular remodeling during AAA progression. Targeting Hb oxidation pathways and neutralizing ferrylHb species may therefore represent promising therapeutic strategies to alleviate oxidative damage and inflammation within the aneurysmal wall, thereby attenuating AAA growth and reducing the risk of life-threatening rupture.

1.8 Role of endothelial and smooth muscle cell dysfunction in abdominal aortic aneurysm pathogenesis

Healthy vascular ECs and SMCs serve as the cornerstone for sustaining vascular homeostasis and ensuring the normal physiological function of the arterial wall. ECs constitute a dynamic semipermeable barrier separating circulating blood from the vessel wall stroma, and they actively modulate vascular permeability, leukocyte transmigration, coagulation cascades, and inflammatory signal transduction. By virtue of the regulated secretion of vasoactive mediators, ECs also exert a pivotal function in adjusting vascular tone and sustaining an intravascular microenvironment characterized by anti-inflammatory and antithrombotic properties.

In parallel, vascular smooth muscle cells are indispensable for preserving the mechanical stability and structural architecture of the arterial wall. SMCs participate in ECM synthesis, turnover, and remodeling processes, thus guaranteeing the resilience and structural integrity of blood vessels under both physiological and pathological mechanical stress. Under homeostatic conditions, SMCs display a contractile phenotype; yet these cells retain pronounced phenotypic plasticity, which enables them to switch toward a synthetic or pro-inflammatory state in response to specific environmental stimuli.

Mounting evidence indicates that endothelial dysfunction represents one of the earliest pathogenic events during AAA initiation. Impairment of endothelial barrier function and dysregulation of inflammatory signaling pathways promote enhanced leukocyte adhesion and infiltration into the vessel wall, thereby triggering and amplifying local

inflammatory responses (93, 94). This pro-inflammatory microenvironment drives phenotypic modulation, apoptotic death, and depletion of SMCs, ultimately disrupting ECM homeostasis and impairing the structural stability of the arterial wall. Collectively, the synergistic dysfunction of ECs and SMCs drives progressive arterial wall degeneration and occupies a central position in the pathogenesis of AAA.

1.9 Heme oxygenase-1 in abdominal aortic aneurysm: mechanistic insights and therapeutic implications

Mounting evidence points to a pivotal protective role of heme oxygenase-1 (HO-1) in the initiation and progression of AAA (95, 96). In murine experimental models, HO-1 deficiency has been shown to expedite aneurysm formation and elevate the vulnerability to aortic rupture, which underscores the enzyme's critical function in maintaining vascular wall structural integrity. Consistently, in human cohorts, genetic polymorphisms correlated with diminished HO-1 inducibility have been associated with higher AAA prevalence rates, implying that the protective mechanism of HO-1 is conserved across different species (97). Collectively, these findings indicate that HO-1 exerts regulatory effects not only on oxidative stress responses but also on inflammatory cascades and ECM remodeling processes, all of which are core pathophysiological events in AAA development.

Intramural hemorrhage within the aneurysmal wall constitutes a major reservoir for Hb and heme accumulation. Hb undergoes spontaneous auto-oxidation, leading to the generation of metHb and reactive oxygen species (ROS) such as superoxide anions (81, 98). This oxidative microenvironment is further exacerbated by ROS derived from

infiltrating neutrophils and macrophages, as well as oxidized lipids released from atherosclerotic plaques. These factors synergistically accelerate Hb oxidation and facilitate heme dissociation from metHb (99). Free heme, in turn, can amplify oxidative stress, trigger endothelial dysfunction, and activate inflammatory signaling pathways, thereby establishing a vicious cycle that may accelerate aneurysmal progression. Despite this mechanistic insight, three key questions remain unresolved: whether heme toxicity acts as a primary causal driver of AAA development, whether metHb accumulation is a universal pathological feature conserved across species, and whether pharmacological induction of HO-1 can effectively decelerate aneurysm growth.

HO-1 acts as both a substrate-dependent enzyme and a transcriptionally regulated protein, with its expression induced in part by heme-mediated inhibition of the transcription factor Bach1 (100-102). Pharmacological agents that can selectively upregulate HO-1 expression without exacerbating oxidative stress have attracted particular research attention. Normosang (heme arginate), a clinically approved therapeutic agent for acute hepatic porphyria (103), can effectively enhance HO-1 expression while circumventing the pro-oxidant effects linked to free heme (104). Experimental evidence has demonstrated that HO-1 induction can alleviate vascular inflammation, suppress matrix metalloproteinase activity, and mitigate oxidative damage in vascular tissues. These properties render Normosang a promising candidate for the development of targeted therapies against AAA.

1.10 Aim of the study

Numerous prior investigations have emphasized that mitigation of macrophage and neutrophil infiltration and suppression of NET generation exert protective impacts against AAA progression (105, 106). Nevertheless, the direct causal function of the crosstalk between macrophages and neutrophils and Hb, especially ferrylHb, the oxidized derivative of Hb, in the pathogenic process of AAA remains to be elucidated. Macrophagesand neutrophils are among the first immune cells recruited to sites of vascular injury and inflammation, where they can release reactive oxygen species, proteases, and NETs, all of which contribute to vascular wall degradation (107, 108). Concurrently, red blood cell extravasation and hemolysis within the aneurysmal wall release cell-free Hb, which can undergo oxidative modifications under the pro-oxidative microenvironment of AAA, forming ferrylHb (109-111). However, whether these processes synergistically exacerbate AAA formation and rupture risk has not been fully elucidated.

The overall aim of this PhD thesis is to define Hb oxidation and heme stress as upstream pathogenic mechanisms in AAA, and to determine how oxidized Hb species promote immune activation and vascular wall injury. By integrating analyses of human AAA samples with mechanistic studies in the angiotensin II (AngII) -induced AAA model in apolipoprotein E-deficient ($ApoE^{-/-}$) mice, this thesis seeks to establish a causal link between hemorrhage-associated Hb oxidation, neutrophil/macrophage responses, and aneurysmal progression, and to evaluate HO-1 as a protective and therapeutically targetable pathway.

This thesis aims to investigate and clarify the following objectives.

Develop translational tools to detect ferrylHb in circulation, and assess whether circulating ferrylHb is associated with ruptured AAA, supporting its potential as a rupture-related biomarker.

Determine the causal effects of Hb and ferrylHb on aneurysm progression, with emphasis on neutrophil and macrophage activation, cell injury, and NET formation within the aortic wall.

Characterize Hb oxidation-associated signatures in AAA, including accumulation of oxidized Hb species, heme loading, and inflammatory immune cell markers in human and experimental mice aneurysmal tissues.

Transcriptomic signatures associated with inflammation and neutrophil activation in human and mouse hemorrhaged AAA, and to determine whether ferrylHb drives similar transcriptomic changes in human macrophages.

How ferrylHb influences neutrophil behavior, including gene programs involved in macrophage recruitment, activation, elastase release with potential elastin degradation, and PAD4-dependent NET formation, thereby linking Hb oxidation to immune mediated vascular wall remodeling.

Heme overload elucidates its impact on ECs and SMCs activation, including induction of IL1β, ICAM1, and NLRP3-dependent inflammatory pathways.

Evaluate the therapeutic relevance of the heme-HO-1 axis, testing whether pharmacological HO-1 induction mitigates aneurysm formation and intramural hemorrhage, while HO-1 inhibition exacerbates disease severity.

In summary, this thesis aims to establish a mechanistic framework in which intramural hemorrhage induces Hb oxidation and heme stress, thereby amplifying neutrophil/macrophage-driven inflammation and vascular wall degeneration in AAA. These findings support the heme-HO-1 pathway as a modifiable upstream target and provide translational opportunities for biomarker development and therapeutic intervention.

2 Methods

2.1 Sex as a biological variable

In the present study, we restricted our investigation to male mice, as the pathological condition being modeled manifests specifically in the male population and therefore cannot be reliably reproduced in females. This sex-specific design allowed us to ensure the biological relevance of the model and to obtain findings that more accurately reflect the clinical characteristics of the disease.

2.2 Ferryl hemoglobin level quantification in serum

Following the generation and characterization of a novel monoclonal antibody targeting ferrylHb (anti-ferrylHb mAb (82)), we developed an in-house sandwich ELISA to quantify ferrylHb antigen levels. The antibody recognizes a specific epitope corresponding to amino acids 32-41 (LLVVYPWTQR) within the β-subunit, which becomes accessible only when Hb undergoes oxidative modification (82).

For this enzyme-linked immunosorbent assay, high-binding 96-well flat bottom ELISA plates (EB, Thermo Fischer Scientific Oy, Vantaa, Finland) were coated with the in-house generated anti-ferrylHb monoclonal antibody (anti-ferrylHb mAb) at a concentration of 10 µg/ml. The coating solution was prepared by diluting the antibody in 0.2 M sodium bicarbonate buffer (pH 9.6) and applied at a volume of 0.1 ml per well, with incubation carried out overnight at 4 °C.

To eliminate non-specific binding, each well was filled with 0.15 ml of blocking buffer (composed of 0.5% bovine serum albumin, 0.5 M sodium chloride, and 0.05% Tween-20 in phosphate-buffered saline, pH 7.2) and incubated for 1 hour at ambient temperature. Following this step, 0.1 ml of either calibration standard solutions or serum/plasma samples (pre-diluted at a ratio of 1:2500 in the same blocking buffer) was added to each well, with a 1 hour incubation period at room temperature.

The detection of bound ferrylHb was implemented by adding 0.1 ml per well of horseradish peroxidase (HRP)-conjugated anti-ferrylHb monoclonal antibody. After sufficient incubation, 3,3′,5,5′-tetramethylbenzidine (TMB) substrate solution (One Component HRP Microwell Substrate, Diarect Ag, Freiburg, Germany) was introduced into each well. After 15 minutes of chromogenic reaction at room temperature, the enzymatic reaction was terminated by adding 0.05 ml of 2 M sulfuric acid to each well. The absorbance of each well was measured at a wavelength of 450 nm using a Labsystems iEMS MF microplate reader (Labsystems Oy, Helsinki, Finland).

It should be noted that a washing procedure was performed three times between every two consecutive incubation steps; the washing solution was phosphate-buffered saline containing 0.05% Tween-20, with a volume of 0.3 ml applied to each well for each wash.

To generate standard curves, serial dilutions of ferrylHb ranging from 2.5 to 100 μg/l were included in each run. The intra-assay coefficients of variation were 4.1%, 5.9%, and 7.1% for control samples containing 189 μg/ml, 98 μg/ml, and 22 μg/ml ferrylHb, respectively, demonstrating good reproducibility of the method.

2.3 Establishment of a murine abdominal aortic aneurysm model

Male ApoE$^{-/-}$ mice aged 8-10 weeks were randomly allocated to receive either AngII infusion or saline infusion. The study was restricted to male animals in order to minimize the confounding effects of female sex hormones on AngII responsiveness and because aortic hematoma occurs predominantly in males in the clinical setting.

All experimental mice were subjected to a 12-week feeding protocol with two distinct dietary regimens: a high-fat diet (HFD) containing 18% protein, 12.6% carbohydrate, 15% fat, and 1.25% cholesterol (sniff Spezialdiäten GmbH, Soest, Germany), or a standard chow diet (STD) as the control. In the last 4 weeks of this dietary intervention, osmotic minipumps (Model 2004; ALZA Scientific Products, Mountain View, CA, USA) were subcutaneously implanted into the mice. These devices were designed to continuously deliver either AngII at a dose of 1000 ng/minute/kg (Sigma-Aldrich Corp., St. Louis, MO, USA) or physiological saline as the vehicle control (Figure 7A).

At study termination (week 12), mice were anesthetized by intraperitoneal administration of ketamine (80 mg/kg) combined with xylazine (5 mg/kg). Following euthanasia, the thoracic and abdominal aorta were carefully exposed, perfused with cold saline, and cleared of surrounding connective tissue. The vessel was excised, rinsed to remove residual intraluminal blood, and dissected into segments. Abdominal aortic sections were processed for aneurysm assessment and histological examination, while parallel samples were snap-frozen for protein analysis. Gross morphological images of the isolated arterial specimens were captured utilizing a Nikon D3200 digital camera (Nikon Corp., Minato, Tokyo, Japan).

2.4 Ultrasonographic assessment of the abdomen in mice

In vivo abdominal aortic imaging was performed using a Vevo 770 high resolution ultrasound system fitted with a 30 MHz linear transducer (VisualSonics, Toronto, Canada). Mice were anesthetized with 1-2% isoflurane, and after abdominal hair removal, they were placed in a supine position on a temperature-maintained imaging stage. A thin coat of ultrasound transmission gel was applied to guarantee ideal acoustic coupling between the transducer and the skin surface.

Longitudinal ultrasound scans of the suprarenal aorta were acquired, spanning from the aortic hiatus down to the anatomical level corresponding to the left renal artery. Images were acquired at mid-systole to minimize variability. The maximal luminal diameter of the abdominal aorta was quantified, and measurements were performed independently by two blinded investigators to ensure objectivity and reproducibility.

2.5 Quantification of blood pressure and heart rate

Systolic blood pressure and heart rate were measured in a noninvasive manner via the CODA tail-cuff blood pressure system (Kent Scientific Corporation), both before and after osmotic pump implantation. Experimental mice were placed in restraint devices mounted on a temperature regulated heating platform, which helped sustain peripheral blood circulation. An occlusion cuff and a volume pressure recording (VPR) cuff were fastened close to the base of the tail, with both connected to the CODA control unit. Each session consisted of ten measurement cycles, and valid readings were

automatically recorded by the CODA software. Data were subsequently exported to Microsoft Excel for calculation of mean values and standard deviations.

2.6 Grading of aneurysm severity

The extent of aortic aneurysm formation was graded using a modified version of the Daugherty classification system, as previously established in our laboratory (112, 113). The classification criteria were established as follows: Stage I refers to morphologically intact aortas with no abnormal changes; Stage II denotes aneurysmal dilatation in the absence of hemorrhage signs; Stage III indicates aneurysms complicated by hemorrhage; and Stage IV represents overt rupture of the aneurysm. Evaluation of aneurysmal specimens was performed independently by three blinded investigators. In cases where initial assessments differed, the observers re-examined the samples and reached a consensus through discussion.

2.7 Histology

Formalin-fixed paraffin-embedded tissue sections (human and murine) of 4 μm thickness were prepared for serial histological and immunohistochemical (IHC) analysis. Conventional stains included hematoxylin-eosin (H&E), Naphthol AS-D (NASD) chloroacetate esterase, Verhoeff-Van Gieson (EVG), and Masson's trichrome. For IHC, slides underwent deparaffinization, antigen retrieval, and antibody labeling following the respective manufacturer's protocols. The antibodies applied were: anti-myeloperoxidase (MPO) (Thermo Scientific, RB373A; 1:1000, 1 hour), anti-Hb (Abcam, ab92492, clone EPR3608; 1:500, 1 hour), anti-ferrylHb (mouse monoclonal

antibody generated in-house; 1:100, 1 hour), and anti-cluster of differentiation 163 (CD163) (Proteintech, Cat. no. 16646-1-AP; 1:500, 1 hour).

After phosphate buffered saline (PBS) washes, slides were incubated with MACH 2 Rabbit HRP-Polymer (Biocare, RP520H, 30 minutes), followed by DAB chromogen development and rinsing in distilled water. Counterstaining was performed with Mayer's hematoxylin (1 minute), then slides were washed under running tap water for 10 min. Finally, specimens were dehydrated through graded ethanol, cleared in xylene, and coverslipped. For image acquisition, sections were digitized using a Mirax Midi scanner (3D Histech, Budapest, Hungary).

2.8 Staining with immunofluorescent techniques

Cells were immobilized through fixation with 3.7% formaldehyde for 15 minutes, and then rendered permeable via incubation with 0.3% Triton X-100 for another 15 minutes. For immunofluorescence staining assays, CD163 and MPO were targeted separately with rabbit anti-CD163 primary antibody (Novus Biologicals, NB110-40686) and rabbit anti-MPO primary antibody (Thermo Scientific, RB373A). Subsequent signal visualization was achieved using Alexa Fluor 488-conjugated goat anti-rabbit IgG $F(ab')_2$ secondary antibody (Cat. no. A11070, Thermo Fisher Scientific, Waltham, MA, USA). In the meantime, ferrylHb was identified with a mouse monoclonal antibody developed in-house, and the corresponding fluorescence signal was visualized with Alexa Fluor 568-conjugated goat anti-mouse IgG $F(ab')_2$ (Cat. no. A11004, Thermo Fisher Scientific). Nuclear counterstaining was conducted with Hoechst 33258. All

primary antibodies against CD163, MPO and ferrylHb were diluted at a ratio of 1:500 and incubated with samples for 1 hour at room temperature, and the secondary antibodies were also used at the same dilution ratio with a 1-hour incubation period.

For paraffin embedded tissue specimens (including human and mouse samples, n = 5 per group), ferrylHb was labeled with mouse anti-human ferrylHb antibody at a 1:1000 dilution for 2 hours, and the labeling signal was visualized by Alexa Fluor 488-conjugated goat anti-mouse IgG $F(ab')_2$ (1:1000 dilution, 2-hour incubation). In parallel, the tissue sections were incubated with rabbit anti-human CD163 antibody (Abcam, ab182422; 1:400 dilution, 2 hours incubation), followed by incubation with Alexa Fluor 647-conjugated goat anti-rabbit IgG (Cat. no. A21244, Thermo Fisher Scientific; 1:1000 dilution, 2 hours incubation) for signal detection.

In supplementary experiments with human samples (n = 5 per group), ferrylHb labeling was repeated with mouse anti-human ferrylHb antibody (1:1000 dilution, 2 hours incubation), and the signal was visualized with Alexa Fluor 488-conjugated goat anti-mouse IgG $F(ab')_2$ (1:1000 dilution, 2 hours incubation). After that, the tissue sections were further incubated with either rabbit anti-human MPO antibody (Cat. no. RB373A, Thermo Fisher Scientific; 1:1000 dilution, 2 hours incubation) or rabbit anti-human carboxypeptidase M (CPM) antibody (Abcam, ab150405, clone EPR8052; 1:200 dilution, 1 hour incubation). The corresponding signals of these two targets were visualized with Alexa Fluor 647-conjugated goat anti-rabbit IgG (Cat. no. A21244, Thermo Fisher Scientific; 1:1000 dilution, 2 hours incubation).

2.9 Western blot

For human derived specimens including healthy arterial tissues (n = 4) and AAA samples (n = 4), tissue homogenization was performed under liquid nitrogen conditions, followed by lysis in a protein extraction buffer formulated with 10 mM Tris-HCl, 5 mM EDTA, 150 mM NaCl (pH 7.2), 1% Triton X-100, 0.5% Nonidet P-40, as well as protease inhibitors (Complete Mini, F. Hoffmann-La Roche, Basel, Switzerland). An aliquot of total protein (50 μg) from each sample was separated via 10% SDS-polyacrylamide gel electrophoresis, and then electro-transferred onto nitrocellulose membranes (Amersham Biosciences, Piscataway, NJ, USA). The prepared membranes were incubated overnight with either HRP-conjugated goat anti-human Hb antibody (Abcam, ab19362-1; dilution ratio 1:15,000) or HRP-labeled mouse anti-human ferrylHb antibody (in house preparation; dilution ratio 1:1000), after which the target bands were visualized through a chemiluminescence detection system (GE Healthcare Life Sciences, Piscataway, NJ, USA).

Murine aneurysm tissue sections (10 mm in length, n = 3 per experimental group) were homogenized in protein lysis buffer, subjected to ice-bath sonication (three cycles of 10 seconds each), and then centrifuged at 12,000 × g for 15 minutes at 4 °C. A total of 18 μg protein from each sample was loaded onto 10% SDS-PAGE gels for separation. The expression level of Hb was detected via incubation with goat anti-human Hb antibody (Abcam, ab19362-1; dilution ratio 1:5000) over an overnight period.

Human neutrophils treated with 10 μM Hb or ferrylHb for 24 hours were lysed, and 20 μl of the supernatant protein was collected for SDS-PAGE separation. The expression

of MPO was evaluated through incubation with rabbit anti-human MPO antibody (Thermo, RB373A; dilution ratio 1:15,000) overnight, followed by a 1-hour incubation with HRP-conjugated anti-rabbit secondary antibody (Cell Signaling, 7074S; dilution ratio 1:15,000).

Neutrophils exposed to 10 μM Hb or phorbol 12-myristate 13-acetate (PMA) for 16 h were lysed, and 20 μg of total protein per sample was resolved using 10% SDS-PAGE gels. The detection of Hb was achieved by overnight incubation with rabbit anti-human Hb antibody (Abcam, ab19362-1; dilution ratio 1:5000).

For neutrophils or macrophages treated with 5 μM ferrylHb or 5 μM GSK484 (ab223598, Abcam) for 16 hours, protein samples with a volume of 37.5 μl (for neutrophils) or a mass of 20 μg (for macrophages) were loaded onto 10% SDS-PAGE gels. The expression of CD163 was probed by overnight incubation with rabbit anti-human CD163 antibody (Proteintech, 16646-1-AP; dilution ratio 1:500), while MPO expression was assessed using rabbit anti-human MPO antibody (Thermo, RB373A; dilution ratio 1:500) with overnight incubation.

2.10 Liquid chromatography-tandem mass spectrometry analysis

For proteomic analysis, murine aortic tissues with ruptured aneurysms (n = 5) and human AAA specimens (n = 5) were subjected to in-solution tryptic digestion. Initially, protein fractions were denatured with 6 M urea (Bio-Rad, Hercules, CA, USA) for 30 min, followed by reduction with 10 mM dithiothreitol at 56 °C for 1 hour. Subsequently, alkylation was implemented using 20 mM iodoacetamide under dark conditions at room

temperature for 45 minutes. Before proceeding with enzymatic hydrolysis, the urea concentration was diluted to 1 M by adding 25 mM ammonium bicarbonate (Sigma-Aldrich, St. Louis, MO, USA). MS-grade modified trypsin (Sciex, Framingham, MA, USA) was introduced at an enzyme-to-protein ratio of 1:25, and the digestion reaction was allowed to proceed overnight at 37 °C. The resultant digested peptides were dried in a speed vacuum concentrator, reconstituted in 1% formic acid, and desalted using C18 PierceTips (ThermoFisher Scientific, Waltham, MA, USA). After a second round of drying, the peptide samples were finally resuspended in 1% formic acid to be ready for liquid chromatography-tandem mass spectrometry (LC-MS/MS) analysis.

Peptide separation and subsequent detection were conducted on an Easy nLC 1200 liquid chromatography system coupled to an Orbitrap Fusion mass spectrometer (Thermo Scientific, Waltham, MA, USA). All samples were first enriched on an ACQUITY UPLC Symmetry C18 trapping column (20 mm × 180 µm, 5 µm, 100 Å; Waters, Milford, MA, USA), and then separated on an Acclaim PepMap RSLC analytical column (75 µm × 250 mm, 2 µm, 100 Å; Thermo Scientific) with a 180-minute gradient elution program. The gradient procedure was set as follows: maintaining 5% solvent B for 5 minutes, elevating to 10% within the next 5 minutes, increasing linearly to 35% over 120 minutes, rising to 50% in 15 minutes, then ramping up to 85% within 5 minutes and holding at this level for 10 minutes, and finally returning to 5% within 1 minute with a 19-minute re-equilibration period. Solvent A was composed of water containing 0.1% formic acid, while solvent B was prepared

with 95% acetonitrile supplemented with 0.1% formic acid, and the entire separation process was performed at a constant flow rate of 400 nl/minute.

Data dependent acquisition mode was adopted for mass spectrometric detection. For each full survey scan covering a mass-to-charge ratio (m/z) range of 350-1600, the top 14 most intense precursor ions were selected for MS/MS fragmentation. The full scan was completed in the Orbitrap analyzer at a resolution of 60,000, with an automatic gain control target of 4.0e5 and operated in profile mode. Higher energy collisional dissociation was employed with a normalized collision energy of 35%, and the resulting product ions were detected in the linear ion trap, with an automatic gain control target of 1.0e6 and operated in centroid mode. To avoid repeated fragmentation of identical precursor ions, dynamic exclusion was activated with an exclusion window set at 45 seconds.

2.11 Processing and analytical pipeline for data

Protein identification was performed using MaxQuant version 2.0.1 (114). Human aortic aneurysm samples were searched against the Human SwissProt database (release 2022.01, 20,394 sequences), while mouse aortic aneurysm samples were analyzed against the Mouse SwissProt database (release 2022.02, 17,082 sequences), together with the MaxQuant-provided contaminants database. Variable modifications included cysteine oxidation, trioxidation, carbamidomethylation, methionine oxidation, and N-terminal acetylation, with up to two missed trypsin cleavage sites permitted.

The resulting datasets were imported into Scaffold 5.0.1 software (Proteome Software, Inc.) for validation. Proteins were considered identified if supported by at least two unique peptides, with a protein false discovery rate of 1% and a minimum peptide probability of 95%.

Structural visualization of Hb was conducted using CAVER Analyst 2.0 software: human Hb structures were based on RCSB PDB entry 1BUW, and mouse Hb structures were based on PDB entry 3HRW.

2.12 Hemoglobin isolation and purification procedures

OxyHb (Fe^{2+}) was fabricated in accordance with protocols established in prior research (115). Specifically, Hb was extracted from fresh blood samples donated by healthy individuals, and further purified through ion-exchange chromatography with a DEAE Sepharose CL-6B column as the separation medium. The resultant product contained 98-99% OxyHb, whereas a small portion (1-2%) of the total protein underwent oxidative modification. Purified Hb aliquots were subjected to snap-freezing in liquid nitrogen immediately after preparation, and then preserved at a temperature of -70 °C for subsequent experimental use. The purity of the final Hb preparation was verified via silver staining assay, and the hemoglobin concentrations were quantified following the method described by Winterbourn (116). It should be noted that all Hb levels reported in the present study were calculated based on the corresponding heme concentrations.

2.13 Analysis of hemoglobin in diverse redox states

Human healthy arterial tissues and AAA specimens (n = 5 per group) were soaked in physiological saline and sonicated on ice using an Ultrasonic Cell Disrupter (Virtis Virsonic 323410), with three cycles of 10 seconds each. The obtained homogenates were centrifuged at 12000 × g for 15 minutes at 4°C, and the resulting supernatants were subjected to spectrophotometric analysis (Beckman Coulter Inc., Brea, CA, USA). Concentrations of oxyHb, metHb, and ferrylHb were computed by applying the formulas outlined below (117):

$[OxyHb] = -75.78OD_{560} + 103.16OD_{576} – 38.39OD_{630}$

$[MetHb] = -26.09OD_{560} + 12.48OD_{576} – 280.70OD_{630}$

$[FerrylHb] = 132.60OD_{560} – 74.10OD_{576} – 68.33OD_{630}$

Mouse aneurysm tissues were processed using the same procedure. For neutrophil experiments, cells treated for 16 h with PMA or Hb were collected, and the redox states of Hb were determined by analyzing their visible absorption spectra.

2.14 Measurement of total heme content

Heme levels in healthy aortic tissues and AAA specimens were quantified following the protocols previously reported in our research and the study by Huy et al (118, 119).

2.15 Isolation of monocytes from human blood and subsequent macrophage treatment

Separation of human blood-derived monocytes and treatment of macrophages were extracted as described previously (82).

2.16 Isolation of peripheral blood neutrophils

Twenty milliliters of anticoagulated blood were collected from healthy donors and transferred into a 50 ml conical tube, followed by dilution with an equal volume of 0.9% physiological saline. The diluted blood sample was gently overlaid onto 10 ml of Histopaque®-1077 (a solution of polysucrose and sodium diatrizoate; Product No: 10771) and subjected to centrifugation at 400 × g for 40 minutes at 24°C. Post-centrifugation, the plasma fraction and mononuclear cell layer were aspirated and discarded. The polymorphonuclear leukocyte-enriched layer, which contained residual erythrocytes, was harvested and resuspended in less than 5 ml of sterile distilled water for 25 seconds to lyse the remaining red blood cells. Isotonic conditions were promptly restored by adding an equal volume of 1.8% sterile saline. The cell suspension was then rinsed with 0.9% physiological saline and centrifuged at 500 × g for 5 minutes at 24°C. Finally, the purified polymorphonuclear leukocytes were resuspended in 500 µl of Dulbecco's Modified Eagle Medium (DMEM) supplemented with 10% glucose (high glucose formulation).

2.17 Neutrophils exposed to hemoglobin or ferryl hemoglobin

Isolated neutrophils were resuspended in DMEM medium and seeded into 24-well culture plates at a volume of 500 µl per well. The cells were subjected to treatment with either 10 µM Hb or 10 µM ferrylHb, followed by incubation at 37°C in a humidified incubator containing 5% carbon dioxide (CO_2) for different time intervals (4, 8, 16, and

24 hours). At each pre-specified time point, the cells were harvested and visualized under a Leica DMC 4500 microscope to acquire images.

For the evaluation of Hb oxidation, neutrophils were initially activated with PMA (10 µg/ml; Product No: P1585) and subsequently treated with 10 µM Hb for a 16-hour period. In an independent experimental setup, human neutrophils were incubated with 5 µM ferrylHb or 5 µM GSK484 (ab223598, Abcam) over a 16-hour duration.

2.18 Polymorphonuclear leukocyte elastase quantification assay

The concentration of polymorphonuclear leukocyte (PMN) elastase was quantified utilizing a Human PMN-Elastase ELISA kit (Affymetrix eBioscience) (120). Briefly, 10 µl of each test sample was mixed with 90 µl of Sample Dilution Buffer in a microtiter plate, followed by incubation at ambient temperature for 60 minutes. After completing the washing step, 150 µl of HRP-conjugated detection reagent was dispensed into each well, and the plate was incubated for another 60 minutes under the same ambient temperature conditions. Subsequent to a second round of washing, 200 µl of TMB substrate was added to each well, and the plate was placed in the dark at ambient temperature for a 30-minute incubation period. The enzymatic reaction was halted by adding 50 µl of Stop Solution to each well, and the absorbance value was measured at a wavelength of 450 nm using a Biotek Synergy HT microplate reader (PMT 49984). All final results were presented in units of ng/ml.

2.19 Transcriptome RNA-Sequencing

To acquire comprehensive transcriptome landscapes, high-throughput mRNA sequencing was conducted on diverse sample types, encompassing human neutrophils stimulated with Hb or ferrylHb (n = 5), aortic aneurysm tissues derived from patients (n = 4), healthy aortic tissues obtained from organ donors (n = 5), and AAA tissues isolated from $ApoE^{-/-}$ mice (n = 5 per experimental group). Total RNA was extracted, quantified, and evaluated for quality via an Agilent BioAnalyzer paired with the Eukaryotic Total RNA Nano Kit (Agilent Technologies, Santa Clara, CA, USA), following the protocols provided by the manufacturer. Sequencing libraries were constructed on the Illumina platform (Illumina, San Diego, CA, USA).

Owing to RNA degradation, ribosomal RNA (rRNA) was depleted using the NEBNext® rRNA Depletion Kit (Human/Mouse/Rat; New England BioLabs). For library preparation, 200 ng of total RNA was processed with the NEBNext® Ultra II RNA Sample Preparation Kit for Illumina (New England BioLabs, Ipswich, MA, USA). Polyadenylated RNAs were captured utilizing oligo(dT)-conjugated magnetic beads and fragmented at 94°C for a 15-minute duration. First-strand complementary DNA (cDNA) was synthesized with random primers, after which second-strand synthesis was performed to produce double-stranded cDNA. Subsequent to end repair and adapter ligation, the resulting fragments were amplified through enrichment polymerase chain reaction (PCR) to construct the sequencing libraries. Sequencing was executed on an Illumina NextSeq500 instrument, employing single-end reads with a 75-cycle length.

2.20 Analysis of RNA-Sequencing data

HISAT2 algorithm was employed to align raw sequencing reads (FASTQ files) against the human or mouse reference genome (GRCh37), yielding BAM files. Subsequent analytical procedures were carried out via iDEP 2.01 (available at http://ge-lab.org/idep/). Following the import of BAM files into iDEP 2.01, normalization was implemented utilizing the DESeq2 algorithm. Differentially expressed genes (DEGs) were pinpointed through comparisons between untreated and ferrylHb-exposed neutrophils, or between aortic aneurysm tissues and healthy aortic tissues, leveraging the DESeq2 test. For four sets of mouse aortic specimens derived from $ApoE^{-/-}$ mice, analysis of variance (ANOVA) was performed, followed by Tukey's post hoc test for multiple pairwise comparisons.

Heatmaps and dot plots were constructed either with GraphPad Prism 10 (GraphPad Software, La Jolla, CA, USA) or were automatically generated by iDEP 2.01. DEG lists underwent further investigation using the Gene Ontology (GO) enrichment module integrated within iDEP 2.01. GO terms meeting the criteria of fold enrichment ≥ 2 and $P < 0.05$ were selected, and the outcomes were visualized based on the -log10 *P*-value. Bar graphs were generated automatically through the iDEP 2.01 platform.

2.21 Cell culture

Human aortic endothelial cells (HAoECs) and human aortic smooth muscle cells (HAoSMCs) were obtained from Lonza (Lonza Group Ltd., Allendale, NJ, USA). HAoECs were maintained in CM199 medium, whereas HAoSMCs were cultured in

DMEM; both media were supplemented with 10% fetal bovine serum (FBS), 100 U/ml penicillin, 100 μg/ml streptomycin, and amphotericin B to ensure optimal growth and sterility. Cells were expanded until reaching approximately 90% confluence and were used between passages 4 and 6. Culture medium was refreshed every 48 hours to maintain nutrient availability and cellular viability.

Heme treatments were performed in serum- and antibiotic-free conditions to avoid interference from external growth factors and antibiotics. A stock solution of hemin chloride was prepared in sterile 20 mM NaOH and subsequently diluted to the desired concentrations in the serum- and antibiotic-free medium. Before treatment, cells were washed twice with Hank's Balanced Salt Solution (HBSS+, pH 7.4) supplemented with Ca^{2+} and Mg^{2+} to remove residual medium. Cells were then exposed to varying concentrations of hemin for 2 hours. Following treatment, cells were washed again with HBSS+, and fresh complete medium containing 10% FBS and antibiotics was added. The cells were further incubated for 3, 6, or 16 hours under standard culture conditions (37°C, 5% CO_2) to assess both early and delayed transcriptional responses to heme.

2.22 Small interfering RNA transfection

To investigate the role of HO-1 in vascular endothelial responses, HAoECs were transfected with Silencer Select small interfering RNA (siRNA) targeting HO-1 (Thermo Fisher Scientific, 4390824, Waltham, MA, USA). A corresponding non-targeting negative control siRNA was purchased from Ambion (Thermo Fisher Scientific, 4390843, Waltham, MA, USA). Transfections were performed using

Oligofectamine (Invitrogen, 12252011, Carlsbad, CA, USA) following the manufacturer's protocol. The final siRNA concentration in all experiments was 10 nmol/l. This approach allowed selective and efficient knockdown of HO-1, enabling the assessment of its regulatory effects on heme-induced inflammatory gene expression.

2.23 RNA isolation and qRT-PCR (quantitative reverse transcription-polymerase chain reaction)

Total RNA was extracted from cells cultured in six-well plates using TriReagent (Zymo Research, R2050-1-200, Irvine, CA, USA) in accordance with the manufacturer's instructions. RNA purity and integrity were confirmed prior to downstream analysis. cDNA was synthesized from 1 μg of total RNA using the High-Capacity cDNA Reverse Transcription Kit (Applied Biosystems, 4368813, Foster City, CA, USA).

Quantitative PCR was performed to determine the expression levels of HO-1, IL1β, intercellular adhesion molecule 1 (ICAM1), and NOD-, LRR- and pyrin domain-containing protein 3 (NLRP3) transcripts using TaqMan Gene Expression Assays (Thermo Fisher Scientific, EP0405, Waltham, MA, USA). GAPDH was used as the endogenous control for normalization (HO-1: Hs01110250; IL1β: Hs01555410_m1; ICAM1: Hs00164932_m1; NLRP3: Hs00918082; GAPDH: Hs02758991_g1). All reactions were run on a C1000 Thermal Cycler coupled with the CFX 96 Real-Time PCR System (Bio-Rad, 785BR03880, Hercules, CA, USA). Relative gene expression levels were calculated using the ΔΔCt method, providing a standardized approach to quantify fold changes in transcript abundance following heme treatment or HO-1 knockdown.

2.24 Statistical analysis

All statistical computations were carried out using GraphPad Prism 10 software (GraphPad Software Inc., La Jolla, CA, USA). Experimental data are presented as mean ± standard error of the mean (SEM), with the exception of measurements for mouse blood pressure, heart rate, and survival rates. The Shapiro-Wilk test was employed to verify the normality of data distribution, while Levene's test was utilized to assess the homogeneity of variances across groups. For datasets that met the assumptions of normality and equal variance, group comparisons were performed using Student's t-test or one-way ANOVA, followed by Sidak's post hoc testing as detailed in the corresponding figure legends. Survival curves were analyzed using the Log-rank test and Gehan-Breslow-Wilcoxon test. Pearson's correlation analysis was applied to explore the association between ferrylHb levels and heme content. A *P* value less than 0.05 was defined as statistically significant.

2.25 Study approval

Enrollment of patients undergoing open surgical repair for aortic aneurysm was conducted in accordance with protocols approved by the Hungarian National Center for Public Health and Pharmacy (approval No. 164482) and the Regional and Institutional Committee on Scientific and Research Ethics of Semmelweis University (approval No. 7891/2012). In addition, the operation and management of the aortic aneurysm biobank were authorized by the Hungarian National Center for Public Health and Pharmacy (approval No. 9882-8/2022) and the Regional and Institutional Committee on Scientific

and Research Ethics of Semmelweis University (approval No. 111/2022). All human related research protocols were implemented in strict compliance with applicable national laws, the relevant EüM decree, and the Helsinki Declaration of the World Medical Association. Written informed consent was obtained from all enrolled patients or their legal representatives prior to the collection of biological samples. Preoperative diagnosis of aortic aneurysm was confirmed via echocardiography or computed tomography/magnetic resonance angiography, with comprehensive clinical evaluation performed by specialist vascular surgeons. Surgical intervention was indicated for infrarenal aortic aneurysms with a diameter of ≥5.5 cm in male patients and ≥5.0 cm in female patients, provided that the aneurysm was unruptured and free of infectious manifestations. Collection, preservation, and experimental utilization of aortic tissue samples were carried out in adherence to European Union legislation, with strict compliance with Hungarian laws governing personal data, health information, and copyright regulations.

An aortic aneurysm biobank was established to support and facilitate translational research on aortic aneurysms. The biological materials stored in this biobank include intraluminal aneurysmal thrombus, aortic wall tissue, peripheral blood, saliva, urine, and anal swabs. Detailed patient demographics, clinical characteristics, and laboratory test results were systematically recorded in a dedicated biobank database. Histopathological analyses of aortic wall tissue samples were performed by board certified specialists in cardiovascular pathology.

Healthy aortic tissue samples were obtained from deceased organ donors with no history of vascular disease, with sample collection conducted within 4-6 hours postmortem. Donor tissue sampling was performed in accordance with international and national regulations governing multi organ donation. The corresponding research protocol was approved by the Regional and Institutional Committee on Scientific and Research Ethics of Semmelweis University (license No. 257/2018). Donor informed consent was deemed non-applicable, as all tissue samples were collected and analyzed on an anonymous basis. In compliance with the EU General Data Protection Regulation, relevant donor information was prospectively retrieved from electronic health record systems.

Comprehensive baseline characteristics of enrolled patients and organ donors are summarized in Table 2 and Table 3, respectively. Isolation of neutrophils and macrophages from the peripheral blood of healthy volunteers was carried out under the auspices of research protocols approved by the Regional Research Ethical Committee (project approval Nos. 3853-2013 and 4699-2016), with detailed donor information presented in Table 4.

Table 2. Clinical features of abdominal aortic aneurysm patients

Clinical parameters	*Corresponding data*
Sampling timeframe	*From January 2022 to March 2025.*
Total sample number	*A total of 81 biological samples were collected for the present study, with sample allocation distributed as follows: 77 samples were assigned for the quantification of ferrylHb levels; 10 samples were designated for histopathological analysis; another 10 samples were allocated to a panel of experimental assays, including*

	spectrophotometric analysis, proteomic profiling, biochemical examinations, molecular biology investigations, and RNA sequencing.
Patient gender distribution	*66 males (66/81, 81.5%); 15 females (15/81, 18.5%).*
Age	*51-83 years (average: 69.3 years, SD: 6.2 years).*
Aneurysm anatomical localization	*Suprarenal (2/81, 2.5%); Infrarenal (46/81, 56.8%); Suprarenal and infrarenal (2/81, 2.5%); Juxta renal (21/81, 25.9%); Thoracal (2/81, 2.5%); Iliac (5/81, 6.2%); No data (3/81, 3.7%).*
Aneurysm morphology	*Fusiform (69/81, 85.2%); Saccular (7/81, 8.6%); Dual (2/81, 2.5%); No data (3/81, 3.7%).*
Symptoms	*Asymptomatic (64/81, 79.0%); Symptomatic (16/81, 19.8%); Uncertain (1/81, 1.2%).*
Maximum axial diameter (mm)	*41-120 mm (average: 63.6 mm, SD: 13.3 mm); No data (3/81, 3.7%).*
Annual aneurysm progression rate (mm/year)	*0-19 mm/year (average: 7.4 mm/year, SD: 4.1 mm/year; 38/81, 46.9%); Primary detected before the surgery (43/81, 53.1%).*
Patient comorbidities and associated clinical conditions	*Hypertension (65/81, 80.2%); Ischemic heart disease (16/81, 19.8%); Type 2 diabetes mellitus (NIDDM; 9/81, 11.1%); Stroke (ischemic and hemorrhagic; 10/81, 12.3%); Hyperlipidemia (14/81, 17.3%); Myocardial infarction (AMI; 12/81, 14.8%); COPD (16/81, 19.8%); Hypothyroidism (5/81, 6.2%); Heart surgery-CABG (1/81, 1.2%); Bronchial asthma (2/81, 2.5%); Glaucoma (4/81, 4.9%); Cancer (17/81, 21.0%).*
Histological assessment of inflammatory	*None (2/81, 2.5%); Mild (4/81, 4.9%); Moderate (7/81, 8.6%); Serious (10/81,*

intensity in abdominal aortic aneurysm	*12.3%); Tertiary lymphoid tissue (29/81, 35.8%); No data (29/81, 35.8%).*
Most frequent medications	*Antiplatelet (58/81, 71.6%); Antacids (19/81, 23.5%); Beta-blocker (37/81, 45.7%); Diuretics (20/81, 24.7%); Allopurinol (11/81, 13.6%); Calcium channel blocker (26/81, 32.1%); ACE inhibitor or AngII receptor antagonists (34/81, 42.0%); Statins (31/81, 38.3%); Alpha 1-receptor blocker (11/81, 13.6%); Levothyroxine (10/81, 12.3%); Anticholinergic (4/81, 4.9%).*

The following is the list of abbreviations used in the study and their corresponding full names.
SD: standard deviation
NIDDM: noninsulin-dependent diabetes mellitus
COPD: chronic obstructive pulmonary disease
CABG: coronary artery bypass surgery
ACE inhibitor: angiotensin-converting-enzyme inhibitor

Table 3. Clinical profile of healthy subjects

Clinical parameters	*Corresponding data*
Sampling timeframe	*From 2022 to 2025*
Total number of samples	*A total of 91 biological samples were collected for the present study, with the allocation of samples as follows: 86 samples were assigned for the quantification of ferrylHb levels; 5 samples obtained from organ donors were allocated to a series of experimental analyses, including histopathological assessment, spectrophotometric measurement, proteomic profiling, biochemical examination, molecular biology investigation, and RNA sequencing.*

Table 4. Neutrophil and macrophage isolation data from healthy blood donor volunteers' whole blood

Clinical parameters	*Corresponding data*
Sampling timeframe	*September 2023-July 2025*

Total number of volunteers	*8*
Total number of samples	*17*
Patient gender distribution	*8 Males (100%)*
Patient age characteristics	*25-62 years (Mean ± SD: 41.1 ± 11.5 years)*

All animal experimental protocols were approved by the Scientific and Research Ethics Committee of the Scientific Council of Health of the Hungarian Government (registration No. 1/2021/DEMÁB) and were implemented in accordance with institutional and national guidelines for the care and use of laboratory animals. C57BL/6 ApoE$^{-/-}$ mice were housed under specific pathogen free conditions at the University of Debrecen, with animal husbandry practices strictly adhering to institutional ethical regulations.

2.26 Data availability

RNA-seq datasets generated in the course of this study have been deposited in the NCBI BioProject database, with the corresponding accession numbers listed as follows: PRJNA1196652, PRJNA1196699, PRJNA594843, and PRJNA1196670.

3 Results

3.1 Ferryl hemoglobin in the circulation of patients with ruptured abdominal aortic aneurysms

We established a monoclonal antibody-based enzyme-linked immunosorbent assay, utilizing an in-house generated anti-ferrylHb monoclonal antibody that exhibits specific binding affinity for ferrylHb (82). This assay was developed to quantitatively determine ferrylHb concentrations in serum samples from two cohorts: patients diagnosed with ruptured AAA and healthy volunteer controls. Blood samples were collected from 40 patients undergoing open vascular surgery for ruptured AAA, as well as from 26 healthy donors who were matched for age and sex and had no history of cardiovascular disease, thereby establishing a rigorous comparative baseline. As illustrated in Figure 1A, serum ferrylHb concentrations were found to be markedly elevated in the AAA patient group (320.12 ± 339.26 μg/ml) relative to healthy controls (122.36 ± 106.53 μg/ml). This represented an approximate 2.6-fold increase in the patient cohort, with the difference reaching statistical significance ($P < 0.01$). These striking findings point to a strong correlation between circulating ferrylHb levels and AAA rupture, and further prompted us to explore the potential mechanistic role of ferrylHb in the pathophysiological progression of AAA.

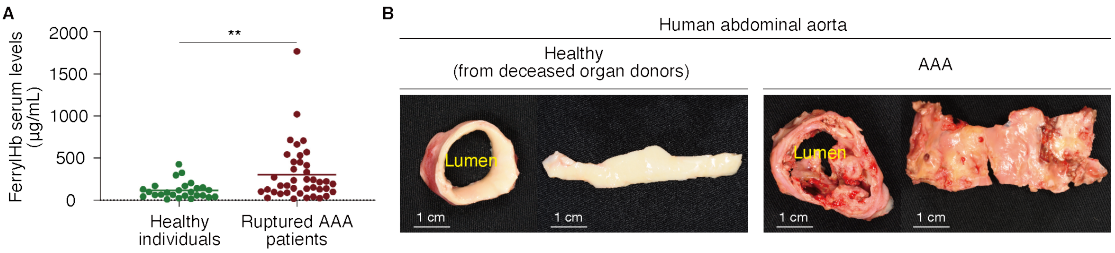

Figure 1. Quantitative detection of circulating ferryl hemoglobin in patients with ruptured abdominal aortic aneurysms.

(A) *A sandwich ELISA was established using monoclonal antibodies with specific affinity for human ferrylHb. This assay was applied to measure ferrylHb concentrations in serum derived from two cohorts: patients with ruptured AAA undergoing open vascular surgery, and healthy donor controls. Experimental data are presented as mean values. Statistical comparisons were performed using the unpaired t-test, with* $^{**}P < 0.01$ *(n = 26 healthy donors; n = 40 AAA patients).* ***(B)*** *Representative macroscopic images are displayed for two tissue types: a hemorrhaged AAA specimen and a healthy aortic tissue sample obtained from deceased organ donors.*

3.2 In human abdominal aortic aneurysms, ferryl hemoglobin accumulates in association with hemorrhage and is taken up by neutrophils and macrophages

To investigate Hb oxidation and ferrylHb accumulation in the pathological context of AAA, we collected aneurysmal tissue specimens from ten patients who underwent open surgical repair for AAA. For comparative analysis, we also obtained healthy aortic tissue samples from five deceased organ donors (Figure 1B). The clinical conditions, comorbidities, and medication histories of the patients are summarized in Table 2, providing a comprehensive overview of the study cohort. As expected, gross examination and histopathological evaluation revealed that the abdominal aortas from AAA patients exhibited partial intramural hemorrhage and mural thrombus formation in contrast to the smooth, intact architecture of healthy aortic tissues.

IHC staining using our previously characterized anti-ferrylHb monoclonal antibody (82) demonstrated a pronounced accumulation of oxidized Hb within the aneurysmal arterial wall, with ferrylHb deposits detected both intracellularly within infiltrating cells and extracellularly within the ECM (Figure 2A and B). Notably, ferrylHb staining was

absent in healthy aortic samples, underscoring the association between hemorrhagic transformation in AAA and local Hb oxidation.

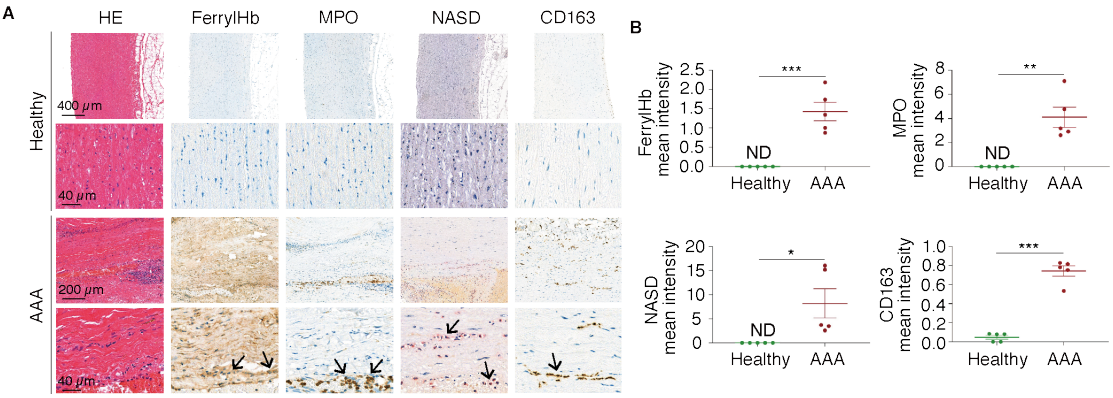

Figure 2. Ferryl hemoglobin accumulates in neutrophils and macrophages within hemorrhaged aortic aneurysm tissue.

(A) *Assays were conducted on tissue samples (n = 5), with detection strategies including H&E staining, as well as IHC staining targeting ferrylHb, MPO, NASD chloroacetate esterase, and CD163.* ***(B)*** *Signal levels corresponding to ferrylHb, MPO, NASD, and CD163 were quantified using the ImageJ software package (n = 5). Statistical significance was defined as follows: $^{*}P < 0.05$; $^{**}P < 0.01$; $^{***}P < 0.001$, with comparisons implemented via unpaired t-test. The abbreviation ND denotes tissue regions where specific staining signals were not detectable.*

Further in-depth histopathological profiling uncovered severe structural disruption of the aortic vessel wall in AAA tissue specimens. This pathological feature was accompanied by the infiltration and accumulation of cells presenting dense, lobulated nuclear morphologies that align with the phenotypic characteristics of granulocytes. These infiltrating cells exhibited positive staining for NASD chloroacetate esterase, a specific phenotypic marker for granulocytes, as well as for MPO, a functional marker that denotes the presence and activation status of neutrophils (121, 122) (Figure 2A and 2B). Importantly, these MPO- and NASD-positive neutrophils were predominantly localized in the adventitia and periadventitial hemorrhagic regions of the aneurysmal

wall, highlighting the spatial association between neutrophil infiltration and intramural hemorrhage in AAA pathophysiology.

Immunohistochemical staining for the hemoglobin scavenger receptor CD163 revealed a markedly increased presence of CD163-positive cells in the AAA tissues compared to healthy controls, suggesting enhanced recruitment or activation of CD163-expressing macrophages within the aneurysmal environment (Figure 2A and B). To explore the potential relationship between ferrylHb accumulation and immune cell activity, we performed double immunostaining for ferrylHb and MPO, which confirmed that ferrylHb was taken up by infiltrating neutrophils within the AAA wall. This observation indicates a mechanistic link between local hemoglobin oxidation and neutrophil-mediated inflammatory responses within AAA.

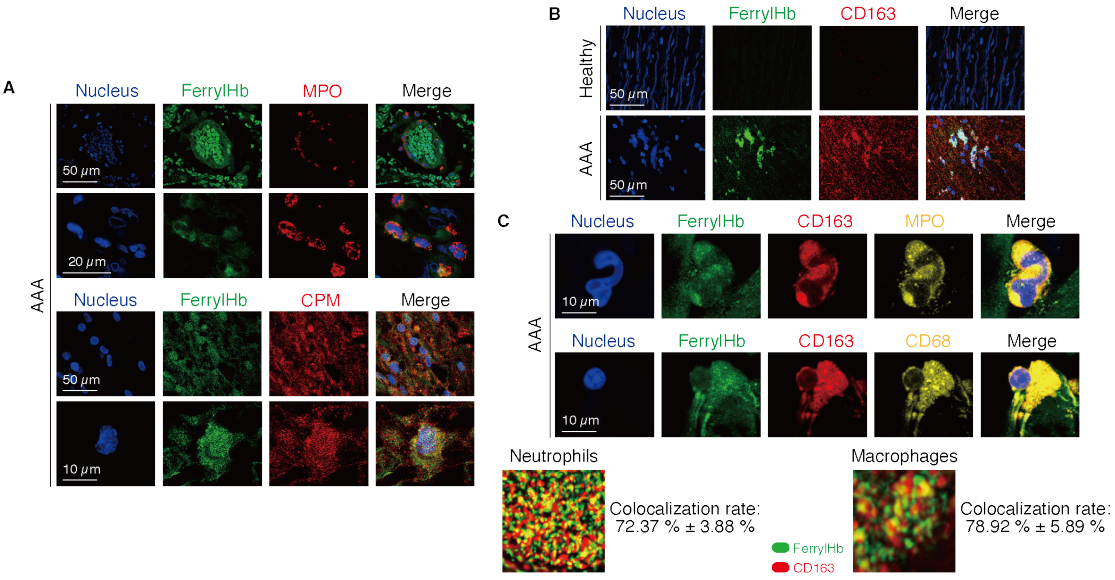

Figure 3. Co-localization of ferryl hemoglobin with neutrophils and macrophages in hemorrhaged aortic tissue.

(A) *Sections harvested from hemorrhagic AAA tissues were subjected to multi-label immunofluorescence staining. Nuclear DNA was labeled with Hoechst 33258 (blue fluorescence); ferrylHb was detected using an Alexa Fluor 488-conjugated anti-ferrylHb antibody (green fluorescence); MPO or CPM were visualized separately via Alexa Fluor 647-conjugated anti-MPO or anti-CPM antibodies (red fluorescence).* ***(B***

and ***C)*** *In a comparable experimental setup, tissue sections derived from both healthy aortas and hemorrhagic AAA tissues were subjected to four-color immunofluorescence staining. Nuclear DNA was labeled with Hoechst 33258 (blue fluorescence); ferrylHb was detected using an Alexa Fluor 488-conjugated anti-ferrylHb antibody (green fluorescence); the CD163 receptor was stained with an Alexa Fluor 647-conjugated anti-CD163 antibody (red fluorescence); MPO or CD68 were labeled separately via Alexa Fluor 568-conjugated anti-MPO or anti-CD68 antibodies (yellow fluorescence). All fluorescence images were acquired using a Leica TCS SP8 gated STED-CW nanoscopic imaging system, a platform endowed with super-resolution imaging capability that exceeds the traditional diffraction limit. Raw imaging data were further processed and deconvolved using Huygens Professional software to optimize image clarity, contrast, and spatial resolution parameters. Representative images presented in this panel were derived from five independent biological samples (n = 5), with scale bars corresponding to 10 μm, 20 μm, or 50 μm as indicated in the figures. Two-dimensional super-resolution imaging validated the spatial colocalization of ferrylHb and the CD163 receptor within macrophage-enriched regions of hemorrhagic AAA tissues. Representative imaging results are displayed, and quantitative analysis of the colocalization rate is presented in the format of mean ± SD (n = 4).*

Additionally, we performed double immunofluorescence staining for ferrylHb and CPM, a surface marker for activated macrophages, revealing significant colocalization of ferrylHb with CPM-positive cells (Figure 3A and B). This finding suggests that not only neutrophils but also macrophages actively internalize oxidized Hb, likely contributing to the inflammatory milieu within the aneurysmal wall. Double immunofluorescence staining also confirmed robust colocalization of ferrylHb with CD163-positive macrophages, reinforcing the involvement of these cells in ferrylHb uptake and potential processing.

Dual immunofluorescence staining assays verified robust colocalization between ferrylHb and the CD163 marker. Quantitative analysis revealed that the colocalization rate of ferrylHb with neutrophil-positive cells reached 72.37% ± 3.88%, while the corresponding rate with CD163-positive macrophages was 78.92% ± 5.89% (Figure 3C). These findings confirm pronounced colocalization of ferrylHb with both

neutrophils and macrophages, thus indicating that these two immune cell populations are actively involved in the uptake of oxidized hemoglobin within AAA lesions.

3.3 In cases of hemorrhaged abdominal aortic aneurysm, hemoglobin is oxidized to the ferryl state, followed by oxidative modification of globin chains and liberation of heme moieties

Hb oxidation and the subsequent production of its highly oxidized ferryl derivative are characterized by the formation of covalently cross-linked Hb, a well-recognized biomarker indicative of ferrylHb presence (82). To verify the existence and clarify the biochemical properties of ferrylHb in human AAA tissues, we carried out Western blot assays on protein extracts isolated from AAA specimens and healthy abdominal arterial tissue samples (Figure 4A and 4B). The results revealed distinct bands corresponding to Hb dimers and tetramers in the AAA samples (upper panel), indicating the formation of globin radicals and subsequent covalent crosslinking of globin chains, a characteristic feature associated with ferrylHb formation under oxidative stress (123). Immunoprecipitation (IP) assays using anti-ferrylHb monoclonal antibodies further confirmed the presence of ferrylHb in AAA samples (lower panel), whereas healthy control tissues exhibited negligible reactivity, reinforcing the association between hemorrhagic transformation in AAA and local Hb oxidation.

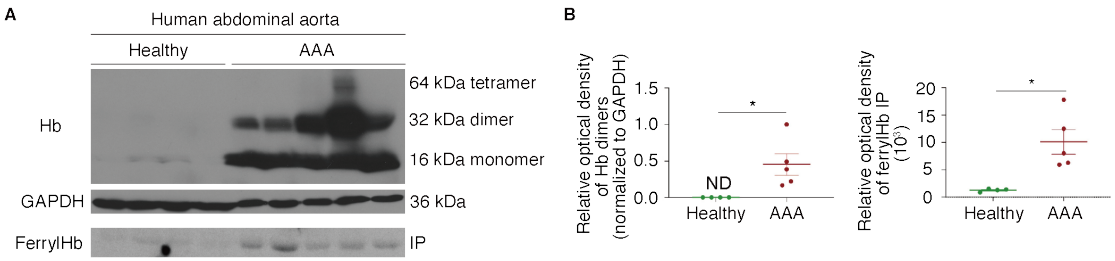

Figure 4. Hemoglobin oxidative modification in tissues from human abdominal aortic aneurysms.

(A) *Representative assay profiles are presented for evaluating and comparing expression levels of Hb dimers (upper panel) and ferrylHb (lower panel), with comparisons drawn between healthy aortic tissue specimens (n = 4) and AAA tissue specimens (n = 5). Western blot assays were implemented with an anti-human Hb antibody to detect total Hb in both healthy and aneurysmal aortic tissue samples.* ***(B)*** *Relative levels of Hb dimers were measured via densitometric analysis and normalized against the expression level of glyceraldehyde-3-phosphate dehydrogenase (GAPDH). For the specific detection of ferrylHb, IP assays were performed using an anti-human ferrylHb antibody for target protein pulldown. Quantitative data corresponding to each protein target were analyzed, with results shown as mean ± SEM for each experimental cohort (n = 4 or 5 per group). Statistical comparisons between healthy and AAA tissue groups were conducted using the unpaired t-test,* $^{*}P < 0.05$.

To further evaluate the oxidation state of Hb in these tissues, we conducted spectral analysis as described previously (82, 85). The absorption spectra of Hb in the ferroHb control samples displayed two characteristic peaks at 542 nm and 577 nm. In contrast, these spectral peaks were significantly diminished in the AAA samples, indicating the oxidation of Hb and the loss of its native spectral features under the pathological conditions present within aneurysmal tissues (Figure 5A). FerrylHb concentrations in the same AAA samples were subsequently quantified using a modified Alayash method (85), which confirmed that ferrylHb levels were markedly elevated in AAA tissues, while healthy controls exhibited undetectable levels of ferrylHb, providing strong biochemical evidence for Hb oxidation within the aneurysmal wall.

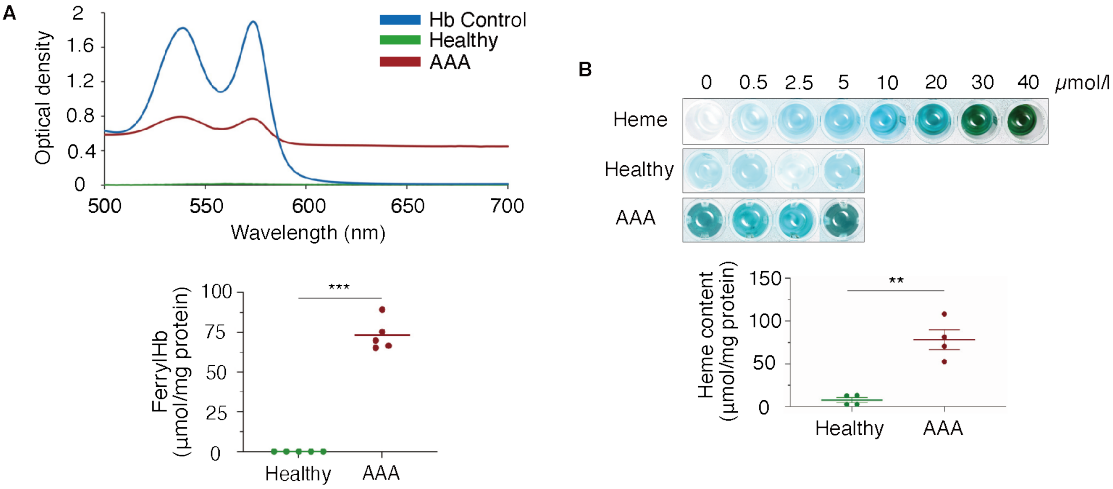

Figure 5. Heme liberation in human abdominal aortic aneurysm samples.

(A) *Assays were carried out on samples from three groups: healthy aortic tissues (n = 5), AAA tissues (n = 5), and Hb control specimens. Concentrations of ferrylHb were measured and the results are presented in the format of mean ± SEM. Statistical comparisons were implemented using the unpaired t-test,* $^{***}P < 0.001$. ***(B)*** *Total heme levels (expressed in µmol/mg protein) were quantified in lysates isolated from human healthy aortic tissues (n = 4) and human AAA tissues (n = 4). Experimental data are displayed as mean ± SEM. Statistical significance was assessed via unpaired t-test,* $^{**}P < 0.01$.

In addition to inducing covalent cross-linking of the globin chains, Hb oxidation can also lead to the destabilization of the heme-globin complex, resulting in the release of the heme prosthetic group and the formation of non-Hb-bound (free) heme, which can exacerbate oxidative stress and inflammation within the vascular wall. To assess this, we measured total heme concentrations in AAA and control tissue samples. The results demonstrated that AAA tissues contained significantly higher levels of free heme (78.29 ± 23.27 µmol/mg protein) compared to healthy control tissues (7.67 ± 5.86 µmol/mg protein), as illustrated in Figure 5B. These findings underscore that the oxidative environment within AAA lesions facilitates the liberation of heme from oxidized Hb, potentially amplifying local inflammatory responses and tissue damage.

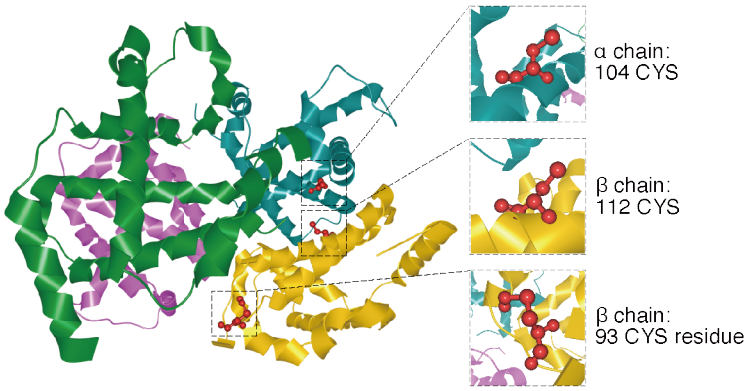

Figure 6. Oxidative modifications of cysteine residues in hemoglobin within human abdominal aortic aneurysm tissues.
Aneurysmal tissue samples (n = 5) were subjected to trypsin digestion prior to LC-MS/MS analysis, which was designed to detect oxidized cysteine (CYS) residues within Hb chains. The specific oxidized CYS sites identified via this approach are listed as follows:
α chain: CYS at position 104, corresponding to the peptide sequence LLSHCLLVTLAAHLPAEFTPAVHASLDKFLASVSTVLTSK.
β chain: CYS at position 112, corresponding to the peptide sequence LLGNVLVCVLAHHFGK.
β chain: CYS at position 93, corresponding to the peptide sequence GTFATLSELHCDKLHVDPENFR.
Three-dimensional visualization of human Hb protein structure was accomplished using CAVER Analyst 2.0 software, with the protein structure data retrieved from the RCSB Protein Data Bank under the entry code 1BUW.

Multiple lines of evidence from prior studies indicate that the βCys93 residue within the Hb molecule serves as a critical site for free radical-induced oxidation, initiating the formation of globin radicals that drive further oxidative modifications (124-126). To directly assess the oxidative modifications occurring at specific cysteine residues within Hb in AAA tissues, we employed high-resolution mass spectrometry analysis. This analysis confirmed the oxidation and trioxidation of the βCys93 residue, which aligns with the role of this residue as a primary site for oxidative attack. Additionally, we identified further oxidative modifications at βCys112 and αCys104 residues (Figure 6), indicating that oxidative modifications of multiple cysteine residues contribute to the structural changes and functional impairments of Hb within the aneurysmal

environment (127). These post-translational modifications are consistent with a heightened oxidative milieu in AAA tissues and likely contribute to the pathophysiological processes underlying aneurysm progression and rupture.

3.4 Hemoglobin conversion to ferryl form marks angiotensin II-triggered abdominal aortic aneurysms in apolipoprotein E knockout mice

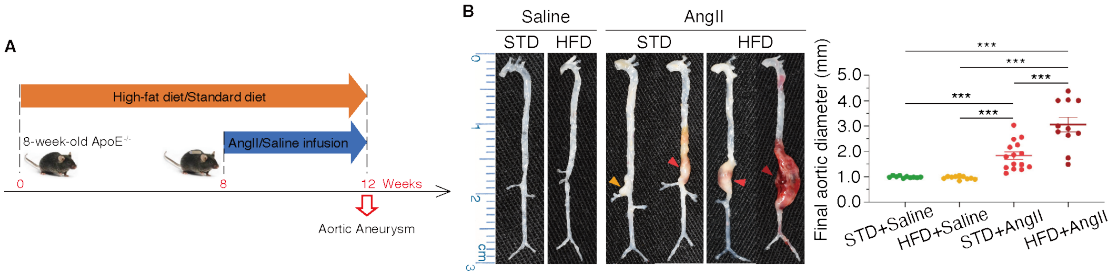

Figure 7. High-fat feeding aggravates angiotensin II-triggered abdominal aortic aneurysm development in apolipoprotein E knockout mice.

(A) *Male ApoE$^{-/-}$ mice at 8 weeks of age were assigned to four dietary cohorts, receiving either a STD or a HFD over a 12-week period. In the final 4 weeks of this dietary intervention, the animals were administered continuous infusion via osmotic pumps, with the infusion agent being either AngII or physiological saline.* ***(B)*** *Images display isolated aortic specimens derived from four experimental groups: saline, AngII, HFD+saline, and HFD+AngII. Yellow arrowheads indicate aneurysm lesions without concurrent hemorrhage; light red arrowheads mark aneurysm lesions accompanied by hemorrhage; dark red arrowheads denote fully ruptured aortic tissues. Maximal suprarenal aortic diameter (in millimeters) was measured at 28 days post-infusion. Statistical comparisons were performed using the unpaired t-test, $^{***}P < 0.001$.*

To further elucidate the mechanistic basis underlying our findings in human AAA, we utilized a well-established murine model of aortic aneurysm formation. ApoE$^{-/-}$ mice, a model characterized by inherent susceptibility to vascular inflammatory responses and atherosclerotic lesion formation, were randomized to receive either a STD or a HFD for a 12-week duration to establish a pro-atherogenic physiological state. Subsequent to dietary intervention, the mice were subjected to continuous subcutaneous infusion of either physiological saline or AngII at a dosage of 1000 ng/kg/min for 28 days, to

trigger AAA development (Figure 7A). The dynamic progression of AAA in these experimental mice was closely tracked via serial ultrasonographic assessments. Abdominal aortic diameter was measured at the baseline time point prior to infusion, as well as at three post-infusion time intervals: 7, 14, and 28 days (Figure 8A). Consistent with previous observations, AngII infusion resulted in progressive dilation of the abdominal aorta, with the aneurysmal expansion being more pronounced in HFD-fed mice compared to STD-fed mice, indicating that dietary lipid loading exacerbates AngII-induced aneurysm development (Figure 7B, Figure 8B). Notably, blood pressure measurements did not show significant differences between AngII-treated STD and HFD groups, suggesting that the observed differences in AAA progression were not attributable to differential blood pressure effects (Figure 9A).

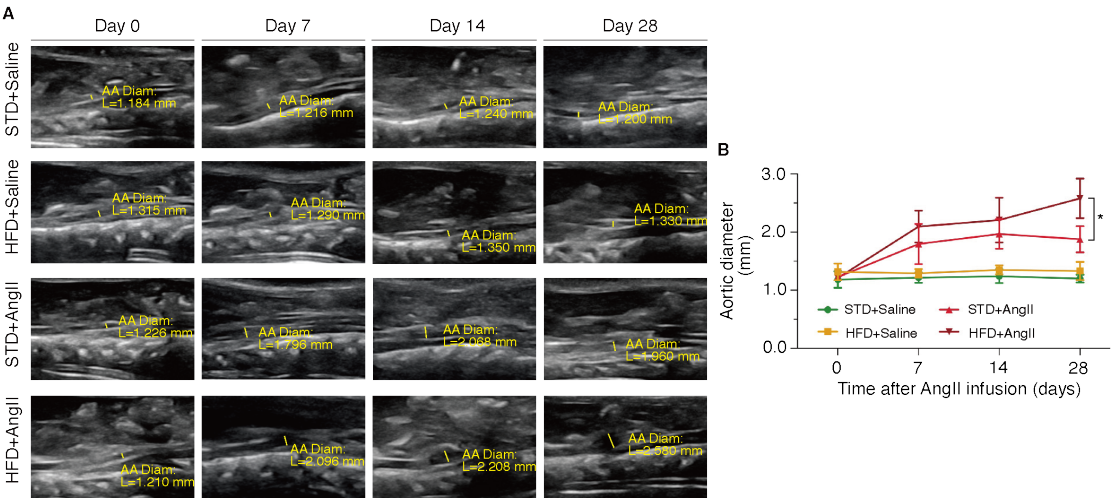

Figure 8. Longitudinal ultrasound assessment of abdominal aortic aneurysm development in angiotensin II-infused mice.

(A) *Representative high-resolution ultrasound images of suprarenal abdominal aortas obtained from different experimental groups. AA, abdominal aorta; L, length.* ***(B)*** *Temporal changes in suprarenal aortic diameter (mm) were quantified by ultrasonography at baseline (day 0) and after 7, 14, and 28 days of AngII infusion. Values are shown as mean ± SEM.* $^{*}P < 0.05$*, unpaired t-test.*

Control groups maintained on STD or HFD without AngII infusion failed to develop aneurysms during the study period, confirming the requirement of AngII for AAA induction in this model. Aortic aneurysms were stratified into four distinct grades based on well-validated histopathological classification standards: Grade I denotes morphologically normal aortic tissue; Grade II represents aortic aneurysm lesions without associated hemorrhage; Grade III refers to aortic aneurysm lesions complicated by hemorrhage; Grade IV indicates fully ruptured aortic tissue (Figure 9B) (128).

Notably, the frequency of aneurysmal hemorrhage (17 out of 19 cases) and rupture (8 out of 19 cases) was markedly elevated in mice subjected to AngII infusion combined with high-fat diet feeding. This trend stood in sharp contrast to the outcomes observed in AngII-infused mice maintained on a standard diet, where hemorrhage occurred in 9 out of 19 cases and rupture in 4 out of 19 cases (Figure 9C and 9D). These findings underscore the critical role of hyperlipidemia and dietary regimens in aggravating aneurysm instability and rupture within the experimental setting of AngII-induced AAA.

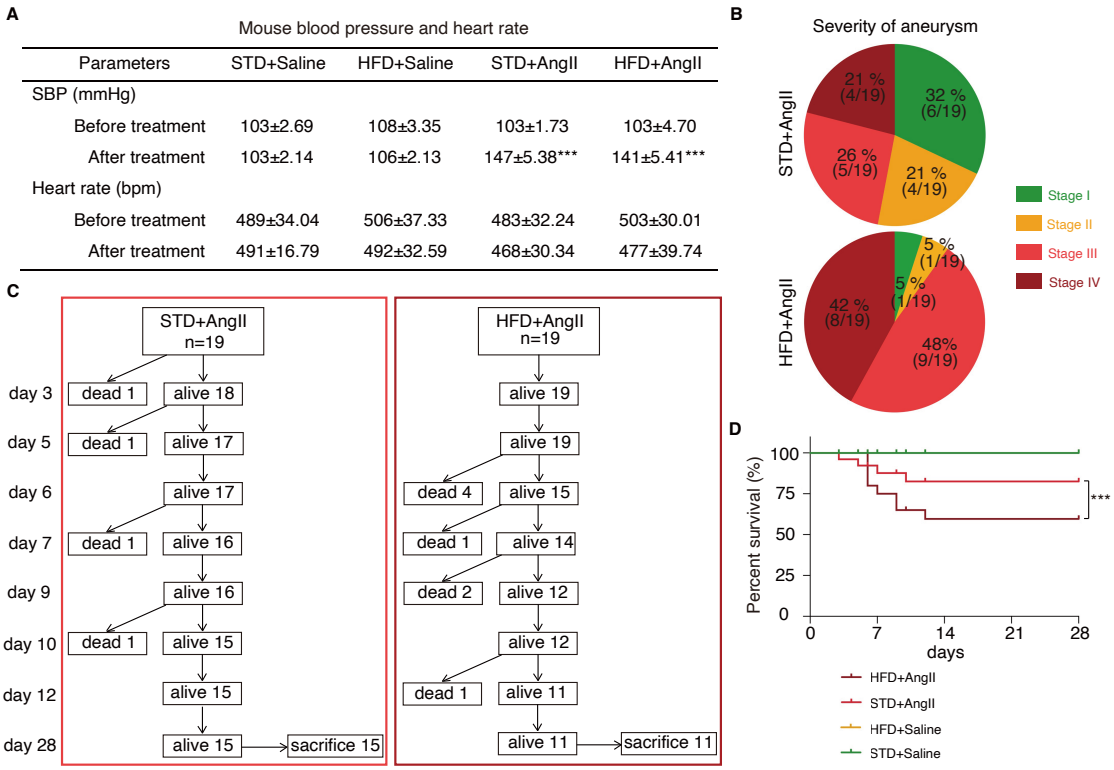

Figure 9. High-fat diet aggravates the severity and rupture frequency of abdominal aortic aneurysms in angiotensin II-infused apolipoprotein E deficient mice.

(A) *Systolic blood pressure (SBP) and heart rate were measured before AngII infusion and after 4 weeks of treatment. Values are shown as mean ± SD.* $^{***}P < 0.001$ *compared with pretreatment SBP within the same group (paired t-test).* ***(B)*** *Distribution of aneurysm severity in mice receiving STD+AngII (n = 19) or HFD+AngII (n = 19). Tissue lesions were classified into four distinct grades according to pathological features: Grade I represent histologically normal aortic tissue; Grade II corresponds to aortic aneurysm lesions without concurrent hemorrhage; Grade III indicates aortic aneurysm lesions accompanied by hemorrhage; Grade IV denotes fully ruptured aortic tissue.* ***(C)*** *Time of aneurysm rupture following AngII infusion in the two dietary groups.* ***(D)*** *Kaplan-Meier survival curves of STD+AngII versus HFD+AngII mice.* $^{***}P < 0.001$*; significance determined by Log-rank and Gehan-Breslow-Wilcoxon tests.*

Given our findings of ferrylHb accumulation in human hemorrhagic AAAs, we sought to determine whether AngII-induced AAA in ApoE$^{-/-}$ mice recapitulates similar Hb oxidation profiles. Spectral profiling of Hb isolated from hemorrhagic AAA tissues identified distinct absorption peaks at 533 nm and 571 nm, a characteristic signature indicative of the presence of oxidized Hb species within these pathological specimens.

Quantitative spectral assays further revealed that the levels of metHb and ferrylHb were markedly elevated relative to ferroHb in hemorrhagic AAA tissues; this elevation was particularly pronounced in ApoE$^{-/-}$ mice subjected to HFD feeding combined with AngII administration (Figure 10A and B).

To obtain supplementary biochemical verification, Western blot assays were conducted on protein lysates extracted from AAA tissues. The results confirmed the presence of Hb dimers and the formation of covalently cross-linked globin chains in HFD-fed, AngII-treated ApoE$^{-/-}$ mice, two hallmark biochemical features that signal the oxidation of Hb to its ferryl state (Figure 11A). Collectively, these data recapitulate the characteristic biochemical signature of ferrylHb observed in human hemorrhagic AAA tissues, thereby implying the existence of evolutionarily conserved Hb oxidation mechanisms during the progression of aneurysmal lesions across species.

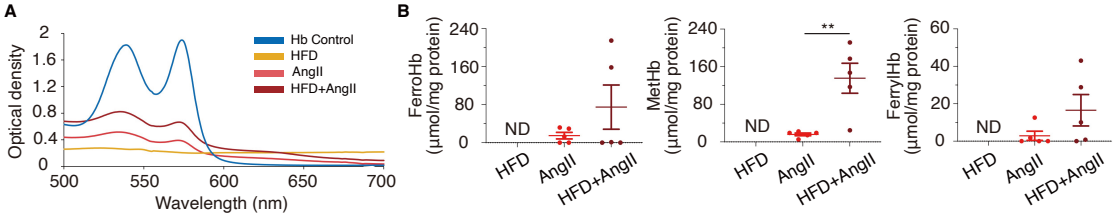

Figure 10. Ferryl hemoglobin is detectable in abdominal aneurysms of high-fat fed mice administered angiotensin II.

(A) *Assays were conducted on samples derived from four experimental cohorts: Hb control, HFD, AngII, and HFD+AngII (AAA) groups, with five biological replicates assigned to each cohort (n = 5 per group).* ***(B)*** *Relative levels of oxyHb, metHb, and ferrylHb were determined via quantification. Experimental results are presented in the format of mean ± SEM. Statistical comparisons between groups were performed using the unpaired t-test, with $P < 0.01$ defined as the threshold for significance. The abbreviation ND denotes components with concentrations below the detectable limit of the assay.*

To pinpoint the specific oxidative modifications occurring within the globin chains, we conducted high-resolution mass spectrometry on proteins extracted from hemorrhaged

mouse aneurysm tissues. Interestingly, while human AAA tissues exhibited oxidative modifications at βCys93, βCys112, and αCys104, analysis of mouse AAA tissues revealed a predominant oxidation localized specifically at the βCys93 residue (Figure 11B). This finding suggests that although the general mechanism of Hb oxidation and ferrylHb formation is conserved, there may be species-specific differences in the patterns of cysteine oxidation within the globin molecule during AAA pathogenesis.

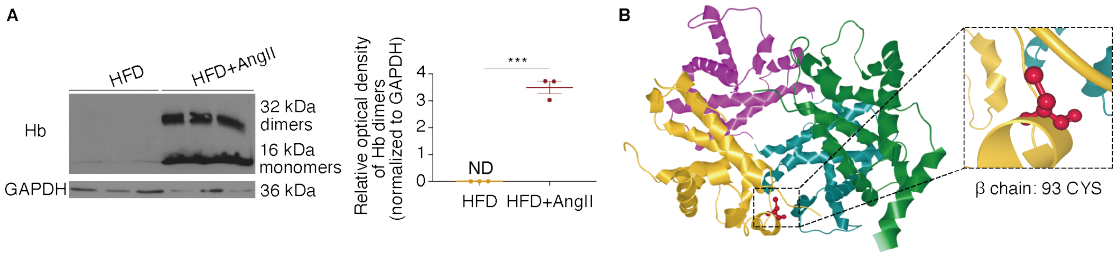

Figure 11. Oxidative changes to cysteine residues in hemoglobin within abdominal aortic aneurysm tissues of mice.

(A) *Western blot analysis of Hb dimers in HFD versus HFD+AngII aortas (n = 3 per group). GAPDH served as a loading control. Densitometric quantification is shown as mean ± SEM.* ***(B)*** *Oxidized CYS residues in globin chains were detected by LC-MS/MS following tryptic digestion of aneurysmal tissue from HFD+AngII-treated mice (n = 4). The primary oxidation hotspot was identified at β93 (sequence GTFASLSELHCDKLHVDPENFR). Structural localization was performed with CAVER Analyst 2.0 software using PDB entry 3HRW.*

Similar to human AAA samples, increased accumulation of oxidized Hb was observed in AAA tissues from HFD-fed mice treated with AngII, which was accompanied by elevated heme levels (Figure 12A). Furthermore, correlation analysis combining ferrylHb and heme measurements from both human and mouse arterial samples revealed a strong positive relationship between ferrylHb concentrations and free heme levels. This correlation was particularly pronounced in hemorrhaged abdominal aneurysms with very high ferrylHb values (R = 0.717, $P = 0.030$) (Figure 12B).

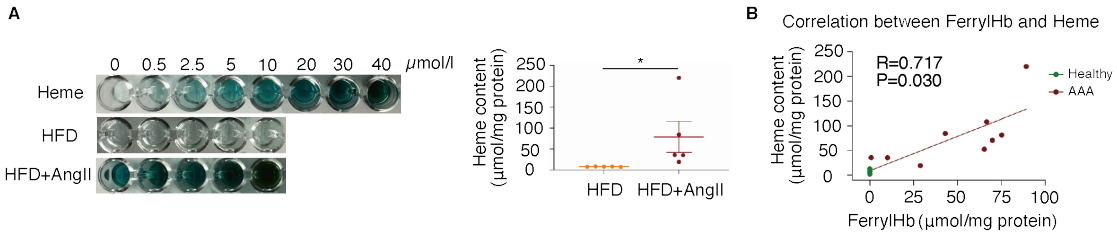

Figure 12. Correlation between ferryl hemoglobin accumulation and elevated heme levels in human and murine abdominal aortic aneurysm tissues.

(A) *Fluorescence-based assays were implemented to detect total heme levels in specimens derived from two experimental cohorts: HFD (n = 5) and HFD+AngII (n = 5). Statistical comparisons between groups were performed using the unpaired t-test, with P < 0.05 defined as the threshold for significance (P < 0.05).* ***(B)*** *Correlation analyses were carried out to explore the association between ferrylHb and heme levels in aortic wall samples isolated from both human and mouse aneurysm tissues. Correlation coefficients (R) and corresponding P values are indicated in the plot. Statistical significance was determined using two-tailed tests, with P < 0.05 regarded as statistically meaningful.*

Collectively, these results demonstrate that AngII-induced AAA in ApoE$^{-/-}$ mice, particularly under hyperlipidemic conditions, recapitulates the oxidative environment of human AAA, characterized by Hb oxidation to the ferryl state, covalent cross-linking of globin chains, liberation of heme moieties, and specific cysteine residue oxidation within the globin structure. These findings substantiate the utility of this murine model for further mechanistic studies on Hb oxidation in AAA and suggest that targeting the oxidative modification of Hb may represent a therapeutic strategy to mitigate inflammation and progression in AAA.

3.5 Hemoglobin is internalized by neutrophils and macrophages in murine hemorrhaged abdominal aortic aneurysms

In human AAA tissues, we previously demonstrated that neutrophils and macrophages actively internalize ferrylHb, linking Hb oxidation with cellular inflammation within the aneurysmal wall. To determine whether a similar mechanism of Hb uptake occurs

in our murine model of hemorrhaged AAA, we performed comprehensive histological and immunohistochemical analyses on aortic tissues from ApoE$^{-/-}$ mice subjected to AngII-induced AAA under either STD or HFD conditions.

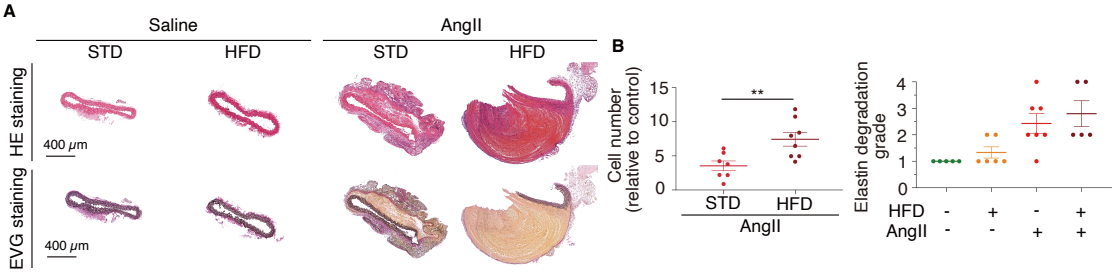

Figure 13. Histological evidence of angiotensin II - and high-fat diet -induced elastin degradation in murine abdominal aortic aneurysms.

(A) *ApoE$^{-/-}$ mice were subjected to AngII infusion for a 4-week period. Suprarenal aortic tissue specimens were then harvested for subsequent histopathological evaluation. Representative micrographs are provided for H&E staining and EVG staining of the collected tissues.* ***(B)*** *Cell count data were normalized against corresponding values derived from control groups, with sample sizes ranging from 7 to 8 per cohort (n = 7-8). Statistical significance was determined via unpaired t-test, with $P < 0.01$ indicating a notable difference between groups. Additionally, the extent of elastin degradation in aortic tissues was quantified, with sample sizes of 5 to 7 per cohort (n = 5-7).*

Histological examination using H&E and EVG staining confirmed that saline-infused control mice maintained normal aortic architecture, characterized by well-preserved and intact elastin layers within the suprarenal aortic segments (Figure 13A and B, Supplemental Figure 1). By sharp contrast, AngII administration triggered overt aneurysm formation, a pathological change accompanied by extensive degradation of elastic fibers within the aortic wall. When comparing AngII-treated mice fed a HFD with those on a STD, the scope and severity of elastic fiber degradation, along with the overall degree of cellular infiltration, were markedly enhanced. This observation underscores the exacerbator role of hyperlipidemia in accelerating aneurysm progression and impairing the structural integrity of the vascular wall.

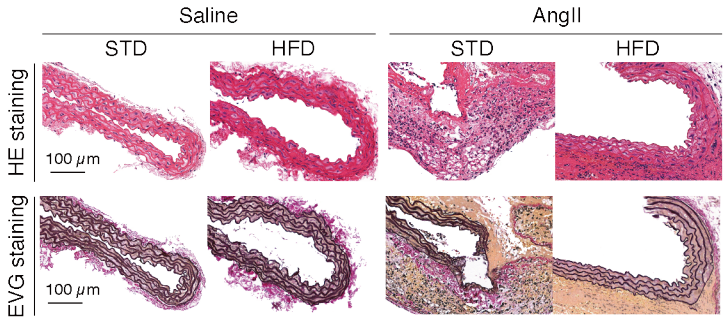

Supplemental Figure 1. High-resolution histological analysis of abdominal aortic aneurysms induced by angiotensin II.

ApoE$^{-/-}$ mice were subjected to AngII administration for a duration of 4 weeks. Suprarenal aortic tissues were subsequently harvested for histological examination. Representative micrographs are shown for H&E staining and EVG elastin staining of aneurysmal tissue sections. Scale bar = 100 μm.

IHC analysis revealed that in the regions of the ruptured and hemorrhagic aortic wall, extracellular accumulation of Hb was evident within the aneurysmal matrix, particularly in areas of elastin disruption and adventitial hemorrhage (Figure 14A). Importantly, high-resolution imaging demonstrated that this extracellular Hb was actively internalized by neutrophils within the lesion sites, as highlighted within magnified boxed regions, indicating that neutrophil-mediated uptake of Hb occurs in the murine model similar to what was observed in human AAA tissues. Similarly, Hb-positive signals were detected in macrophages (arrows) located in the same area. The internalization of Hb by neutrophils and macrophages in the hemorrhagic AAA microenvironment points to an evolutionarily conserved mechanism. Through this pathway, neutrophils and macrophages interact with oxidized Hb in the context of intramural hemorrhage, which may foster local oxidative stress responses and amplify inflammatory signal transduction within the aneurysmal wall.

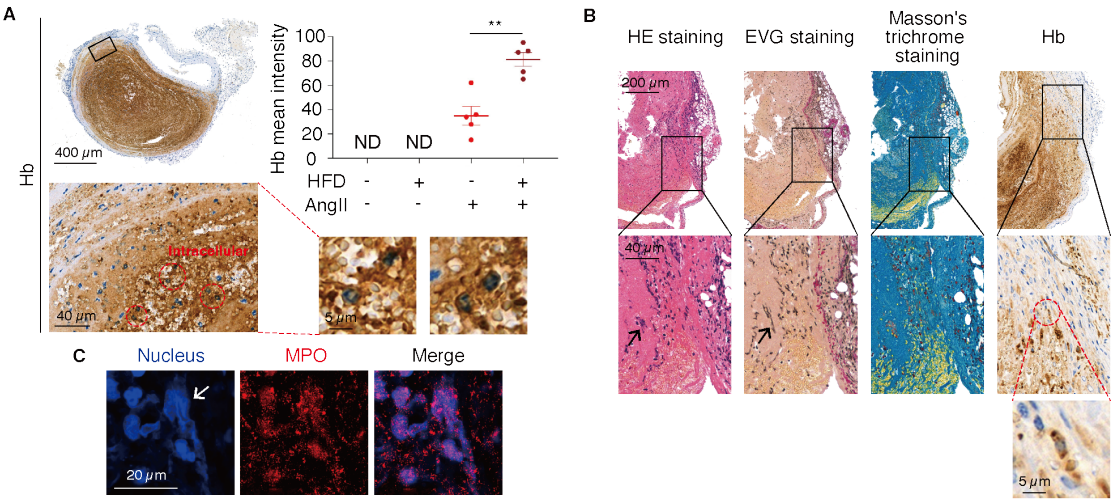

Figure 14. Hemoglobin internalization by neutrophils and macrophages in murine hemorrhaged abdominal aortic aneurysms.

(A) *The assay was designed to characterize the localization and distribution patterns of Hb within the aneurysmal vessel wall. Areas presenting positive intracellular Hb signals are demarcated by red dashed circles. High-magnification micrographs displayed in the right-side insets highlight neutrophil populations, which are identified by their typical multilobed nuclear morphology and concurrent positive cytoplasmic Hb staining; this finding confirms the intracellular presence of Hb in these immune effector cells. Quantitative assessments of Hb staining intensity and spatial distribution across tissue sections were carried out using the ImageJ software package. Experimental data are presented as mean values generated from five independent tissue samples (n = 5). Statistical comparisons between groups were executed via unpaired t-test, with $P < 0.01$ defined as the threshold for statistical significance. The abbreviation ND indicates tissue regions where specific Hb staining signals were not detectable.* ***(B)*** *Images display results from H&E, EVG, Masson's trichrome, and Hb immunostaining assays. Insets enclosed by red dashed circles in the right-hand panels highlight tissue regions with intracellular Hb accumulation; these Hb-positive cells are identified as macrophages based on their characteristic large, round, mononuclear morphological features. Lower-panel micrographs provide high-magnification views that delineate detailed tissue microarchitectural characteristics, with arrows pointing to NET structures, a key hallmark of neutrophil activation and inflammatory responses in AAA lesions.* ***(C)*** *Tissue sections were derived from mouse models with AAA induced by AngII infusion combined with an HFD. Samples were stained with Hoechst 33258 for visualizing nuclear DNA (blue fluorescence) and an Alexa Fluor 647-conjugated anti-MPO antibody for labeling MPO protein (red fluorescence). Fluorescence imaging was accomplished using a Leica TCS SP8 gated STED-CW nanoscopic microscope, a platform endowed with super-resolution imaging capacity. Acquired raw images were further processed via deconvolution using Huygens Professional software to optimize image clarity, contrast, and spatial resolution parameters. Scale bars correspond to 20 μm, and arrows marked in the images denote NET structures.*

To further delineate the inflammatory progression within advanced aneurysm tissues, we extended the AngII infusion regimen to a 15-week duration for the assessment of late-stage pathological manifestations. Notably, this prolonged intervention elicited the formation of NETs within advanced aneurysmal lesions; such structures were identified via the detection of extracellular DNA decorated with neutrophil-derived enzymes including MPO and NE (Figure 14B and C). The emergence of NETs in these late-stage lesions implies an additional dimension of neutrophil-mediated inflammation, which may interact with extracellular Hb to propagate oxidative stress and proteolytic activity within the aneurysmal microenvironment.

Collectively, these findings illustrate that in AngII-induced hemorrhagic AAAs of $ApoE^{-/-}$ mice, extracellular Hb is released within the aneurysmal wall and undergoes active internalization by neutrophils and macrophages, a pattern that recapitulates observations in human AAA specimens. Moreover, the development of NETs within advanced aneurysm tissues underscores the intricate interplay between Hb oxidation, neutrophil activation, and macrophage function, a regulatory network that may contribute to the progression and destabilization of AAA lesions in this murine model.

3.6 Ferryl hemoglobin uptake by neutrophils also occurs via cluster of differentiation 163 (CD163)

CD163, a class B member of the scavenger receptor superfamily (129), exerts a pivotal function in Hb homeostasis under hemolytic conditions. It accomplishes this by binding to Hb-haptoglobin complexes, then mediating their internalization and lysosomal breakdown, actions that alleviate oxidative damage and suppress inflammatory

reactions within affected tissues (130, 131). Of note, CD163-driven clearance of free Hb can proceed independently of haptoglobin, ensuring efficient elimination of potentially cytotoxic extracellular Hb from the tissue microenvironment (82).

Building on these findings, we investigated whether ferrylHb uptake in neutrophils within aneurysmal tissues also occurs via CD163-mediated mechanisms. In AngII- and HFD-induced AAA tissues from ApoE$^{-/-}$ mice, immunofluorescence analysis revealed a marked colocalization of ferrylHb with CD163 within infiltrating neutrophils and macrophages, indicating active engagement of CD163 with oxidized Hb within the hemorrhagic microenvironment (Figure 15A). Notably, such expression patterns and colocalization of CD163 with ferrylHb were absent in aortic tissues obtained from healthy control mice, highlighting a disease-specific upregulation and utilization of this pathway during AAA progression.

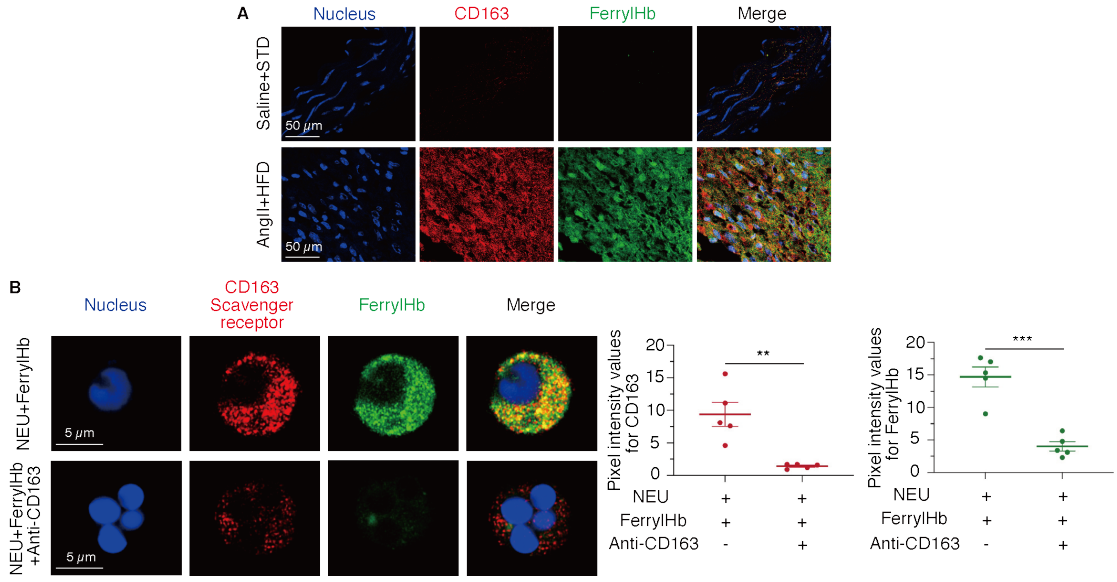

Figure 15. Cluster of differentiation 163 mediates ferryl hemoglobin uptake by neutrophils in murine abdominal aortic aneurysm tissues.

(A) *The assay was conducted to detect ferrylHb and CD163-positive neutrophils/macrophages, with comparisons drawn between aneurysmal aortas from the HFD+AngII cohort and control aortas from the STD+Saline cohort.* ***(B)***

Neutrophils (NEUs) isolated from healthy volunteer donors were treated with ferrylHb for 16 hours, with a parallel group receiving ferrylHb treatment combined with CD163 blockade. Cells were subjected to triple staining: Hoechst 33258 for labeling DNA (blue fluorescence), Alexa Fluor 488-conjugated anti-ferrylHb antibody (green fluorescence), and anti-CD163 antibody (red fluorescence). Imaging acquisition was implemented using a Leica TCS SP8 gated STED-CW microscope, followed by image deconvolution via the Huygens Professional software. Scale bar = 5 μm. Pixel intensity values corresponding to red and green fluorescence signals were quantified with the ImageJ software (n = 5). $^{**}P < 0.01$, $^{***}P < 0.001$.

To further validate the functional role of CD163 in ferrylHb uptake, we pretreated isolated neutrophils with a CD163-blocking antibody prior to exposure to ferrylHb. This blockade resulted in a substantial reduction in ferrylHb internalization by neutrophils, underscoring the essential role of CD163 in mediating ferrylHb uptake in these cells. Quantitative analysis revealed a significant decrease in ferrylHb-positive neutrophils upon CD163 inhibition, confirming the specificity of this receptor-mediated process (Figure 15B).

Collectively, these findings illustrate that CD163 expressed on neutrophils actively mediates the internalization and clearance of ferrylHb in the setting of AngII and HFD induced AAA. This regulatory mechanism likely serves as a critical protective pathway, alleviating ferrylHb-associated oxidative stress and inflammatory responses within the aneurysmal microenvironment. Simultaneously, it highlights a previously undervalued role of neutrophil expressed CD163 in maintaining vascular homeostasis during the progression of hemorrhagic AAA.

3.7 Transcriptomic signature of human hemorrhaged abdominal aortic aneurysms correlated with inflammation and neutrophil activation

To further dissect the molecular cascades governing the initiation and progression of AAA, we conducted bulk RNA sequencing (RNA-seq) assays on aneurysmal tissue specimens harvested from patients diagnosed with hemorrhaged AAA. These tissue profiles were then subjected to comparative analysis against samples derived from healthy abdominal aortic tissues. This analytical strategy enabled the identification of DEGs and facilitated the delineation of relevant biological pathways that might mediate the pathophysiological processes of AAA.

Principal component analysis (PCA) uncovered distinct transcriptomic signatures that clearly segregated AAA tissue samples from healthy control specimens. Biological replicates corresponding to each experimental group clustered closely together, which attested to the robustness and reproducibility of the acquired data. Of note, the first PC1 accounted for 55.45% of the total variance across the dataset, a result that underscores the extensive transcriptomic alterations associated with AAA pathogenesis (Figure 16A).

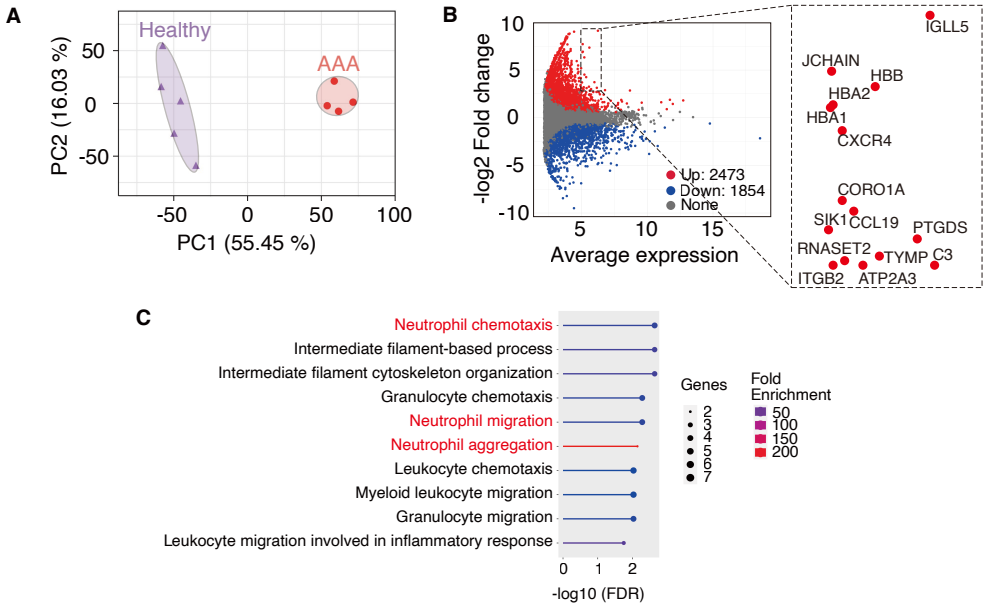

Figure 16. Distinct transcriptomic signature between human healthy aortic tissue and hemorrhaged abdominal aortic aneurysm.

(A) *Assays were conducted on tissue samples obtained from healthy donor cohorts (n = 5, marked by purple circles) and AAA patient cohorts (n = 4, marked by red circles). PCA results indicated a distinct separation between the two experimental groups. Principal components were calculated via unit variance scaling combined with singular value decomposition (SVD) coupled with imputation; PC1 and PC2 contributed to 55.45% and 16.03% of the total variance across the dataset, respectively.* ***(B)*** *Genes with significant upregulation are marked in red, those with notable downregulation are shown in blue, and genes without statistical expression differences are displayed in gray. The embedded small plot highlights the DEGs with the most prominent upregulation trends.* ***(C)*** *The analysis screened out the top 10 significantly enriched biological process terms, which were ranked according to the value of -log10 (false discovery rate, FDR). A heatmap was generated to exhibit the expression patterns of representative marker genes linked to the most heavily affected pathways, and these genes were further categorized into three distinct functional clusters.*

A transcriptomic profiling analysis across all experimental samples identified 4,327 DEGs in total. Among these transcriptomic alterations, 2,473 genes exhibited significant upregulation and 1,854 genes displayed marked downregulation in AAA tissues relative to healthy vascular wall specimens (Figure 16B). Notably, a substantial proportion of the upregulated genes were enriched in biological pathways linked to neutrophil activation, inflammatory signal transduction, oxidative stress responses, and

iron metabolic processes. These enrichment patterns imply that neutrophil-mediated inflammatory cascades and iron homeostasis regulatory mechanisms play central roles in driving AAA pathogenesis.

To further delineate the biological processes correlated with these transcriptomic variations, we conducted GO enrichment assays. The results highlighted robust associations with core neutrophil-related biological events, including “Neutrophil Chemotaxis,” “Neutrophil Migration,” and “Neutrophil Aggregation” (Figure 16C). These transcriptomic signatures align well with histopathological evidence documenting extensive neutrophil infiltration in aneurysmal lesions, suggesting that neutrophil-driven inflammatory responses may actively promote aneurysmal wall degeneration and disease progression.

A targeted analysis focusing on neutrophil-associated gene expression patterns revealed pronounced upregulation of several critical neutrophil functional markers. These included S100A8, which encodes a calcium-binding protein involved in neutrophil activation and chemotaxis; ADAM8, a metalloproteinase gene implicated in ECM remodeling and neutrophil migration; DOCK8, which regulates cytoskeletal rearrangements essential for neutrophil motility; and SELL (L-selectin), a gene critical for mediating neutrophil adhesion and transmigration across the vascular endothelium (Figure 17). The elevated expression of these genes further underscores the pivotal involvement of neutrophil activation and recruitment processes in shaping the pro-inflammatory microenvironment of hemorrhagic AAA.

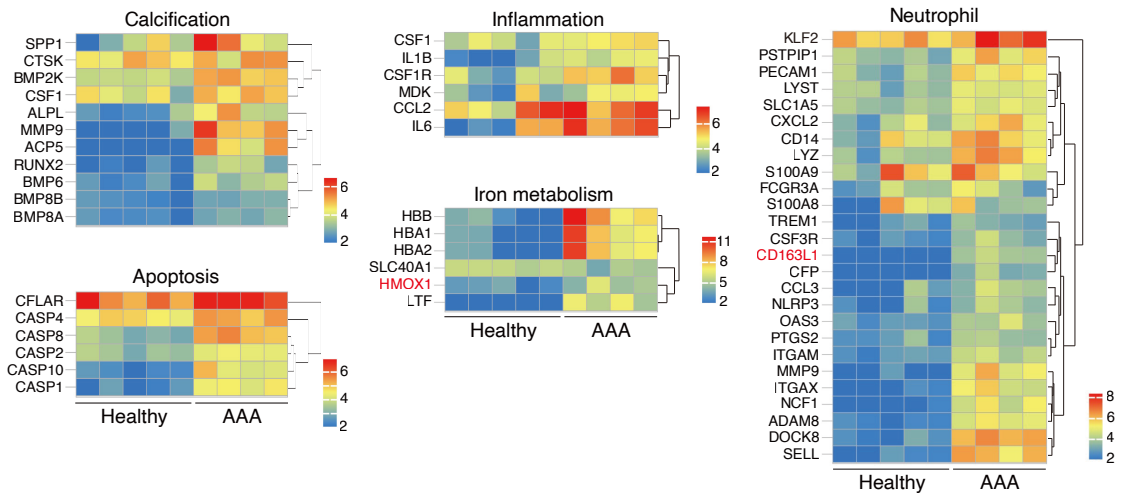

Figure 17. Upregulation of neutrophil activation markers and pro-inflammatory cytokines in hemorrhaged abdominal aortic aneurysms.

The analysis focused on five functional gene categories, namely calcification, apoptosis, inflammation, neutrophil activation and iron metabolism. Expression patterns of genes within these categories were systematically compared between healthy aortic tissue specimens and AAA tissue samples.

Beyond the enrichment of neutrophil activation-related pathways, our transcriptomic assays also revealed significant dysregulation of multiple key inflammatory genes in hemorrhagic AAA tissues. Specifically, the genes encoding IL1β and IL6 showed marked upregulation in AAA samples compared with healthy control tissues. As core mediators of inflammatory cascades, these two cytokines are known to amplify neutrophil recruitment and activation, while simultaneously sustaining the chronic inflammatory microenvironment that typifies aneurysmal progression.

Furthermore, an analysis targeting iron metabolism-related genes demonstrated notable expression dysregulation within AAA tissues. Genes including hemoglobin subunit beta (HBB), HMOX1, and lactotransferrin (LTF) exhibited distinctly altered expression profiles in aneurysmal tissues relative to control specimens. The upregulation of HBB may reflect extracellular Hb accumulation within the aneurysmal wall subsequent to intramural hemorrhage. In contrast, HMOX1, a stress-responsive enzyme responsible

for heme catabolism, is typically induced under conditions of oxidative stress and heme overload. Meanwhile, the elevated expression of LTF, which encodes lactoferrin, a critical iron-binding protein, suggests the activation of an adaptive response aimed at mitigating iron-mediated oxidative damage within the aneurysmal microenvironment.

Collectively, these transcriptomic findings underscore the tight interplay between ferrylHb accumulation, iron metabolism dysregulation, and neutrophil-mediated inflammation in the pathogenesis of AAA. The concurrent upregulation of inflammatory cytokine genes and iron homeostasis regulatory genes provides molecular evidence supporting our histological and biochemical observations: that ferrylHb accumulation within hemorrhagic AAA lesions may act as a key trigger for neutrophil recruitment and activation, thereby amplifying local inflammatory responses and oxidative stress within the aneurysmal wall. This mechanistic insight may facilitate the identification of novel therapeutic targets, which can be leveraged to modulate inflammation and oxidative injury in AAA and ultimately prevent disease progression and life-threatening aortic rupture.

3.8 Ferryl hemoglobin triggers transcriptomic alterations in human monocytes that overlap with those seen in abdominal aortic aneurysms

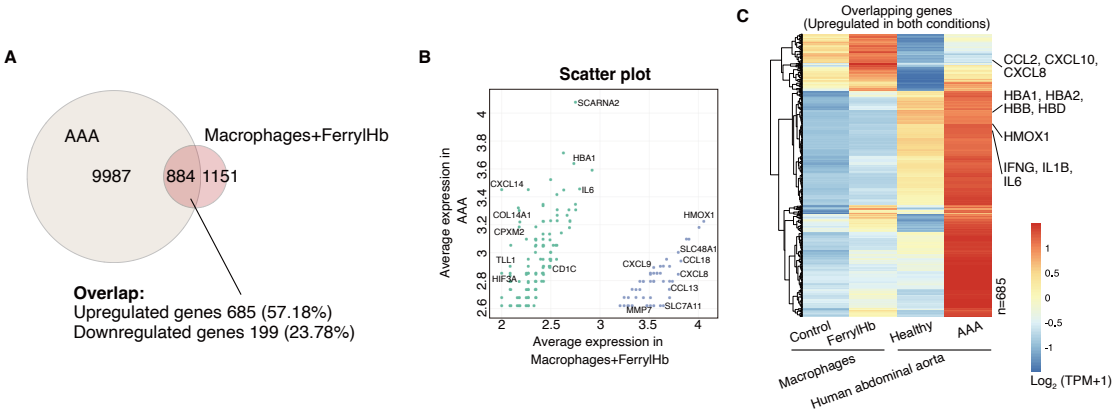

Figure 18. Comparative analysis of human abdominal aortic aneurysms versus human macrophages exposed to ferryl hemoglobin.

(A) *Venn diagram showing the overlap of DEGs between human AAA versus healthy aortic tissues (yellow) and macrophages exposed to ferrylHb for 8 hours (red).* ***(B)*** *Scatter plot illustrating shared DEGs between AAA and ferrylHb-treated macrophages. The Y-axis represents DEGs from AAA versus healthy tissue, and the X-axis represents DEGs from ferrylHb-treated versus control macrophages. Genes with |logFC| > 2 were considered significant; the most highly regulated genes are labeled.* ***(C)*** *Heatmap of 685 upregulated overlapping DEGs identified. Expression values are represented as log2(TPM+1).*

To investigate the molecular impact of ferrylHb on macrophages in greater detail, and to better understand its potential involvement in the pathophysiology of AAA, we carried out a systematic comparative transcriptomic analysis. DEGs were obtained from human AAA biopsy specimens as well as from *in vitro* experiments in which primary human macrophages were exposed to ferrylHb for 8 hours. Cross-comparison of the two transcriptomic datasets uncovered a striking and biologically relevant overlap in DEGs. Specifically, a total of 884 DEGs were shared between the two cohorts, among which 685 genes showed upregulated expression and 199 genes exhibited downregulated expression (Figure 18A). This notable overlap accounted for 57.18% of the upregulated transcripts and 23.78% of the downregulated transcripts identified in

ferrylHb-treated macrophages. These proportional distributions strongly indicate that ferrylHb may serve as a core driver of the transcriptional reprogramming events observed in aneurysmal tissue specimens. The above findings imply that the cellular response triggered by ferrylHb stimulation in macrophages recapitulates, to a considerable extent, the molecular alterations detected in clinical human AAA samples. In depth analysis of these overlapping DEGs further identified a cohort of genes with well-documented functions in vascular pathological processes and immune regulatory networks. For instance, transcripts encoding oxidative stress-responsive enzymes, including HMOX1 and hemoglobin subunit alpha 1 (HBA1), displayed consistent upregulation across both datasets, which points to redox homeostasis imbalance and heme-mediated cellular stress as prominent molecular characteristics of AAA (Figure 18B). Concurrently, canonical pro-inflammatory mediators such as IL6, CCL8, and CCL9 were found to be robustly upregulated in the overlapping gene set, underscoring the capacity of ferrylHb to potentiate macrophage-initiated inflammatory cascades. Furthermore, multiple members of the MMP family, which are pivotal effectors of ECM degradation and vascular structural remodeling, were also enriched among the overlapping DEGs. This enrichment establishes a direct molecular link between ferrylHb exposure and the pathological processes that undermine aortic wall structural integrity.

To provide a broader view of the shared transcriptional response, we generated a heatmap using the 685 consistently upregulated DEGs (Figure 18C). This visualization revealed striking similarities in the expression patterns between ferrylHb-treated

macrophages and AAA tissues. Genes related to inflammatory signaling pathways, such as IFNG, IL1B, IL6, CCL2, CXCL10, and CXCL8, were among the most prominently induced, indicating an activated immune phenotype. Likewise, iron metabolism-related genes, including HMOX1, HBA1, HBA2, HBB, and HBD, showed robust induction in both contexts, providing further support for a mechanistic link between ferrylHb-mediated oxidative stress, heme metabolism, and the immune-inflammatory environment characteristic of AAA.

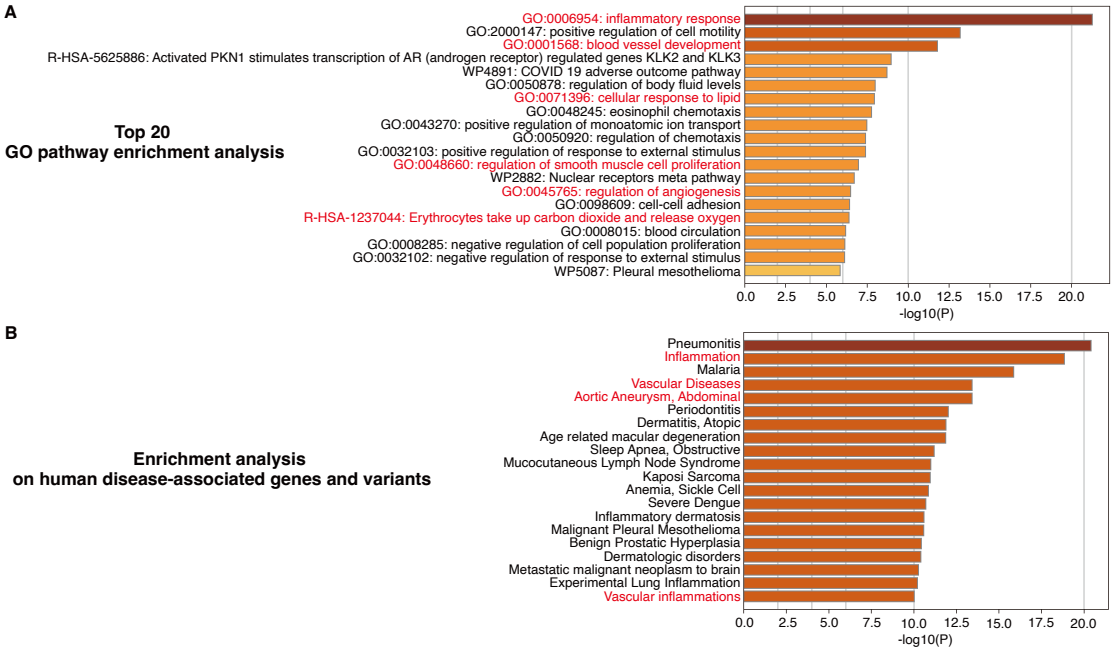

Figure 19. Gene Ontology and disease enrichment analyses reveal ferryl hemoglobin-driven transcriptomic signatures relevant to vascular injury and abdominal aortic aneurysm.

(A) *The visualization presents the top 20 enriched biological process terms. Classification of functionally related terms was carried out on the basis of kappa similarity coefficients exceeding 0.3, and the term with the strongest statistical significance within each cluster was selected as the representative label. For inclusion in the final analysis, terms were required to meet three criteria: P value < 0.01, enrichment factor > 1.5, and association with no fewer than 3 genes.* ***(B)*** *The most prominently associated disease terms are exhibited in the plot, with ranking determined by the value of -log10 (P-value) and grouping performed according to semantic similarity. Statistical significance was defined by an adjusted P value < 0.05, and only terms satisfying this threshold were included in the results.*

Beyond descriptive comparisons, functional enrichment analyses were performed to further interpret the biological significance of these overlapping DEGs. GO enrichment highlighted multiple biological processes of relevance, most prominently those associated with inflammatory responses, blood vessel development, vascular remodeling, and angiogenesis (Figure 19A and Table 5). These results not only reinforce the observed upregulation of inflammatory cytokines and chemokines but also connect ferrylHb exposure to pathways that regulate vascular homeostasis and structural integrity, both of which are central to aneurysm progression.

Table 5. Top 20 clusters together with their representative enriched terms

GO	Category	Description	Count	%	Log10(*P*)	Log10(q)
GO:0006954	GO Biological Processes	inflammatory response	66	8.49	-21.27	-16.93
GO:2000147	GO Biological Processes	positive regulation of cell motility	53	6.82	-13.19	-10.02
GO:0001568	GO Biological Processes	blood vessel development	46	5.92	-11.80	-8.87
R-HSA-5625886	Reactome Gene Sets	Activated PKN1 stimulates transcription of AR (androgen receptor) regulated genes KLK2 and KLK3	14	1.80	-8.96	-6.20
WP4891	WikiPathways	COVID 19 adverse	8	1.03	-8.71	-5.99

		outcome pathway				
GO:0050878	GO Biological Processes	regulation of body fluid levels	31	3.99	-7.98	-5.32
GO:0071396	GO Biological Processes	cellular response to lipid	41	5.28	-7.93	-5.28
GO:0048245	GO Biological Processes	eosinophil chemotaxis	8	1.03	-7.76	-5.17
GO:0043270	GO Biological Processes	positive regulation of monoatomic ion transport	21	2.70	-7.47	-4.94
GO:0050920	GO Biological Processes	regulation of chemotaxis	22	2.83	-7.39	-4.88
GO:0032103	GO Biological Processes	positive regulation of response to external stimulus	42	5.41	-7.39	-4.88
GO:0048660	GO Biological Processes	regulation of smooth muscle cell proliferation	19	2.45	-6.96	-4.51
WP2882	WikiPathways	Nuclear receptors meta pathway	26	3.35	-6.70	-4.27
GO:0045765	GO Biological Processes	regulation of angiogenesis	28	3.60	-6.48	-4.07
GO:0098609	GO Biological Processes	cell-cell adhesion	36	4.63	-6.41	-4.01

R-HSA-1237044	Reactome Gene Sets	Erythrocytes take up carbon dioxide and release oxygen	6	0.77	-6.38	-3.99
GO:0008015	GO Biological Processes	blood circulation	31	3.99	-6.17	-3.84
GO:0008285	GO Biological Processes	negative regulation of cell population proliferation	45	5.79	-6.13	-3.81
GO:0032102	GO Biological Processes	negative regulation of response to external stimulus	31	3.99	-6.10	-3.79
WP5087	WikiPathways	Pleural mesothelioma	30	3.86	-5.84	-3.58

In the GO enrichment analysis of overlapping DEGs from AAA versus healthy aorta and ferrylHb-treated macrophages versus control, all annotated genes in the genome were used as background. For each term, "Count" indicates the number of input genes associated with that ontology, "%" refers to the proportion of input genes mapped to the term, "Log10(P)" represents the P-value (calculated by cumulative hypergeometric distribution), and "Log10(q)" denotes the Benjamini-Hochberg adjusted P-value (132). Enriched terms were selected based on $P < 0.01$, enrichment factor > 1.5 (ratio of observed to expected counts), and a minimum of three genes. To reduce redundancy, terms were hierarchically clustered using kappa statistics as a similarity metric, with sub-trees showing similarity > 0.3 merged into clusters. The most significant term within each cluster was chosen as its representative.

To complement GO analysis, we performed disease enrichment analysis using the DisGeNET database (133) via the Metascape platform (134). This analytical strategy uncovered significant correlations between the overlapping DEGs and human disorders defined by vascular damage and chronic inflammatory responses. Notably, robust enrichment signals were observed for AAA itself, along with associated pathological conditions including vascular inflammation and arteriosclerotic lesions (Figure 19B

and Table 6). These results furnish independent evidence confirming that the transcriptomic program driven by ferrylHb possesses high relevance to the pathological mechanisms of AAA.

Table 6. Summary of enrichment analysis in Disease Gene Network (133)

GO	Description	Count	%	Log10(*P*)	Log10(q)
C3714636	Pneumonitis	68	8.80	-20.00	-16.00
C0021368	Inflammation	53	6.80	-19.00	-15.00
C0024530	Malaria	60	7.70	-16.00	-12.00
C0042373	Vascular Diseases	56	7.20	-13.00	-10.00
C0162871	Aortic Aneurysm, Abdominal	51	6.60	-13.00	-10.00
C0031099	Periodontitis	53	6.80	-12.00	-8.70
C0011615	Dermatitis, Atopic	56	7.20	-12.00	-8.60
C0242383	Age related macular degeneration	53	6.80	-12.00	-8.60
C0520679	Sleep Apnea, Obstructive	42	5.40	-11.00	-8.00
C0026691	Mucocutaneous Lymph Node Syndrome	36	4.60	-11.00	-7.80
C0036220	Kaposi Sarcoma	42	5.40	-11.00	-7.80
C0002895	Anemia, Sickle Cell	39	5.00	-11.00	-7.70
C0019100	Severe Dengue	20	2.60	-11.00	-7.60

C3875321	Inflammatory dermatosis	36	4.60	-11.00	-7.50
C0812413	Malignant Pleural Mesothelioma	38	4.90	-11.00	-7.50
C1704272	Benign Prostatic Hyperplasia	54	6.90	-10.00	-7.40
C0037274	Dermatologic disorders	47	6.00	-10.00	-7.40
C0220650	Metastatic malignant neoplasm to brain	36	4.60	-10.00	-7.30
C0887898	Experimental Lung Inflammation	14	1.80	-10.00	-7.30
C0947751	Vascular inflammations	31	4.00	-10.00	-7.10

Finally, to further clarify the associations among enriched functional categories and intuitively visualize the global network architecture underlying the ferrylHb driven response, we constructed a network plot with the use of Cytoscape 5. In this graphical representation, each node stood for an enriched term, whereas the edges reflected the functional relatedness between these terms. Nodes were color coded either according to their cluster identity (Figure 20A) or based on their statistical significance (Figure 20B). This analysis uncovered interconnected pathway modules, with inflammatory signaling, oxidative stress response, and vascular remodeling emerging as core network hubs. These findings thus highlight ferrylHb as a pivotal upstream regulator that orchestrates multiple pathological cascades relevant to the progression of AAA.

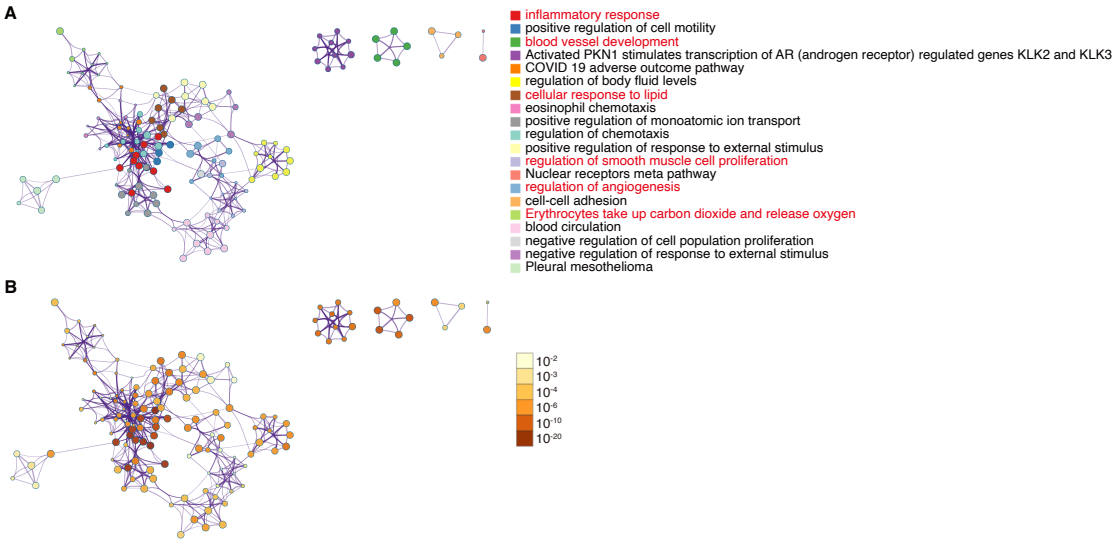

Figure 20. Network of enriched terms linking human abdominal aortic aneurysms and human macrophages treated with ferryl hemoglobin.

*(**A**) Colored by cluster ID, where nodes that share the same cluster ID are typically close to each other; (**B**) colored by P-value, where terms containing more genes tend to have a more significant P-value.*

3.9 Transcriptomic signatures of ruptured murine aneurysms mirror those detected in human hemorrhagic aneurysms.

To comprehensively delineate the molecular landscape associated with aneurysm rupture and hemorrhage *in vivo*, we performed bulk RNA-seq analysis on abdominal aortic tissues obtained from ApoE$^{-/-}$ mice subjected to HFD+AngII, STD+AngII, HFD+Saline, and STD+Saline (healthy controls). Despite the inherent genetic variability typically observed in human samples, the transcriptomic profiles of the HFD+AngII and STD+AngII groups clustered distinctly and consistently among biological replicates compared to healthy controls (Figure 21A), demonstrating the robustness and reproducibility of the AngII-induced AAA mouse model in capturing relevant pathophysiological signatures.

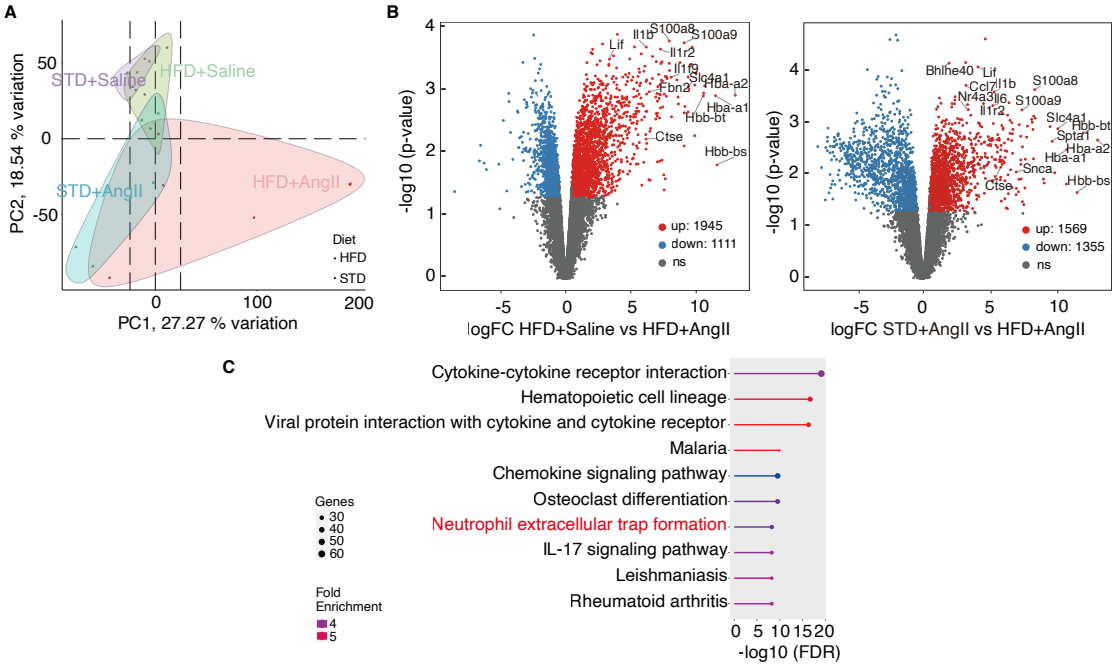

Figure 21. Distinct transcriptomic signatures in mouse aortic tissues.

(A) *The plot presents transcriptomic data derived from mouse arterial tissues across four distinct experimental cohorts: STD+Saline (n = 5, purple), STD+AngII (n = 5, blue), HFD+Saline (n = 5, green) and HFD+AngII (n = 5, pink). Principal components were computed via unit variance scaling combined with SVD coupled with imputation. Among the extracted components, PC1 accounted for 27.27% of total variance, while PC2 explained 18.54% of variance across the dataset.* ***(B)*** *Two comparison pairs were analyzed: HFD+Saline versus HFD+AngII, and STD+AngII versus HFD+AngII. In the plots, red dots stand for significantly upregulated genes, blue dots represent markedly downregulated genes, and gray dots denote genes without differential expression between the compared groups.* ***(C)*** *The diagram displays the top 10 enriched biological pathways, which were ranked according to the value of -log10 (FDR).*

Pairwise comparisons were conducted to identify DEGs reflective of aneurysm severity and rupture risk under hyperlipidemic and hypertensive conditions. The comparison between HFD+Saline and HFD+AngII groups identified 3,056 DEGs, with 1,945 genes upregulated and 1,111 genes downregulated (Figure 21B), indicating the profound transcriptomic remodeling associated with AngII infusion in the context of hyperlipidemia. Similarly, the comparison between STD+AngII and HFD+AngII tissues revealed 2,924 DEGs (1,569 upregulated, 1,355 downregulated), further

highlighting the exacerbating impact of dietary hyperlipidemia on aneurysm transcriptomes.

Among the top-ranked DEGs, those linked to neutrophil biological functions (S100A8, S100A9), core inflammatory cytokines (IL6, IL1β, CCL7, IL1R2), and hemoglobin family members (HBA-A1, HBA-A2, HBB-BT, HBB-BS) exhibited significant expression perturbations in AngII-treated experimental groups. This expression dysregulation was particularly pronounced in the HFD+AngII cohort, a pattern that aligns well with the molecular signatures detected in clinical samples of human hemorrhagic AAA. These genes are well documented to modulate neutrophil activation, chemotactic migration, inflammatory cascade amplification, and iron metabolic processes within the aneurysmal microenvironment, which corresponds precisely to the mechanistic pathways previously delineated in our human derived datasets.

To further decipher the biological implications of these DEGs, we conducted an unbiased GO enrichment analysis. The results revealed robust enrichment in functional pathways including “NET formation”, “Inflammatory Response”, “Iron Ion Homeostasis”, and “Response to Oxidative Stress” (Figure 21C). These enrichment profiles mirror the pathway activation signatures observed in human hemorrhagic AAA tissue specimens.

To evaluate alterations in cellular composition within aneurysmal lesions, we employed Granulator to perform deconvolution analysis on bulk RNA-seq datasets. The analysis results demonstrated that neutrophils constituted the most abundant cell population within the aneurysmal tissues (Figure 22). This finding underscores the pivotal

contribution of neutrophil-driven inflammatory responses and NET formation to the progression and rupture of AAA.

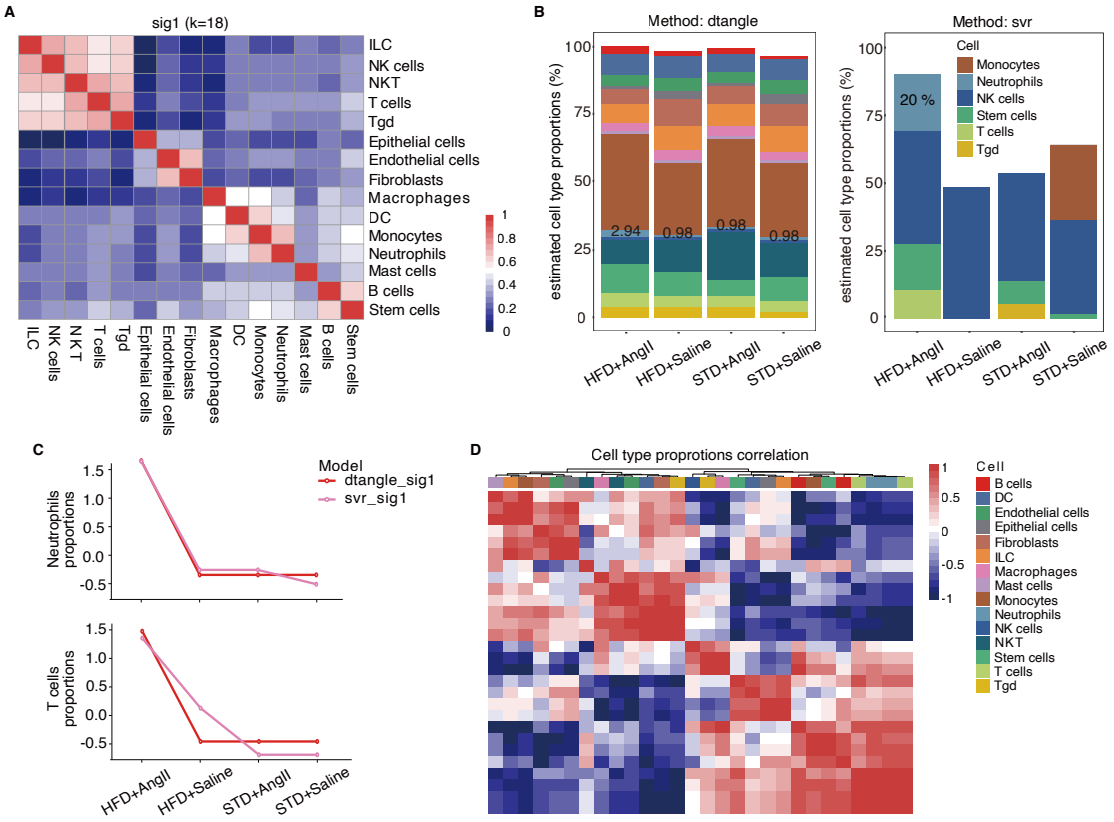

Figure 22. Cell composition matrix and cell types in RNA-seq mouse abdominal aortic aneurysms.

(A) *Cell-type similarity matrix of all reference profiles based on Kendall Rank Correlation Coefficient, highlighting transcriptionally related clusters. Condition number (k) was used to evaluate the stability of the reference matrix.* ***(B)*** *Estimated cell-type coefficients and proportions (percentage) were inferred from bulk RNA-seq using two prediction models (dtangle and SVR).* ***(C)*** *Deconvolution of bulk RNA-seq data showing the relative abundance of individual cell types within the mixed aortic tissue population.* ***(D)*** *Correlation heatmap of estimated cell-type proportions across different deconvolution methods, clustered by collinearity of cell type and model.*

Finally, a targeted evaluation of gene expression signatures related to neutrophil activation, pro-inflammatory signaling, iron metabolism, calcification, and apoptosis revealed that the HFD+AngII group exhibited markedly higher levels of these signatures compared to the STD+AngII and control groups (Figure 23). This pattern

supports the notion that diet-induced hyperlipidemia synergizes with AngII-mediated hypertension to exacerbate inflammation, oxidative stress, and iron dysregulation within the aneurysmal wall, thereby increasing the likelihood of rupture.

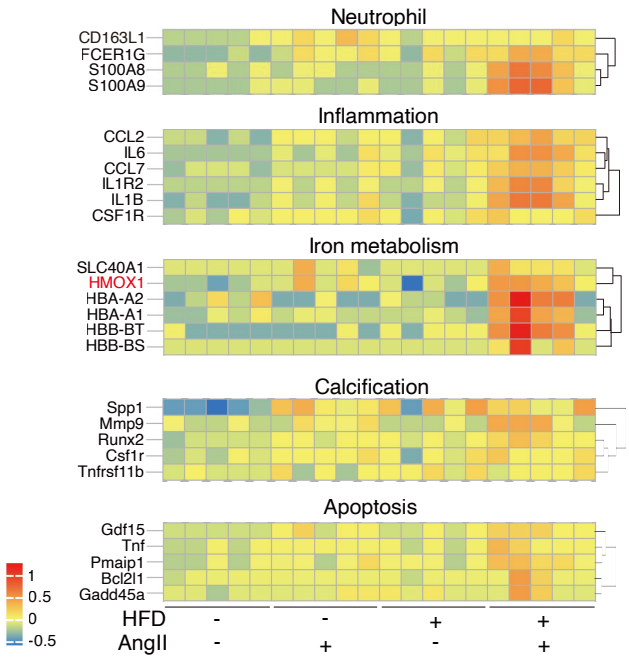

Figure 23. Enriched neutrophil, inflammatory, iron metabolism, calcification, and apoptosis pathways in mouse aortic tissues.

Heatmap of gene markers related to neutrophil activity, inflammation, iron metabolism, calcification, and apoptosis across the four experimental groups.

3.10 Neutrophils exhibit transcriptional activity upon ferryl hemoglobin stimulation, upregulation of genes linked to macrophage recruitment

To elucidate the potential mechanistic link between ferrylHb uptake by neutrophils in aneurysmal tissues and the transcriptomic changes observed at the tissue level, we conducted bulk RNA-Seq analysis on primary human neutrophils exposed to ferrylHb or Hb for 4 hours (Figure 24A). This approach aimed to determine whether ferrylHb

could elicit a distinct transcriptional program in neutrophils, thereby contributing to the inflammatory microenvironment characteristic of AAA.

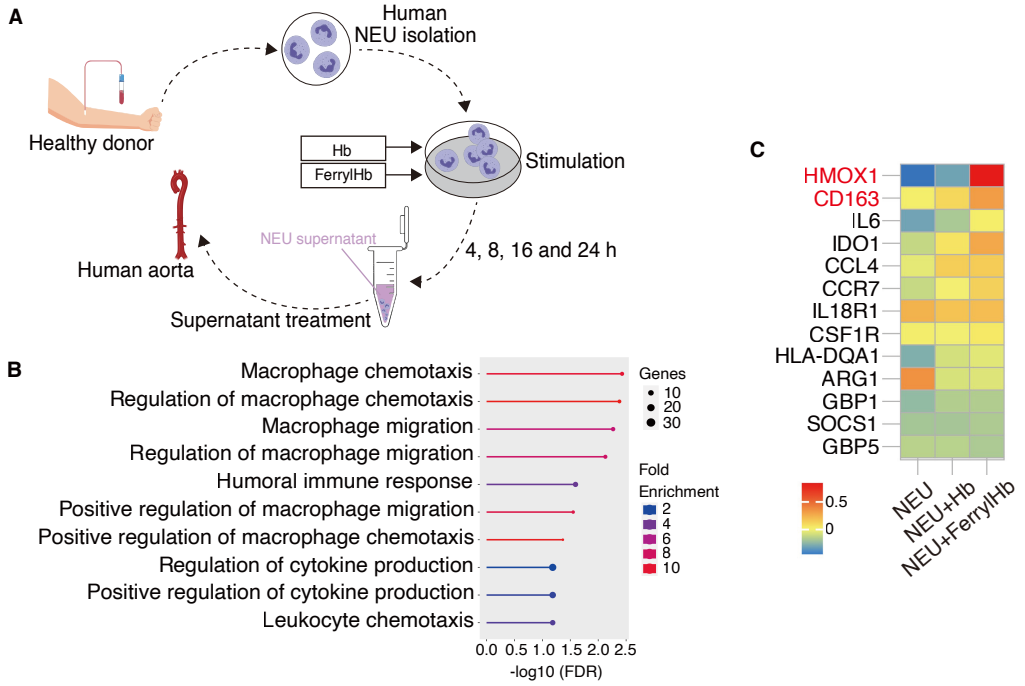

Figure 24. Neutrophils activated by ferryl hemoglobin exhibit a time dependent response, upregulation of genes associated with the recruitment of macrophages.

(A) *Human NEUs were purified from peripheral blood samples of healthy volunteer donors, then subjected to treatment with 10 µmol/l Hb or ferrylHb, followed by incubation periods of 4, 8, 16, or 24 hours. RNA-seq profiling was implemented on the NEU samples after 4 hours of incubation. For assessing the influence of neutrophil-secreted elastase on vascular ECM components, cell culture supernatants were incubated with sections of human aortic tissues overnight, prior to the subsequent evaluation of elastin structural integrity.* ***(B)*** *Analyses were conducted on DEGs identified in NEUs exposed to Hb or ferrylHb, with five biological replicates assigned to each experimental group (n = 5).* ***(C)*** *The heatmap displays expression patterns of DEGs linked to macrophage-associated signaling pathways, and four biological replicates were included in each group (n = 4).*

Gene set enrichment analysis and GO network enrichment analysis (Figure 24B and 24C) demonstrated that neutrophils exposed to ferrylHb exhibited robust transcriptional activity, which stands in sharp contrast to the conventional view that neutrophils are transcriptionally quiescent terminal effector cells. Pathways with elevated expression

in ferrylHb treated neutrophils encompassed inflammatory signal transduction, oxidative stress response, and iron ion homeostasis, a transcriptional profile that aligns well with the molecular signatures identified in human and murine aneurysmal tissue specimens.

Notably, GO enrichment analysis also identified a series of pathways associated with macrophage chemotaxis and migration, including “Macrophage Chemotaxis”, “Regulation of Monocyte Chemotaxis”, and “Positive Regulation of Macrophage Migration”. These findings imply that ferrylHb activated neutrophils may actively participate in the recruitment of macrophages within the aneurysmal microenvironment, thereby amplifying local inflammatory cascades and accelerating the progression and rupture of abdominal aortic aneurysms.

In addition, several top GO terms were related to cellular uptake and secretion processes, such as “Macrophage Phagocytosis” and “Regulation of Endocytosis”, highlighting the interplay between neutrophil activation and the subsequent recruitment and activation of macrophages. These processes are central to the clearance of oxidized Hb species and cellular debris during intramural hemorrhage, linking ferrylHb-driven neutrophil activation to downstream macrophage-mediated effector functions in AAA pathology.

A detailed analysis of DEGs between control and ferrylHb-treated neutrophils revealed the upregulation of several chemokines and cytokines, including CCL4, CCR7, IL18R1, and IL6, all of which are known to facilitate macrophage recruitment and activation within inflamed vascular tissues. Notably, many of these inflammatory genes have previously been reported to be elevated in human aneurysm tissues and are key

mediators of the inflammatory microenvironment driving AAA progression (Supplemental Figure 2).

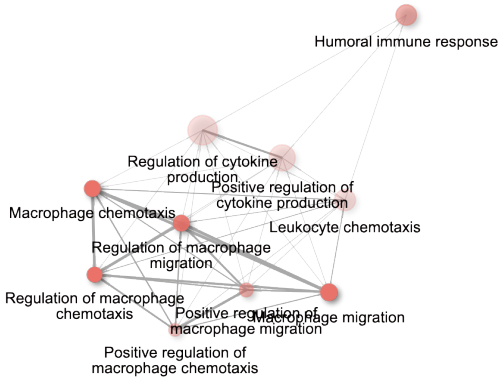

Supplemental Figure 2. Gene Ontology network illustrate differentially expressed genes enriched in neutrophils treated by hemoglobin or ferryl hemoglobin.

3.11 Neutrophil activation takes place in response to ferryl hemoglobin.

To further confirm the activation of neutrophils in response to ferrylHb exposure, we quantified the release of MPO and NE, two key markers of neutrophil degranulation and activation, following a 24-hour incubation with ferrylHb or Hb.

As shown in Figure 25A, ferrylHb stimulation led to a robust increase in extracellular MPO levels, indicating significant degranulation and activation of neutrophils. Although exposure to Hb for 24 hours also elevated MPO release compared to the control group, the magnitude was notably lower than that observed with ferrylHb treatment. In contrast, no detectable levels of extracellular MPO were found in untreated neutrophils, confirming that the observed activation was specific to Hb exposure.

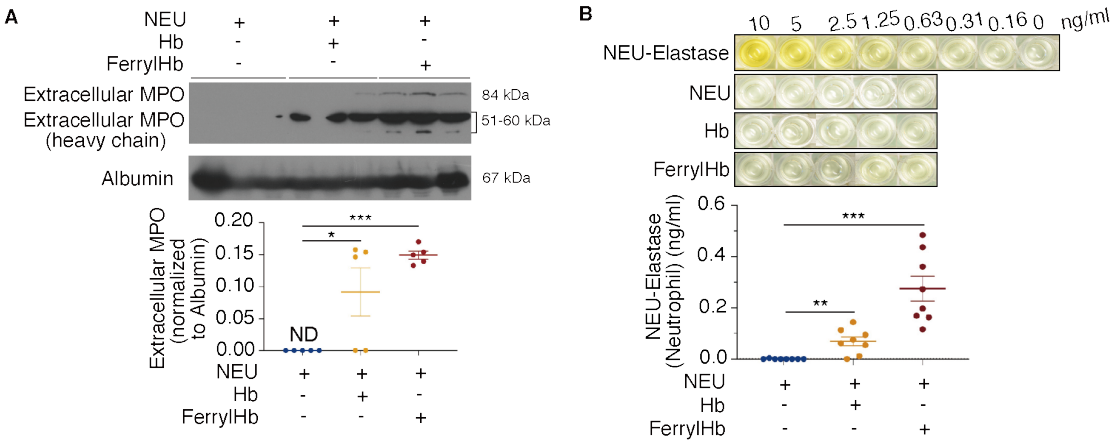

Figure 25. Neutrophils stimulated by ferryl hemoglobin display a time-dependent response, releasing elastase and myeloperoxidase.

(A) *Extracellular MPO and MPO heavy chain were detected in supernatants by Western blot; albumin served as loading control. Quantification is shown as mean ± SEM (n = 5/group).* $^{*}P < 0.05$; $^{***}P < 0.001$; *unpaired t-test. ND, not detected.* ***(B)*** *NEU elastase release quantified by ELISA; concentrations expressed as ng/ml (n = 8/group).* $^{**}P < 0.01$; $^{***}P < 0.001$; *unpaired t-test.*

Similarly, analysis of NE release revealed a significant induction following exposure to both ferrylHb and Hb (Figure 25B). However, ferrylHb exposure resulted in a nearly threefold increase in extracellular elastase concentration compared to native Hb, underscoring the superior pro-inflammatory and activating potential of ferrylHb on neutrophils.

Given previous reports suggesting that neutrophils possess the capacity to oxidize Hb in the extracellular environment (135, 136), we next examined whether Hb oxidation occurred during the 24-hour incubation period in the presence of neutrophils. Spectral profiling verified that ferrylHb constituted 16.26% of the total Hb pool following 24 hours of co-incubation with neutrophils (Figure 26A and B). This result demonstrates that neutrophils are capable of promoting the oxidation of Hb to its ferryl form during extended periods of interaction.

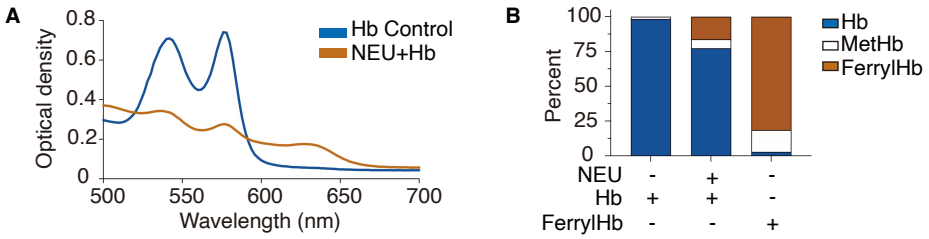

Figure 26. Relative proportions of hemoglobin redox states.

***(A** and **B)** Relative proportions of Hb redox states determined by visible spectrum analysis, expressed as percentage of total heme.*

Collectively, these findings illustrate that ferrylHb acts as a potent activator of neutrophils, triggering the secretion of MPO and elastase. Simultaneously, it maintains its oxidized ferryl state when in the presence of neutrophils, thereby perpetuating an oxidative and inflammatory microenvironment within aneurysmal lesions.

3.12 Neutrophil-released elastase aggravates human aortic elastin degradation

To evaluate the functional consequences of neutrophil activation by ferrylHb on vascular tissue integrity, supernatants from neutrophils stimulated with ferrylHb were applied to human aortic tissue sections and incubated overnight at room temperature. Elastin degradation was assessed by EVG staining, where elastin fibers are visualized as dark purple structures.

As expected, positive control artery segments treated with purified elastase (2 units/ml) exhibited pronounced elastin degradation compared to untreated negative control segments, which displayed well-preserved elastic fibers (Figure 27A). Similarly, tissue incubated with supernatants from unstimulated neutrophils showed intact and well-organized elastic fibers throughout the aortic wall.

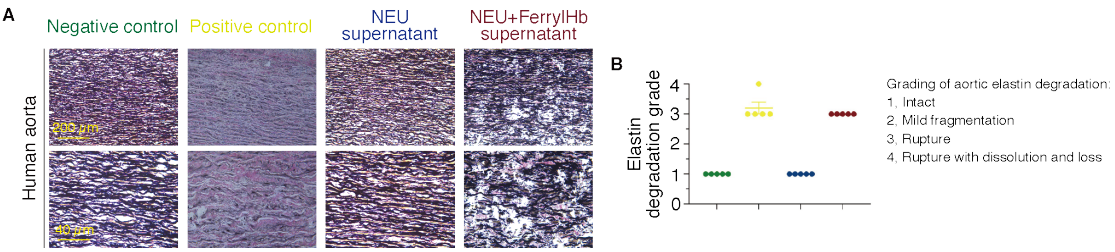

Figure 27. Ferryl hemoglobin activated neutrophils display a time-dependent reaction, intensifying the degradation of aortic elastin.

(A) *Human aortic tissue sections were incubated with four conditions: negative control (DMEM), positive control (elastase, 2 U/ml), NEU supernatant, and ferrylHb-treated NEU supernatant.* ***(B)*** *The structural state of elastin was examined through EVG staining, and the staining results were assigned a four-level scoring standard as follows: grade 1 denotes intact elastin architecture; grade 2 corresponds to slight elastin fragmentation; grade 3 indicates the occurrence of elastin rupture; grade 4 represents elastin rupture accompanied by tissue dissolution and fiber loss.*

In contrast, incubation with supernatants from ferrylHb-stimulated neutrophils resulted in extensive fragmentation of elastin fibers throughout the vessel wall, indicative of enhanced elastolytic activity. Quantitative grading of elastin degradation confirmed a significant increase in elastin breakdown following treatment with ferrylHb-activated neutrophil supernatants compared to both negative controls and unstimulated neutrophil groups (Figure 27B).

These findings highlight the pathophysiological relevance of NE release triggered by ferrylHb in promoting elastin degradation, a critical event contributing to the weakening of the aortic wall in AAA.

3.13 Hemoglobin elicits NETosis, a program mediating the generation of neutrophil extracellular traps

Exposure of neutrophils to ferrylHb for 4 hours triggered a pronounced transcriptional response, and a subset of neutrophils treated with either ferrylHb or Hb for prolonged periods (16-24 hours) underwent cell death, as shown in Supplemental Figure 3. Given

that NETosis has been previously observed in human AAA tissues (64, 75) and we detected NET formation in our mouse model of hemorrhaged AAA, we investigated whether Hb itself can induce NETosis.

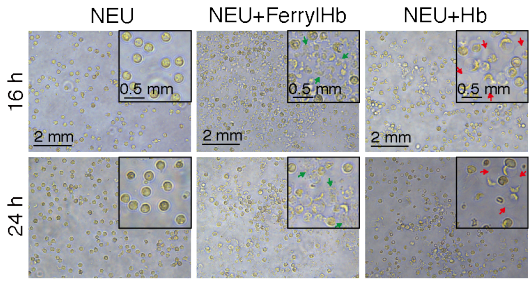

Supplemental Figure 3. Representative images of neutrophils.

Representative images of neutrophils, obtained from 5 independent experiments/donors, are shown at 16 and 24 hours. Green arrows denote dead cells, while red arrows indicate lipid deposits.

As illustrated in Figure 28A, treatment with both ferrylHb and Hb induced the release of NETs into the extracellular space, comparable to the well-established neutrophil activator PMA (137-139). Using STED nanoscopy, extracellular DNA, MPO, and ferrylHb were found to co-localize within NET structures.

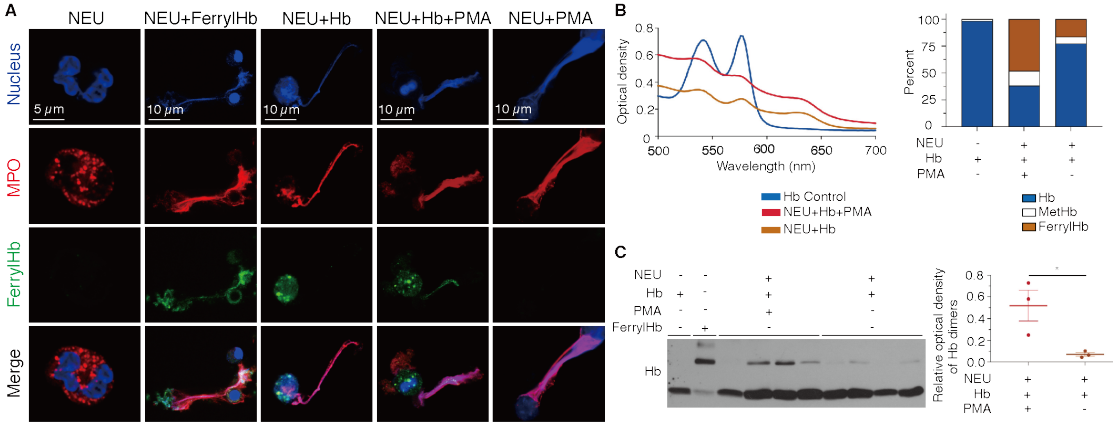

Figure 28. Internalization of ferryl hemoglobin by neutrophils leads to NETosis.

(A) *Human NEUs from healthy donors were exposed to PMA, PMA+Hb, Hb, or ferrylHb and visualized by confocal microscopy. DNA was labeled with Hoechst (blue), MPO with Alexa Fluor 647 (red), and ferrylHb with Alexa Fluor 488 (green). Representative images are shown.* ***(B)*** *Spectral analysis of Hb oxidation states*

expressed as relative percentages. ***(C)*** *Detection of intracellular Hb and ferrylHb in NEUs by Western blot (n = 4). Quantification is presented.*

Importantly, ferrylHb was detected not only in neutrophils stimulated directly with ferrylHb but also in those treated with Hb alone or in combination with PMA, indicating that Hb undergoes oxidation to ferrylHb during NETosis induction. This was further corroborated by spectrophotometric measurements and Western blot analyses (Figure 28B and C), which confirmed the generation of ferrylHb by neutrophils after 24 hours of Hb exposure, even in the absence of PMA.

3.14 Peptidylarginine deiminase 4 inhibition attenuates ferryl hemoglobin - induced NETosis while preserving intracellular activation

To further clarify the regulatory mechanisms governing ferrylHb-triggered NET formation (NETosis), we explored the function of PAD4. This enzyme acts as a key mediator of histone citrullination and chromatin decondensation, two indispensable processes that enable the release of NETs (140, 141). By utilizing GSK484, a highly selective inhibitor targeting PAD4, we assessed whether blocking PAD4 activity could alleviate ferrylHb-induced NET generation, while at the same time retaining the intracellular activation of neutrophils.

As presented in Figure 29A, results from Western blot assays demonstrated that neutrophils co-administered with ferrylHb and GSK484 exhibited a notable decrease in the extracellular release of MPO ($P = 0.0193$) when compared with cells treated with ferrylHb alone. This outcome verified the efficient suppression of NET extrusion. Notably, GSK484 intervention also led to a reduction in the expression level of CD163 ($P = 0.0911$), a change that approached statistical significance. This finding implies that

PAD4 inhibition may partially weaken the neutrophil activation and surface receptor modulation induced by ferrylHb.

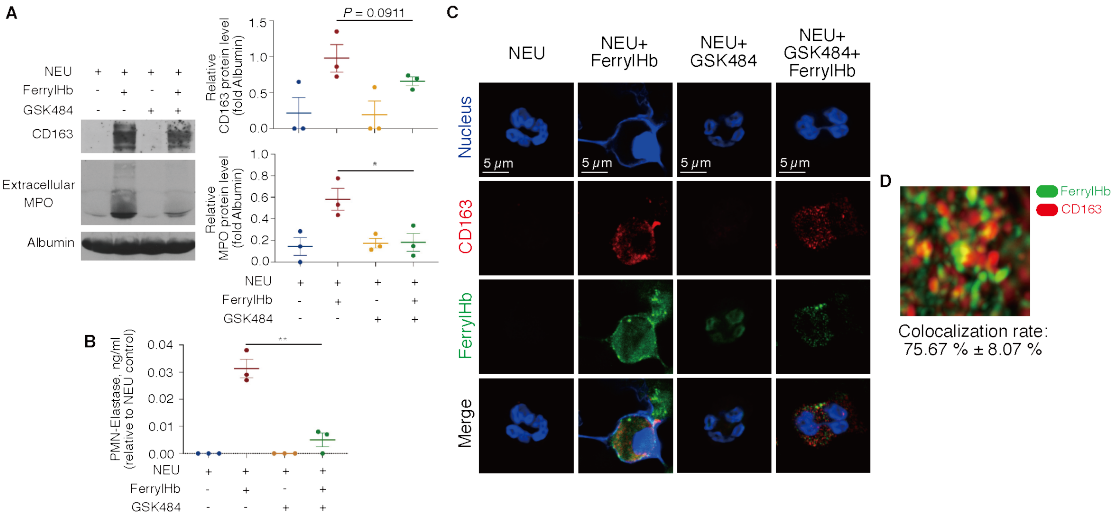

Figure 29. Peptidylarginine deiminase 4 inhibition attenuates ferryl hemoglobin - modulated neutrophil activation.

(A) *Western blot of supernatants showing CD163 and extracellular MPO, with or without PAD4 inhibitor (GSK484). Results are mean ± SEM (n = 3).* $^{*}P < 0.05$*, paired t-test.* ***(B)*** *The concentration of NEU-elastase in the samples was determined via ELISA. A microplate reader was employed to detect the absorbance value of each well at the wavelength of 450 nm, with the final NEU-elastase levels calculated and presented in the unit of ng/ml. Statistical comparisons between groups were performed using the unpaired t-test, and a significant difference was defined as* $P < 0.01$ *(with three biological replicates included per group, n = 3).* ***(C)*** *Immunofluorescence co-staining of NEUs for DNA (blue), CD163 (red), and ferrylHb (green). Scale bar, 5 μm.* ***(D)*** *Super-resolution imaging confirmed co-localization of ferrylHb and CD163 receptor. Colocalization rates are shown as mean ± SD (n = 3).*

In alignment with the above observations, immunofluorescence assays (Figure 29B) further validated the inhibitory action of GSK484 on NET formation. Neutrophils exposed to ferrylHb showed extensive extracellular DNA release, with concurrent colocalization of MPO and ferrylHb-a hallmark indicative of NET production. In contrast, the introduction of GSK484 led to a dramatic decline in the abundance of extracellular NET structures. It is important to emphasize that although NET release was inhibited, the intracellular expression of CD163 and MPO remained detectable.

This result suggests that PAD4 inhibition specifically blocks the process of chromatin extrusion, without completely abrogating the intracellular signaling pathways responsible for neutrophil activation.

Quantitative analyses revealed that the colocalization efficiency of ferrylHb with CD163 in neutrophils reached 75.67% ± 8.07% (Figure 29C), which underscores the tight spatial correlation between ferrylHb and its scavenger receptor during the activation process. This finding, combined with the reduced extracellular MPO levels and diminished NET structures, highlights a clear functional separation between PAD4-dependent NETosis and PAD4-independent intracellular activation cascades that are triggered by ferrylHb. Consistent with the data obtained from neutrophils, macrophages treated with ferrylHb displayed elevated CD163 expression in a PAD4-dependent fashion. The application of GSK484 reversed this upregulation trend, pointing to a pivotal role of PAD4 in mediating the macrophage response induced by ferrylHb (Figures 30A and 30B).

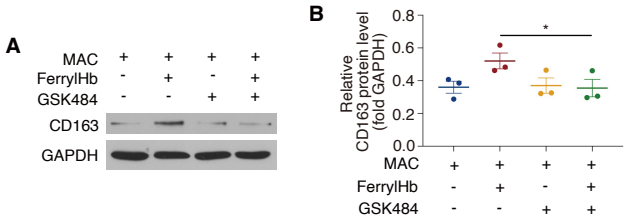

Figure 30. Peptidylarginine deiminase 4 inhibition attenuates ferryl hemoglobin - modulated macrophage activation.

(A) *CD163 expression in macrophages (MACs) analyzed by Western blot. MACs were treated with GSK484. Protein load was 20 µg/lane.* ***(B)*** *Quantification is expressed as mean ± SEM (n = 3).* $^{*}P < 0.05$*, paired t-test.*

Taken together, these results demonstrate that PAD4 serves as a core mediator of ferrylHb-induced NETosis. Pharmacological inhibition of PAD4 by GSK484 can

effectively suppress NET formation, while simultaneously preserving neutrophil viability and maintaining intracellular pro-inflammatory activation. These findings provide novel mechanistic insights into the role of PAD4 in regulating ferrylHb-driven inflammatory responses. Moreover, they support the potential of PAD4 inhibition as a promising therapeutic strategy for hemorrhagic AAA-a strategy that could limit NET-associated tissue damage while preserving the essential immune functions of neutrophils.

3.15 Heme-induced inflammatory activation in vascular endothelial and smooth muscle cells is modulated by heme oxygenase-1

Mounting research findings confirm that endothelial dysfunction acts as an early pivotal event in AAA pathogenesis, fostering inflammatory activation within the gradually degenerating arterial wall (93). Among molecular mediators linked to this process, IL1β and ICAM1 exert central effects on AAA initiation and advancement (142-145). Of note, ICAM1 expression is transcriptionally controlled by IL1β signaling cascades. Based on these insights, we explored whether heme exposure provokes inflammatory responses in vascular ECs and whether such reactions are modulated by HO-1.

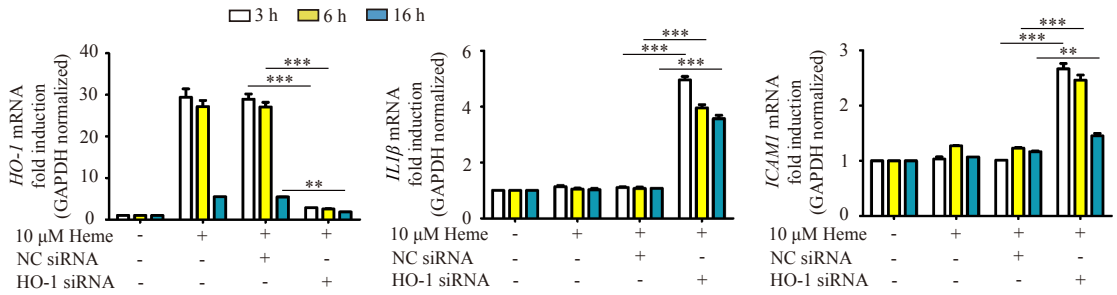

Figure 31. Heme-induced inflammatory signaling in human aortic endothelial cells is restrained by heme oxygenase-1.

HAoECs were transfected with siRNAs directed against HO-1 or with a non-targeting control siRNA. After achieving effective gene silencing, the cells were exposed to 10 μM heme for 2 hours in medium devoid of serum and antibiotics. Subsequent to this treatment phase, the culture medium was substituted with complete growth medium supplemented with 10% fetal calf serum and antimicrobial agents. Relative mRNA expression levels of HO-1, IL1β, and ICAM1 were quantified at 3, 6, and 16 hours post-heme exposure. All data are presented as mean ± SEM from three separate independent experiments (n = 3). Statistical analyses were conducted using two-way ANOVA followed by Sidak's multiple comparisons test. Significance levels are denoted as $^{*}P < 0.05$, $^{**}P < 0.01$, and $^{***}P < 0.001$.

ECs treated with 10 μM heme exhibited robust HO-1 upregulation, which aligns with the enzyme's well-documented role as a stress-inducible cytoprotective factor (Figure 31). Intriguingly, when HO-1 expression remained unimpaired, heme alone failed to induce significant changes in IL1β or ICAM1 mRNA abundances, implying effective suppression of endothelial inflammatory activation. In contrast, selective silencing of HO-1 enabled heme stimulation to markedly elevate both IL1β and ICAM1 expression. These outcomes indicate that HO-1 serves as a key endogenous inhibitor of heme-driven inflammatory signaling in ECs, thereby curbing excessive cytokine biosynthesis and adhesion molecule production during endothelial activation.

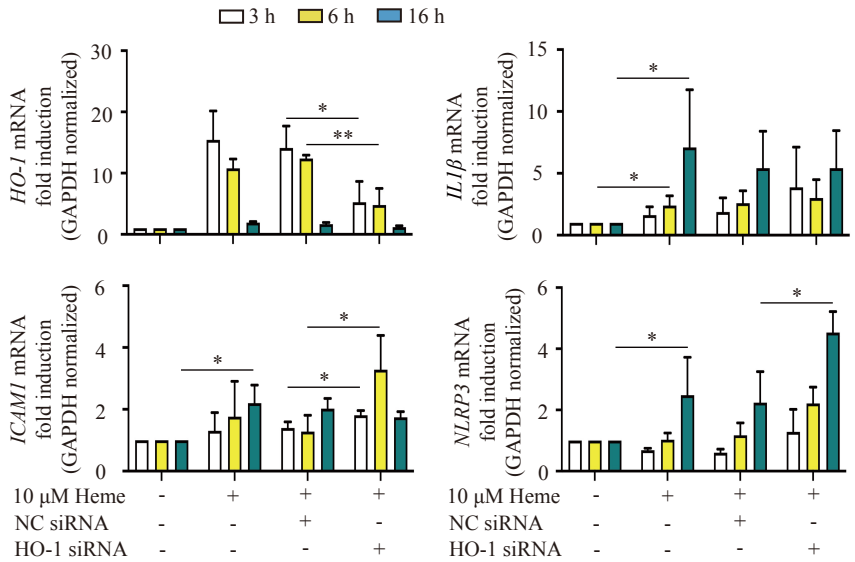

Figure 32. Heme promotes inflammasome-related inflammatory responses in human aortic smooth muscle cells under the control of heme oxygenase-1.

HAoSMCs were transfected with HO-1-targeted siRNAs or non-targeting control siRNAs prior to heme stimulation. The cells were incubated with 10 μM heme for 2 hours under conditions lacking serum and antibiotics, after which fresh growth medium supplemented with 10% fetal calf serum and antimicrobial agents was added. Relative mRNA expression levels of HO-1, IL1β, ICAM1, and NLRP3 were evaluated at 3, 6, and 16 hours following heme exposure. Experimental results are presented as mean ± SEM from three independent experiments (n = 3). Statistical significance was analyzed via two-way ANOVA combined with Sidak's post hoc multiple comparisons test. Significance levels are indicated as $^{*}P < 0.05$, $^{**}P < 0.01$, and $^{***}P < 0.001$.

SMCs displayed a distinct inflammatory response pattern compared to ECs following heme exposure. In these cells, heme treatment alone was sufficient to trigger the expression of both IL1β and ICAM1. Silencing HO-1 did not further boost IL1β mRNA levels, suggesting that IL1β induction in SMCs is governed by HO-1-independent mechanisms. Notably, heme exposure substantially increased the expression of NLRP3-a core constituent of the inflammasome complex-and this upregulation was further enhanced after HO-1 knockdown. Consistent with heightened inflammasome activation, ICAM1 expression was also elevated in heme-treated SMCs and further amplified in the absence of HO-1 (Figure 32).

Collectively, these data demonstrate that heme functions as a potent pro-inflammatory stimulus in both ECs and SMCs of the vascular wall. Importantly, the intensity and characteristics of these inflammatory responses are differentially regulated by HO-1 in a cell type-specific manner. While HO-1 exerts a strong anti-inflammatory effect in ECs by inhibiting IL1β-ICAM1 signaling cascades, its regulatory role in SMCs preferentially targets inflammasome-associated pathways. These findings underscore the critical function of HO-1 in sustaining vascular homeostasis under heme-induced stress and highlight its potential relevance in mitigating inflammation during AAA pathogenesis.

3.16 Normosang (heme arginate) alleviates the progression of abdominal aortic aneurysm in mice

To further evaluate the functional role of HO-1 in maintaining vascular integrity and mounting an adaptive response during the development of AAA, we next used a pharmacological approach to modulate HO-1 activity *in vivo*. ApoE$^{-/-}$ mice on HFD receiving AngII infusion were treated intraperitoneally with Normosang (heme arginate), a clinically used heme formulation that potently induces HO-1 expression, either alone or in combination with tin protoporphyrin IX (SnPP), a competitive inhibitor of HO-1 enzymatic activity (Figure 33A). This experimental design allowed us to distinguish between the effects of HO-1 induction per se and the consequences of blocking its catalytic function in the same pathological setting. Macroscopic inspection of the aortas showed that Normosang administration markedly attenuated aneurysm formation and substantially reduced the incidence and extent of intramural hemorrhage compared with the AngII+HFD group (Figure 33B). In contrast, concomitant treatment with SnPP almost completely abolished the protective effect of Normosang, resulting in aneurysms that were morphologically similar in size and appearance to those observed in the AngII+HFD mice without HO-1 induction.

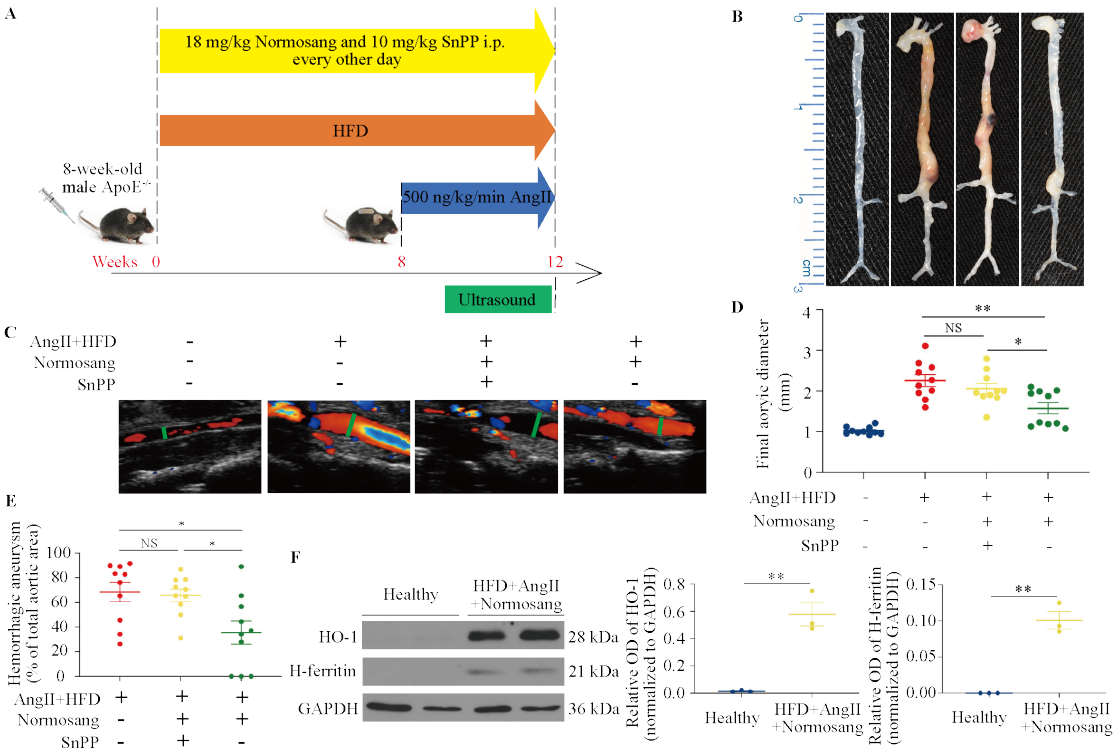

Figure 33. Normosang (heme arginate) retards the progression of angiotensin II-induced abdominal aortic aneurysm in mice via heme oxygenase-1.

(A) *Schematic representation of the experimental design showing intraperitoneal administration of the heme synthesis inhibitor Normosang and the heme degradation inhibitor SnPP in AngII+HFD-treated mice.* ***(B)*** *Representative macroscopic images of aortas from four experimental groups: Control, AngII+HFD (AAA), AngII+HFD+Normosang+SnPP, and AngII+HFD+Normosang.* ***(C)*** *Representative high-frequency ultrasound frames of aortas.* ***(D)*** *Quantification of the final aortic diameters across the four experimental groups. Maximal suprarenal abdominal aortic diameter (in mm) measured from the isolated aorta.* ***(E)*** *Quantitative comparison of the percentage of hemorrhagic aneurysms among the AngII+HFD, AngII+HFD+Normosang+SnPP, and AngII+HFD+Normosang groups. Results are shown as average value ± SEM (n = 10). Statistical significance was determined using an unpaired t-test: *P < 0.05, **P < 0.01, NS no significant.* ***(F)*** *Western blot analysis of HO-1 and H-ferritin in healthy control and AngII+HFD+Normosang-treated mice. Western blot densitometry values are shown as mean ± SEM (n = 3 per group). **P < 0.01 using unpaired t-test.*

These macroscopic findings were corroborated by high-frequency ultrasound imaging, which provided a quantitative assessment of the luminal dimensions over time. Mice treated with Normosang displayed significantly smaller abdominal aortic diameters throughout the observation period, indicating a clear suppression of aneurysmal

expansion (Figure 33C). When SnPP was co-administered, this benefit was lost and luminal diameters increased again, approaching those measured in the AngII+HFD group. Consistently, final aortic diameters at the end of the experiment were significantly reduced in the Normosang-treated mice, whereas SnPP partially or fully restored aneurysmal dilatation to control levels (Figure 33D). Quantitative analysis of lesion phenotype further revealed that the proportion of hemorrhagic aneurysms was markedly lower in the AngII+HFD+Normosang group, but this improvement was reversed by SnPP co-treatment (Figure 33E). Together, these data demonstrate that pharmacological induction of HO-1 by Normosang confers a robust macroscopic and functional protection against AAA progression and intramural bleeding, and that this protection critically depends on intact HO-1 enzymatic activity.

To clarify whether these functional effects were indeed associated with modulation of HO-1 signaling in the vascular wall, we next examined protein expression of HO-1 and its downstream iron-handling partner H-ferritin. Western blot analysis showed that Normosang treatment markedly increased vascular expression of HO-1 and H-ferritin compared with healthy controls, confirming efficient induction of the HO-1 pathway at the tissue level (Figure 33F). In agreement with these biochemical data, immunohistochemistry demonstrated strong up-regulation and broader distribution of HO-1 and H-ferritin in the aortic wall of Normosang-treated mice relative to AngII+HFD animals, whereas SnPP co-treatment blunted this response (Figure 34A). These findings support the concept that HO-1, together with H-ferritin, promotes

vascular protection by enhancing heme degradation and safe iron sequestration within the aneurysmal wall.

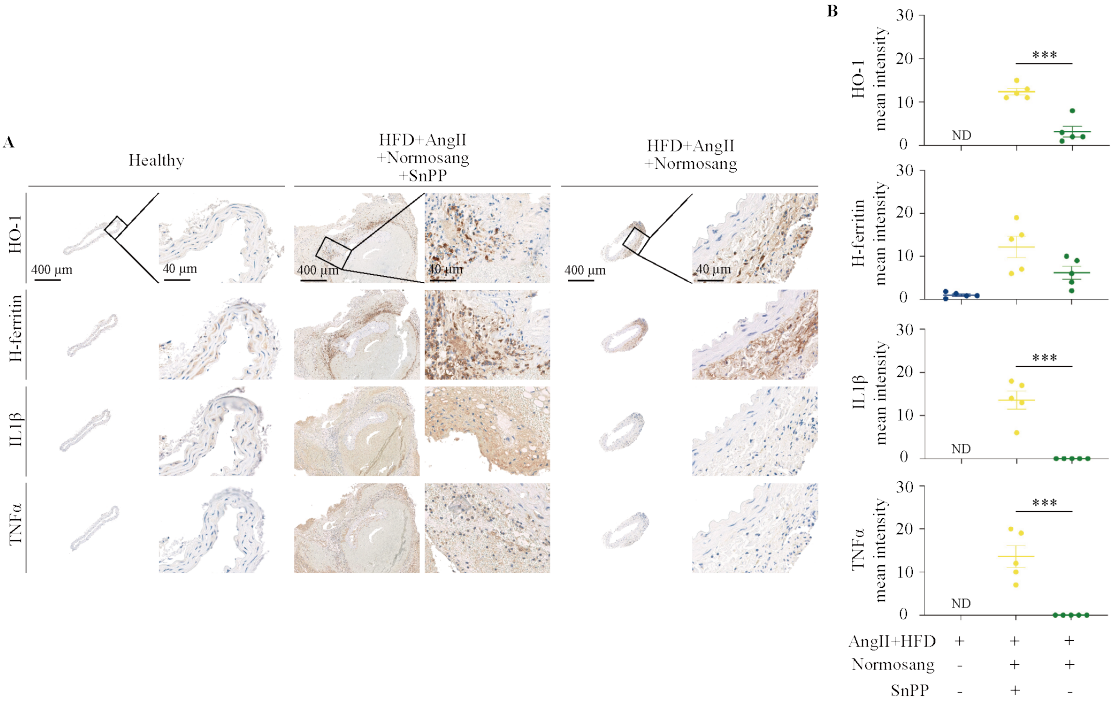

Figure 34. Normosang (heme arginate)-induced heme oxygenase-1 expression can suppress vascular wall inflammation.

***(A** and **B)** IHC analysis of HO-1, H-ferritin, IL1β and TNFα in healthy control, AngII+HFD+Normosang+SnPP-treated and AngII+HFD+Normosang-treated mice. Results are shown as average value ± SEM (n = 5). Statistical significance was determined using an unpaired t-test: ***P < 0.001, ND, not detectable.*

Finally, to link HO-1 induction to the inflammatory milieu of AAA, we evaluated the expression of pro-inflammatory cytokines in the aorta. Normosang treatment was associated with a significant reduction in IL1β and TNFα expression compared with AngII+HFD mice (Figure 34B), indicating that HO-1 induction dampens local inflammatory activation. Importantly, SnPP co-treatment abolished this anti-inflammatory effect, restoring IL1β and TNFα levels towards those seen in the AngII+HFD group, in line with the loss of structural and functional protection. Collectively, these results indicate that pharmacological induction of HO-1 by

Normosang exerts a dual protective action in AAA by stabilizing the vascular wall and suppressing inflammation, whereas inhibition of HO-1 activity with SnPP abrogates these benefits and exacerbates aneurysm severity.

4 Discussion

Hb undergoes inherent, continuous auto-oxidation, a process that generates metHb alongside superoxide anions (146-148). This oxidative cascade is drastically intensified in inflammatory microenvironments, where ROS secreted by neutrophils and macrophages further speed up Hb oxidation and amplify tissue oxidative stress (81, 82, 121).

This work represents the first investigation to confirm the presence of oxidized Hb-specifically ferrylHb-in the circulation of ruptured AAA patients undergoing open vascular surgery. This observation indicates that substantial Hb oxidation occurs during the hemorrhagic transformation of AAA lesions. Our core objectives were to identify the source of Hb oxidation in human hemorrhagic AAA, clarify the mechanisms underlying ferrylHb formation, and elucidate its cellular metabolism and contributions to AAA pathophysiology.

We detected significant ferrylHb production and accumulation in ruptured human AAA tissues, as evidenced by the presence of Hb dimers, tetramers, and multimers in lesion sites. These results align with ferryl group formation in the heme-iron moiety and the generation of protein-bound ferryl radicals, consistent with prior biochemical characterizations of ferrylHb. Integrating proteomic and mass spectrometric analyses, we observed oxidative modifications of βCys93, βCys112, and αCys104 residues in human samples-further validating transient ferrylHb species as key participants in AAA

progression and supporting their role in amplifying oxidative stress within aneurysmal walls.

The AngII-induced AAA model in $ApoE^{-/-}$ mice recapitulated key pathological features of human AAA, including Hb oxidation and intramural hemorrhage. This validation confirms the model's suitability for mechanistic investigations into ferrylHb synthesis and downstream inflammatory signaling cascades.

Immunohistochemical staining with anti-ferrylHb antibodies demonstrated that ferrylHb localizes not only extracellularly in intramural hematomas but also within neutrophils and macrophages in lesion tissues. Most ferrylHb-positive cells exhibited morphological and immunophenotypic markers (MPO^+, $NASD^+$, CPM^+) characteristic of neutrophils and macrophages, highlighting their active involvement in ferrylHb uptake and processing in hemorrhagic AAA tissues.

Unbiased genome-wide RNA sequencing analyses in human and murine AAA models showed hemorrhagic aneurysms are defined by increased neutrophil infiltration and proinflammatory transcriptional reprogramming-consistent with prior observations of neutrophil accumulation in AAA (62). Importantly, ferrylHb exposure in human monocytes induced transcriptomic changes that significantly overlapped with gene expression patterns in human AAA tissues, indicating ferrylHb may act as a key upstream regulator of inflammatory and oxidative stress pathways in aneurysmal tissues.

Given that ferrylHb accumulates extracellularly in AAA vessel walls and is subsequently internalized by neutrophils, we established an *in vitro* model using human

neutrophils exposed to ferrylHb to mimic *in vivo* conditions. Immunofluorescence and Z-Stack-STED nanoscopy revealed strong colocalization of ferrylHb with CD163 in neutrophils, and treatment with a CD163-blocking antibody drastically reduced ferrylHb internalization. These results confirm neutrophils take up ferrylHb via CD163 receptor-mediated endocytosis independent of haptoglobin, consistent with our prior findings of CD163-mediated ferrylHb uptake by macrophages in atherosclerotic lesions (82).

Following internalization, ferrylHb triggers a series of cellular responses in neutrophils, including transcriptional activation of genes involved in inflammatory reactions and macrophage recruitment-many of which are known to be upregulated in AAA tissues. Prolonged ferrylHb exposure induced neutrophil degranulation, releasing elastase and MPO to exacerbate aortic elastin degradation. Furthermore, ferrylHb stimulation induced NETosis, which further amplifies local inflammation and tissue remodeling processes.

We further demonstrated that PAD4 inhibition with GSK484 markedly reduces ferrylHb-induced NET formation while preserving intracellular activation. This highlights a PAD4-dependent mechanism that specifically mediates chromatin decondensation and NET release without impairing essential neutrophil immune functions. Decoupling NETosis from intracellular activation underscores a potential therapeutic approach to limit NET-associated tissue damage while retaining critical neutrophil-mediated host defense in AAA. Consistent with neutrophil findings, ferrylHb stimulation of macrophages induced PAD4-dependent upregulation of CD163.

Vessel wall inflammation is a core driver of AAA development, and our results identify heme as a central mediator linking oxidative stress to vascular injury. In both human AAA and AngII-induced murine AAA, Hb released from intramural hemorrhage undergoes oxidation to metHb, releasing free heme that activates ECs and SMCs, upregulates IL-1β, ICAM1, and NLRP3 expression, and amplifies local inflammatory responses. HO-1, an inducible stress protein, counteracts heme-mediated cytotoxicity by degrading heme into biliverdin, CO, and iron; ferritin then sequesters iron to limit oxidative damage. Pharmacological induction of HO-1 using heme arginate (Normosang) enhanced these protective mechanisms, increased H-ferritin expression, and reduced aneurysm formation and intramural hemorrhage. In contrast, HO-1 inhibition exacerbated inflammation and AAA severity. These results underscore the heme-HO-1 axis as a pivotal regulator of AAA pathogenesis, linking heme-induced stress to inflammation and vascular remodeling, and support HO-1 induction as a viable therapeutic strategy.

In conclusion, this study uncovers a previously unrecognized interplay between neutrophils, macrophages, and Hb in AAA pathogenesis. Intramural hemorrhage and subsequent Hb oxidation to ferrylHb drive neutrophil and macrophage activation, degranulation, elastin degradation, and NET formation-all critical processes in AAA development and progression (129-131). The presence of ferrylHb in the bloodstream of ruptured AAA patients, derived from intramural hemorrhage and Hb oxidation, highlights its potential utility as a biomarker for disease progression and rupture risk stratification.

Summary

Abdominal aortic aneurysm (AAA) exerts a profound influence on cardiovascular homeostasis via inflammation-driven pathological alterations and intramural bleeding events, which impair the structural integrity of vascular walls and elevate the risk of fatal rupture in affected individuals. In this research, oxidized hemoglobin (Hb), particularly the ferrylHb (Fe^{4+}) subtype, was detected in the peripheral circulation of patients suffering from ruptured AAA. This finding signifies the systemic spread of oxidative stress-derived byproducts, which correlate closely with the severity of the disease. The present study was designed to pinpoint the origin of Hb oxidation that leads to ferrylHb production, both in human AAA lesions complicated by hemorrhage and in an experimental AAA model induced by angiotensin II (AngII) in apolipoprotein E-deficient ($ApoE^{-/-}$) mice. Simultaneously, the research aimed to clarify the metabolic fate of ferrylHb and its corresponding pathophysiological impacts.

FerrylHb formation was confirmed within hemorrhagic AAA tissues obtained from human subjects. This process was characterized by the oxidative modification of three specific cysteine residues-βCys93, αCys104 and βCys112-located on the globin chains of Hb. Concomitantly, covalently bonded globin dimers, tetramers and higher order multimers were generated; these oligomeric complexes represent the end products of interactions between Hb, neutrophils and macrophages within the pathologically altered arterial wall. Notably, the AngII-induced AAA model in $ApoE^{-/-}$ mice recapitulated these key pathological features of human AAA, exhibiting prominent vascular wall hemorrhagic transformation and robust ferrylHb synthesis. Employing a newly

generated monoclonal antibody targeting ferrylHb for immunohistochemical assays, the study demonstrated that extracellular ferrylHb is internalized by neutrophils through a CD163 receptor-mediated endocytic pathway, thereby triggering granulocyte activation in the aortic wall microenvironment.

Upon ferrylHb uptake, neutrophils exhibited enhanced transcriptional activity skewed toward a proinflammatory phenotype. Specifically, genes associated with chemotactic signaling, cytokine biosynthesis and macrophage recruitment were markedly upregulated. Sustained exposure to ferrylHb triggered neutrophil degranulation, resulting in the release of elastase and myeloperoxidase. These proteolytic enzymes accelerate elastin degradation, which in turn contributes to the structural weakening of the aortic wall. Moreover, ferrylHb stimulation promoted the formation of neutrophil extracellular traps, a process that fosters a local microenvironment characterized by heightened inflammation and thrombogenic potential within the aneurysmal tissue.

Transcriptomic profiling via RNA sequencing was performed on human AAA tissues, with healthy aortic tissues serving as controls. The analysis identified 4,327 differentially expressed genes (DEGs), among which 2,473 genes were significantly upregulated and 1,854 genes were downregulated. Functional annotation of these DEGs revealed strong associations with biological processes including neutrophil activation, inflammatory response, iron metabolic regulation, vascular calcification and cellular apoptosis. Gene ontology enrichment analysis further highlighted three core biological processes: neutrophil chemotaxis, neutrophil migration and neutrophil aggregation, which collectively underscore the pivotal role of neutrophils in the pathophysiological

progression of AAA. Notably, ruptured human AAA tissues displayed a distinct transcriptomic signature, with 43% of DEGs overlapping with those identified in human macrophages exposed to ferrylHb *in vitro*. Within this set of 884 overlapping genes, functional clusters related to inflammatory modulation, angiogenic signaling and tissue remodeling were identified.

Mechanistic investigations conducted on endothelial cells and vascular smooth muscle cells revealed that heme exposure induces the expression of interleukin-1β (IL-1β), intercellular adhesion molecule 1 (ICAM1) and NLR family pyrin domain containing 3 (NLRP3). This proinflammatory response was attenuated by the upregulation of heme oxygenase-1 (HO-1). Pharmacological induction of HO-1 using Normosang exerted a protective effect, mitigating aneurysm progression and suppressing local inflammation. In contrast, inhibition of HO-1 activity exacerbated disease severity. These results identify the heme-HO-1-H-ferritin signaling axis as a key regulatory module in AAA pathogenesis and a promising candidate for therapeutic targeting.

In summary, the present study elucidates that the crosstalk between oxidized Hb and neutrophils and macrophages within the aortic wall microenvironment plays an active role in driving ferrylHb generation, immune cell activation and extracellular matrix degradation-all of which are critical processes that promote AAA progression. Furthermore, the detection of ferrylHb in the circulation of patients with ruptured AAA highlights its potential utility as a diagnostic biomarker for evaluating disease activity and stratifying rupture risk. These mechanistic insights provide a rational basis for developing targeted therapies that interfere with the Hb-neutrophil-macrophage axis,

with the goal of alleviating inflammation and proteolytic damage in AAA and opening new avenues for clinical intervention.

Key words

Abdominal aortic aneurysm; Hemoglobin oxidation; Ferryl hemoglobin; Neutrophil granulocytes; Neutrophil extracellular traps; Macrophages; Aortic wall remodeling; CD163 receptor; Iron metabolism; Heme oxygenase-1.

References

1. Ramadan A, Al-Omran M, and Verma S. The putative role of autophagy in the pathogenesis of abdominal aortic aneurysms. *Atherosclerosis.* 2017;257(Complete):288-96.
2. Hadi T, Boytard L, Silvestro M, Alebrahim D, Jacob S, Feinstein J, et al. Macrophage-derived netrin-1 promotes abdominal aortic aneurysm formation by activating MMP3 in vascular smooth muscle cells. *Nature Communications.* 2018;9(1).
3. Li DY, Busch A, Jin H, Chernogubova E, Pelisek J, Karlsson J, et al. H19 Induces Abdominal Aortic Aneurysm Development and Progression. *Circulation.* 2018;138(15):1551-68.
4. Yildirim H, van Lammeren GW, Unlu C, van Dongen EP, van de Mortel RH, and de Vries JP. Long-term outcome and quality of life after ruptured abdominal aortic aneurysm repair. *Vascular.* 2018;26(3):231-8.
5. Jing Yu SL, Jianhua Huang, and Wang W. Current Theories and Clinical Trial Evidence for Limiting Human Abdominal Aortic Aneurysm Growth. 2017.
6. Raaz U, Zollner AM, Schellinger IN, Toh R, Nakagami F, Brandt M, et al. Segmental aortic stiffening contributes to experimental abdominal aortic aneurysm development. *Circulation.* 2015;131(20):1783-95.
7. Jeanmonod D, Yelamanchili VS, and Jeanmonod R. *StatPearls*. Treasure Island (FL); 2025.
8. Shaw PM, Loree J, and Oropallo A. *StatPearls*. Treasure Island (FL); 2025.

9. Avishay DM, and Reimon JD. *StatPearls*. Treasure Island (FL); 2025.

10. Blackstock CD, and Jackson BM. Open Surgical Repair of Abdominal Aortic Aneurysms Maintains a Pivotal Role in the Endovascular Era. *Semin Intervent Radiol.* 2020;37(4):346-55.

11. Wainess RM, Dimick JB, Cowan JA, Henke PK, Stanley JC, and Upchurch GR. Epidemiology of Surgically Treated Abdominal Aortic Aneurysms in the United States, 1988 to 2000. *Vascular.* 2004;12(4):218-24.

12. Acosta S, ?gren M, Bengtsson H, Bergqvist D, Lindblad B, and Zdanowski Z. Increasing incidence of ruptured abdominal aortic aneurysm: A population-based study. *Journal of Vascular Surgery.* 2006;44(2):237-43.

13. Kokje VBC, Hamming JF, and Lindeman JHN. Pharmaceutical Management of Small Abdominal Aortic Aneurysms: A Systematic Review of the Clinical Evidence. *European Journal of Vascular & Endovascular Surgery the Official Journal of the European Society for Vascular Surgery.* 2015;62(6):1680.

14. Kent KC, Zwolak RM, Egorova NN, Riles TS, Manganaro A, Moskowitz AJ, et al. Analysis of risk factors for abdominal aortic aneurysm in a cohort of more than 3 million individuals. 2010;52(3):539-48.

15. Puech-Leão P, Molnar LJ, Oliveira IRD, and Cerri GG. Prevalence of abdominal aortic aneurysms - A screening program in São Paulo, Brazil. *Sao Paulo Medical Journal.* 2004;122(4):158-60.

16. Grøndal N, Søgaard R, Henneberg EW, and Lindholt JS. The Viborg vascular (VIVA) screening trial of 65-74 year old men in the central region of Denmark:

Study protocol. *Trials.* 2010;11(1):67.

17. Lindholt MJS, S?rensen J, S?gaard R, and Henneberg EW. Long-term benefit and cost-effectiveness analysis of screening for abdominal aortic aneurysms from a randomized controlled trial. 2010;97(6):826-34.

18. Lindholt JS, and S?gaard R. Population Screening and Intervention for Vascular Disease in Danish Men (VIVA): A Randomised Controlled Trial. *Lancet.* 2017;66(6):1912.

19. Lindholt JS, Rasmussen LM, Sogaard R, Lambrechtsen J, Steffensen FH, Frost L, et al. Baseline findings of the population-based, randomized, multifaceted Danish cardiovascular screening trial (DANCAVAS) of men aged 65-74 years. *Br J Surg.* 2019;106(7):862-71.

20. Ashton HA, Buxton MJ, Day NE, Kim LG, and G SB. The Multicentre Aneurysm Screening Study (MASS) into the effect of abdominal aortic aneurysm screening on mortality in men: A randomised controlled trial. *Lancet.* 2002;360(9345):1531-9.

21. Ashton HA, Gao L, Kim LG, Druce PS, Thompson SG, and Scott RAP. Fifteen-year follow-up of a randomized clinical trial of ultrasonographic screening for abdominal aortic aneurysms. *British Journal of Surgery.* 2007;94(6):696-701.

22. Thompson SG, Ashton HA, Gao L, Buxton MJ, and Scott RAP. Final follow-up of the Multicentre Aneurysm Screening Study (MASS) randomized trial of abdominal aortic aneurysm screening. 2013;57(5):1447-8.

23. Svensjo S, Bjorck M, Gurtelschmid M, Djavani Gidlund K, Hellberg A, and

Wanhainen A. Low prevalence of abdominal aortic aneurysm among 65-year-old Swedish men indicates a change in the epidemiology of the disease. *Circulation.* 2011;124(10):1118-23.

24. Wanhainen A, Hultgren R, Linne A, Holst J, Gottsater A, Langenskiold M, et al. Outcome of the Swedish Nationwide Abdominal Aortic Aneurysm Screening Program. *Circulation.* 2016;134(16):1141-8.

25. Castro-Ferreira R, Barreira R, Mendes P, Couto P, Peixoto F, Aguiar M, et al. First Population-Based Screening of Abdominal Aortic Aneurysm in Portugal. *Ann Vasc Surg.* 2019;59:48-53.

26. Salvador-Gonzalez B, Martin-Baranera M, Borque-Ortega A, Saez-Saez RM, de Albert-Delas Vigo M, Carreno-Garcia E, et al. Prevalence of Abdominal Aortic Aneurysm in Men Aged 65-74 Years in a Metropolitan Area in North-East Spain. *Eur J Vasc Endovasc Surg.* 2016;52(1):75-81.

27. Gianfagna F, Veronesi G, Tozzi M, Tarallo A, Borchini R, Ferrario MM, et al. Prevalence of Abdominal Aortic Aneurysms in the General Population and in Subgroups at High Cardiovascular Risk in Italy. Results of the RoCAV Population Based Study. *Eur J Vasc Endovasc Surg.* 2018;55(5):633-9.

28. Derezinski TL, Formankiewicz B, Migdalski A, Brazis P, Jakubowski G, Woda L, et al. The prevalence of abdominal aortic aneurysms in the rural/urban population in central Poland - Gniewkowo Aortic Study. *Kardiol Pol.* 2017;75(7):705-10.

29. Mccaul KA, Lawrence-Brown M, Dickinson JA, and Norman PE. Long-term

Outcomes of the Western Australian Trial of Screening for Abdominal Aortic Aneurysms: Secondary Analysis of a Randomized Clinical Trial. 2016;176(12).

30. Routine Screening for Abdominal Aortic Aneurysm during Clinical Transthoracic Echocardiography in a Korean Population. *Echocardiography.* 2010;27(10):1182-7.

31. Adachi K, Iwasawa T, and Ono T. Screening for abdominal aortic aneurysms during a basic medical checkup in residents of a Japanese rural community. 2000;30(7):594-9.

32. Cheng SWK, Ting ACW, and Tsang SHY. Epidemiology and Outcome of Aortic Aneurysms in Hong Kong. 2003;27(2):241-5.

33. Balder J-W, Rimbert A, Zhang X, Viel M, and Kuivenhoven JA. Genetics, Lifestyle, and Low-Density Lipoprotein Cholesterol in Young and Apparently Healthy Women. *Circulation.* 2018;137(8):820-31.

34. Krumholz HM, Keenan PS, Jr JEB, Bufalino VJ, Chernew ME, Epstein AJ, et al. Standards for Measures Used for Public Reporting of Efficiency in Health Care: A Scientific Statement From the American Heart Association Interdisciplinary Council on Quality of Care and Outcomes Research and the American College of Cardiology Foundation. 2008;52(18):1518-26.

35. Dimusto PD, Lu G, Ghosh A, Roelofs KJ, Sadiq O, McEvoy B, et al. Increased JNK in Males Compared with Females in a Rodent Model of Abdominal Aortic Aneurysm. *Journal of Surgical Research.* 2012;176(2):687-95.

36. Trenner M, Kuehnl A, Reutersberg B, Salvermoser M, and Eckstein HH.

Nationwide analysis of risk factors for in ospital mortality in patients undergoing abdominal aortic aneurysm repair. *British Journal of Surgery.* 2018;105(4).

37. Cornuz, and J. Risk factors for asymptomatic abdominal aortic aneurysm: Systematic review and meta-analysis of population-based screening studies. *European Journal of Public Health.* 2004;14(4):343-9.

38. Schena M, Shalon D, Davis RW, and Brown PO. Quantitative Monitoring of Gene Expression Patterns with a Complementary DNA Microarray. *Science.* 1995;270(5235):467-70.

39. Tung WS, Lee JK, and Thompson RW. Simultaneous analysis of 1176 gene products in normal human aorta and abdominal aortic aneurysms using a membrane-based complementary DNA expression array. *Journal of Vascular Surgery.* 2001;34(1):143-50.

40. Ono N, Suzuki S, Furusawa C, Shimizu H, and Yomo T. *3d International ICST Conference on Bio-Inspired Models of Network, Information, and Computing Systems*. 2008.

41. Azazi EAA, Bakir SM, Mohtady HA, and Almonem AA. Circulating chemokine eotaxin and chemokine receptor CCR3 in allergic patients. *Egyptian Journal of Immunology.* 2007;14(2):73-82.

42. Rakkola R, Matikainen S, and Nyman TA. Proteome analysis of human macrophages reveals the upregulation of manganese-containing superoxide dismutase after toll-like receptor activation. *Proteomics.* 2010;7(3):378-84.

43. Mcgall G, Labadie J, and Brock P. Light-directed synthesis of high-density oligonucleotide arrays using semiconductor photoresists. *Proceedings of the National Academy of Sciences of the United States of America.* 1996;93(24):p.13555-60.

44. Ahn SK, Choe TB, and Kwon TJ. The gene expression profile of human umbilical vein endothelial cells stimulated with lipopolysaccharide using cDNA microarray analysis. *International Journal of Molecular Medicine.* 2003;12(2):231-6.

45. Seto SW, Chang D, Kiat H, Wang N, and Bensoussan A. Chinese Herbal Medicine as a Potential Treatment of Abdominal Aortic Aneurysm. *Front Cardiovasc Med.* 2018;5:33.

46. Maegdefessel L, Spin JM, Raaz U, Eken SM, Toh R, Azuma J, et al. miR-24 limits aortic vascular inflammation and murine abdominal aneurysm development. *Nat Commun.* 2014;5:5214.

47. Li T, Yu B, Liu Z, Li J, Ma M, Wang Y, et al. Homocysteine directly interacts and activates the angiotensin II type I receptor to aggravate vascular injury. *Nat Commun.* 2018;9(1):11.

48. Ultee KHJ, Soden PA, Zettervall SL, Mccallum JC, and Schermerhorn ML. The perioperative effect of concomitant procedures during open infrarenal abdominal aortic aneurysm repair. *Journal of Vascular Surgery.* 2016;64(4):934-40.e1.

49. Veith FJ, and Paraskevas KI. Endovascular vs. Open Repair of Abdominal

Aortic Aneurysms and Renal Function. *Current Vascular Pharmacology.* 2017;15(2):-.

50. Wang Y, and Shi GP. Mast cell chymase and tryptase in abdominal aortic aneurysm formation. *Trends Cardiovasc Med.* 2012;22(6):150-5.

51. Rosales C. Neutrophils at the crossroads of innate and adaptive immunity. *J Leukoc Biol.* 2020;108(1):377-96.

52. Shafqat A, Khan JA, Alkachem AY, Sabur H, Alkattan K, Yaqinuddin A, et al. How Neutrophils Shape the Immune Response: Reassessing Their Multifaceted Role in Health and Disease. *Int J Mol Sci.* 2023;24(24).

53. Yuan Y, Sun C, Liu X, Hu L, Wang Z, Li X, et al. The Role of Neutrophil Extracellular Traps in Atherosclerosis: From the Molecular to the Clinical Level. *J Inflamm Res.* 2025;18:4421-33.

54. Ji YM, Li T, Qin YH, Xiao SY, Lv YH, Dong Y, et al. Neutrophil Extracellular Traps (NETs) in Sterile Inflammatory Diseases. *J Inflamm Res.* 2025;18:7989-8004.

55. Sorensen OE, and Borregaard N. Neutrophil extracellular traps - the dark side of neutrophils. *J Clin Invest.* 2016;126(5):1612-20.

56. Brinkmann V, Reichard U, Goosmann C, Fauler B, Uhlemann Y, Weiss DS, et al. Neutrophil extracellular traps kill bacteria. *Science.* 2004;303(5663):1532-5.

57. Wang H, Kim SJ, Lei Y, Wang S, Wang H, Huang H, et al. Neutrophil extracellular traps in homeostasis and disease. *Signal Transduct Target Ther.* 2024;9(1):235.

58. Geng X, Wang DW, and Li H. The pivotal role of neutrophil extracellular traps in cardiovascular diseases: Mechanisms and therapeutic implications. *Biomed Pharmacother.* 2024;179:117289.

59. Phillipson M, and Kubes P. The neutrophil in vascular inflammation. *Nat Med.* 2011;17(11):1381-90.

60. Sorvillo N, Cherpokova D, Martinod K, and Wagner DD. Extracellular DNA NET-Works With Dire Consequences for Health. *Circ Res.* 2019;125(4):470-88.

61. Yuan Z, Lu Y, Wei J, Wu J, Yang J, and Cai Z. Abdominal Aortic Aneurysm: Roles of Inflammatory Cells. *Front Immunol.* 2020;11:609161.

62. Ibrahim N, Bleichert S, Klopf J, Kurzreiter G, Hayden H, Knobl V, et al. Reducing Abdominal Aortic Aneurysm Progression by Blocking Neutrophil Extracellular Traps Depends on Thrombus Formation. *JACC Basic Transl Sci.* 2024;9(3):342-60.

63. Yan H, Zhou HF, Akk A, Hu Y, Springer LE, Ennis TL, et al. Neutrophil Proteases Promote Experimental Abdominal Aortic Aneurysm via Extracellular Trap Release and Plasmacytoid Dendritic Cell Activation. *Arterioscler Thromb Vasc Biol.* 2016;36(8):1660-9.

64. Yang S, Chen L, Wang Z, Chen J, Ni Q, Guo X, et al. Neutrophil extracellular traps induce abdominal aortic aneurysm formation by promoting the synthetic and proinflammatory smooth muscle cell phenotype via Hippo-YAP pathway. *Transl Res.* 2023;255:85-96.

65. Rombouts KB, van Merrienboer TAR, Ket JCF, Bogunovic N, van der Velden

J, and Yeung KK. The role of vascular smooth muscle cells in the development of aortic aneurysms and dissections. *Eur J Clin Invest.* 2022;52(4):e13697.

66. Lu H, Du W, Ren L, Hamblin MH, Becker RC, Chen YE, et al. Vascular Smooth Muscle Cells in Aortic Aneurysm: From Genetics to Mechanisms. *J Am Heart Assoc.* 2021;10(24):e023601.

67. Shi D, Zhang M, Zhang Y, Shi Y, Liu X, Wu X, et al. The Pathophysiological Role of Vascular Smooth Muscle Cells in Abdominal Aortic Aneurysm. *Cells.* 2025;14(13).

68. Silvestre-Roig C, Braster Q, Wichapong K, Lee EY, Teulon JM, Berrebeh N, et al. Externalized histone H4 orchestrates chronic inflammation by inducing lytic cell death. *Nature.* 2019;569(7755):236-40.

69. Xiong Y, Liu S, Liu Y, Zhao J, Sun J, Li Y, et al. PI3Kgamma promotes neutrophil extracellular trap formation by noncanonical pyroptosis in abdominal aortic aneurysm. *JCI Insight.* 2024;9(16).

70. Ibrahim N, Eilenberg W, Neumayer C, and Brostjan C. Neutrophil Extracellular Traps in Cardiovascular and Aortic Disease: A Narrative Review on Molecular Mechanisms and Therapeutic Targeting. *Int J Mol Sci.* 2024;25(7).

71. Wei M, Wang X, Song Y, Zhu D, Qi D, Jiao S, et al. Inhibition of Peptidyl Arginine Deiminase 4-Dependent Neutrophil Extracellular Trap Formation Reduces Angiotensin II-Induced Abdominal Aortic Aneurysm Rupture in Mice. *Front Cardiovasc Med.* 2021;8:676612.

72. Zhu J, Meganathan I, MacAruthur R, and Kassiri Z. Inflammation in Abdominal

Aortic Aneurysm: Cause or Comorbidity? *Can J Cardiol.* 2024;40(12):2378-91.

73. Knight JS, Luo W, O'Dell AA, Yalavarthi S, Zhao W, Subramanian V, et al. Peptidylarginine deiminase inhibition reduces vascular damage and modulates innate immune responses in murine models of atherosclerosis. *Circ Res.* 2014;114(6):947-56.

74. Klopf J, Brostjan C, Eilenberg W, and Neumayer C. Neutrophil Extracellular Traps and Their Implications in Cardiovascular and Inflammatory Disease. *Int J Mol Sci.* 2021;22(2).

75. Meher AK, Spinosa M, Davis JP, Pope N, Laubach VE, Su G, et al. Novel Role of IL (Interleukin)-1beta in Neutrophil Extracellular Trap Formation and Abdominal Aortic Aneurysms. *Arterioscler Thromb Vasc Biol.* 2018;38(4):843-53.

76. Rezkalla SH, Dharmashankar KC, Abdalrahman IB, and Kloner RA. No-reflow phenomenon following percutaneous coronary intervention for acute myocardial infarction: incidence, outcome, and effect of pharmacologic therapy. *J Interv Cardiol.* 2010;23(5):429-36.

77. Wang J, Lindholt JS, Sukhova GK, Shi MA, Xia M, Chen H, et al. IgE actions on CD4+ T cells, mast cells, and macrophages participate in the pathogenesis of experimental abdominal aortic aneurysms. *EMBO Mol Med.* 2014;6(7):952-69.

78. Liao M, Liu CL, Lv BJ, Zhang JY, Cheng L, Cheng X, et al. Plasma cytokine levels and risks of abdominal aortic aneurysms: A population-based prospective

cohort study. *Ann Med.* 2015;47(3):245-52.

79. Stone JR, Bruneval P, Angelini A, Bartoloni G, Basso C, Batoroeva L, et al. Consensus statement on surgical pathology of the aorta from the Society for Cardiovascular Pathology and the Association for European Cardiovascular Pathology: I. Inflammatory diseases. *Cardiovasc Pathol.* 2015;24(5):267-78.

80. Bonaca MP, and O'Gara PT. Diagnosis and management of acute aortic syndromes: dissection, intramural hematoma, and penetrating aortic ulcer. *Curr Cardiol Rep.* 2014;16(10):536.

81. Balla J, Jacob HS, Balla G, Nath K, Eaton JW, and Vercellotti GM. Endothelial-cell heme uptake from heme proteins: induction of sensitization and desensitization to oxidant damage. *Proc Natl Acad Sci U S A.* 1993;90(20):9285-9.

82. Potor L, Hendrik Z, Patsalos A, Katona E, Mehes G, Poliska S, et al. Oxidation of Hemoglobin Drives a Proatherogenic Polarization of Macrophages in Human Atherosclerosis. *Antioxid Redox Signal.* 2021;35(12):917-50.

83. Gibson JF, and Ingram DJE. Location of Free Electrons in Porphin Ring Complexes. *Nature.* 1956;178(4538):871-2.

84. Harel S, and Kanner J. The generation of ferryl or hydroxyl radicals during interaction of haemproteins with hydrogen peroxide. *Free Radic Res Commun.* 1988;5(1):21-33.

85. Meng F, and Alayash AI. Determination of extinction coefficients of human hemoglobin in various redox states. *Anal Biochem.* 2017;521:11-9.

86. Patel RP, Svistunenko DA, Darley-Usmar VM, Symons MC, and Wilson MT. Redox cycling of human methaemoglobin by H2O2 yields persistent ferryl iron and protein based radicals. *Free Radic Res.* 1996;25(2):117-23.

87. Bozza MT, and Jeney V. Pro-inflammatory Actions of Heme and Other Hemoglobin-Derived DAMPs. *Front Immunol.* 2020;11:1323.

88. Peng F, Xia J, Niu H, Feng X, Zheng T, He X, et al. Systemic immune-inflammation index is associated with aneurysmal wall enhancement in unruptured intracranial fusiform aneurysms. *Front Immunol.* 2023;14:1106459.

89. Conger AK, Tomasek T, Riedmann KJ, Douglas JS, Berkey LE, Ware LB, et al. Hemoglobin increases leukocyte adhesion and initiates lung microvascular endothelial activation via Toll-like receptor 4 signaling. *Am J Physiol Cell Physiol.* 2023;324(3):C665-C73.

90. Fujii J, Kurahashi T, Konno T, Homma T, and Iuchi Y. Oxidative stress as a potential causal factor for autoimmune hemolytic anemia and systemic lupus erythematosus. *World J Nephrol.* 2015;4(2):213-22.

91. Campomayor NB, Kim HJ, and Kim M. Pro-Oxidative and Inflammatory Actions of Extracellular Hemoglobin and Heme: Molecular Events and Implications for Alzheimer's and Parkinson Disease. *Biomol Ther (Seoul).* 2025;33(2):235-48.

92. Katsu M, Niizuma K, Yoshioka H, Okami N, Sakata H, and Chan PH. Hemoglobin-induced oxidative stress contributes to matrix metalloproteinase activation and blood-brain barrier dysfunction in vivo. *J Cereb Blood Flow*

Metab. 2010;30(12):1939-50.

93. DeRoo E, Stranz A, Yang H, Hsieh M, Se C, and Zhou T. Endothelial Dysfunction in the Pathogenesis of Abdominal Aortic Aneurysm. *Biomolecules.* 2022;12(4).

94. Xiao X, Li C, Huang X, Chen G, Huang X, Song F, et al. Single-cell RNA sequencing reveals that NRF2 regulates vascular smooth muscle cell phenotypic switching in abdominal aortic aneurysm. *FASEB J.* 2024;38(13):e23707.

95. Ho YC, Wu ML, Gung PY, Chen CH, Kuo CC, and Yet SF. Heme oxygenase-1 deficiency exacerbates angiotensin II-induced aortic aneurysm in mice. *Oncotarget.* 2016;7(42):67760-76.

96. Azuma J, Wong RJ, Morisawa T, Hsu M, Maegdefessel L, Zhao H, et al. Heme Oxygenase-1 Expression Affects Murine Abdominal Aortic Aneurysm Progression. *PLoS One.* 2016;11(2):e0149288.

97. Schillinger M, Exner M, Mlekusch W, Domanovits H, Huber K, Mannhalter C, et al. Heme oxygenase-1 gene promoter polymorphism is associated with abdominal aortic aneurysm. *Thromb Res.* 2002;106(2):131-6.

98. Nagy E, Eaton JW, Jeney V, Soares MP, Varga Z, Galajda Z, et al. Red cells, hemoglobin, heme, iron, and atherogenesis. *Arterioscler Thromb Vasc Biol.* 2010;30(7):1347-53.

99. Bunn HF, and Jandl JH. Exchange of heme among hemoglobin molecules. *Proc Natl Acad Sci U S A.* 1966;56(3):974-8.

100. Tenhunen R, Marver HS, and Schmid R. The enzymatic catabolism of

hemoglobin: stimulation of microsomal heme oxygenase by hemin. *J Lab Clin Med.* 1970;75(3):410-21.

101. Shibahara S, Yoshida T, and Kikuchi G. Induction of heme oxygenase by hemin in cultured pig alveolar macrophages. *Arch Biochem Biophys.* 1978;188(2):243-50.

102. Sun J, Hoshino H, Takaku K, Nakajima O, Muto A, Suzuki H, et al. Hemoprotein Bach1 regulates enhancer availability of heme oxygenase-1 gene. *EMBO J.* 2002;21(19):5216-24.

103. Herrick AL, McColl KE, Moore MR, Cook A, and Goldberg A. Controlled trial of haem arginate in acute hepatic porphyria. *Lancet.* 1989;1(8650):1295-7.

104. Balla J, Balla G, Jeney V, Kakuk G, Jacob HS, and Vercellotti GM. Ferriporphyrins and endothelium: a 2-edged sword-promotion of oxidation and induction of cytoprotectants. *Blood.* 2000;95(11):3442-50.

105. Tian Z, Zhang Y, Zheng Z, Zhang M, Zhang T, Jin J, et al. Gut microbiome dysbiosis contributes to abdominal aortic aneurysm by promoting neutrophil extracellular trap formation. *Cell Host Microbe.* 2022;30(10):1450-63 e8.

106. Eliason JL, Hannawa KK, Ailawadi G, Sinha I, Ford JW, Deogracias MP, et al. Neutrophil depletion inhibits experimental abdominal aortic aneurysm formation. *Circulation.* 2005;112(2):232-40.

107. Castanheira FVS, and Kubes P. Neutrophils and NETs in modulating acute and chronic inflammation. *Blood.* 2019;133(20):2178-85.

108. Aymonnier K, Amsler J, Lamprecht P, Salama A, and Witko-Sarsat V. The

neutrophil: A key resourceful agent in immune-mediated vasculitis. *Immunol Rev.* 2023;314(1):326-56.

109. Rubio-Navarro A, Amaro Villalobos JM, Lindholt JS, Buendia I, Egido J, Blanco-Colio LM, et al. Hemoglobin induces monocyte recruitment and CD163-macrophage polarization in abdominal aortic aneurysm. *Int J Cardiol.* 2015;201:66-78.

110. Jeney V, Balla G, and Balla J. Red blood cell, hemoglobin and heme in the progression of atherosclerosis. *Front Physiol.* 2014;5:379.

111. Qin Z, Yang M, Lu Z, Babu VS, Li Y, Shi F, et al. The Oxidative Injury of Extracellular Hemoglobin Is Associated With Reactive Oxygen Species Generation of Grass Carp (Ctenopharyngodon idella). *Front Immunol.* 2022;13:843662.

112. Ren P, Hughes M, Krishnamoorthy S, Zou S, Zhang L, Wu D, et al. Critical Role of ADAMTS-4 in the Development of Sporadic Aortic Aneurysm and Dissection in Mice. *Sci Rep.* 2017;7(1):12351.

113. Daugherty A, Manning MW, and Cassis LA. Angiotensin II promotes atherosclerotic lesions and aneurysms in apolipoprotein E-deficient mice. *J Clin Invest.* 2000;105(11):1605-12.

114. Cox J, and Mann M. MaxQuant enables high peptide identification rates, individualized p.p.b.-range mass accuracies and proteome-wide protein quantification. *Nat Biotechnol.* 2008;26(12):1367-72.

115. Silva G, Jeney V, Chora A, Larsen R, Balla J, and Soares MP. Oxidized

Hemoglobin Is an Endogenous Proinflammatory Agonist That Targets Vascular Endothelial Cells. *J Biol Chem.* 2009;284(43):29582-95.

116. Winterbourn CC. Oxidative Reactions of Hemoglobin. *Method Enzymol.* 1990;186:265-72.

117. Meng FT, and Alayash AI. Determination of extinction coefficients of human hemoglobin in various redox states. *Anal Biochem.* 2017;521:11-9.

118. Huy NT, Xuan Trang DT, Uyen DT, Sasai M, Harada S, and Kamei K. An improved colorimetric method for quantitation of heme using tetramethylbenzidine as substrate. *Anal Biochem.* 2005;344(2):289-91.

119. Gall T, Petho D, Nagy A, Hendrik Z, Mehes G, Potor L, et al. Heme Induces Endoplasmic Reticulum Stress (HIER Stress) in Human Aortic Smooth Muscle Cells. *Front Physiol.* 2018;9:1595.

120. Cavaliere FM, Prezzo A, Bilotta C, Iacobini M, and Quinti I. The lack of BTK does not impair monocytes and polymorphonuclear cells functions in X-linked agammaglobulinemia under treatment with intravenous immunoglobulin replacement. *PLoS One.* 2017;12(4):e0175961.

121. Lau D, Mollnau H, Eiserich JP, Freeman BA, Daiber A, Gehling UM, et al. Myeloperoxidase mediates neutrophil activation by association with CD11b/CD18 integrins. *Proc Natl Acad Sci U S A.* 2005;102(2):431-6.

122. Korai M, Purcell J, Kamio Y, Mitsui K, Furukawa H, Yokosuka K, et al. Neutrophil Extracellular Traps Promote the Development of Intracranial Aneurysm Rupture. *Hypertension.* 2021;77(6):2084-93.

123. Posta N, Csosz E, Oros M, Petho D, Potor L, Kallo G, et al. Hemoglobin oxidation generates globin-derived peptides in atherosclerotic lesions and intraventricular hemorrhage of the brain, provoking endothelial dysfunction. *Lab Invest.* 2020;100(7):986-1002.

124. Alayash AI. betaCysteine 93 in human hemoglobin: a gateway to oxidative stability in health and disease. *Lab Invest.* 2021;101(1):4-11.

125. Jana S, Strader MB, and Alayash AI. The Providence Mutation (betaK82D) in Human Hemoglobin Substantially Reduces betaCysteine 93 Oxidation and Oxidative Stress in Endothelial Cells. *Int J Mol Sci.* 2020;21(24).

126. Pimenova T, Pereira CP, Gehrig P, Buehler PW, Schaer DJ, and Zenobi R. Quantitative mass spectrometry defines an oxidative hotspot in hemoglobin that is specifically protected by haptoglobin. *J Proteome Res.* 2010;9(8):4061-70.

127. Jia Y, Buehler PW, Boykins RA, Venable RM, and Alayash AI. Structural basis of peroxide-mediated changes in human hemoglobin: a novel oxidative pathway. *J Biol Chem.* 2007;282(7):4894-907.

128. Ramanath VS, Oh JK, Sundt TM, 3rd, and Eagle KA. Acute aortic syndromes and thoracic aortic aneurysm. *Mayo Clin Proc.* 2009;84(5):465-81.

129. Onofre G, Kolackova M, Jankovicova K, and Krejsek J. Scavenger receptor CD163 and its biological functions. *Acta Medica (Hradec Kralove).* 2009;52(2):57-61.

130. Nielsen MJ, Andersen CB, and Moestrup SK. CD163 binding to haptoglobin-hemoglobin complexes involves a dual-point electrostatic receptor-ligand

pairing. *J Biol Chem.* 2013;288(26):18834-41.

131. Kristiansen M, Graversen JH, Jacobsen C, Sonne O, Hoffman HJ, Law SK, et al. Identification of the haemoglobin scavenger receptor. *Nature.* 2001;409(6817):198-201.

132. Hochberg Y, and Benjamini Y. More powerful procedures for multiple significance testing. *Stat Med.* 1990;9(7):811-8.

133. Pinero J, Bravo A, Queralt-Rosinach N, Gutierrez-Sacristan A, Deu-Pons J, Centeno E, et al. DisGeNET: a comprehensive platform integrating information on human disease-associated genes and variants. *Nucleic Acids Res.* 2017;45(D1):D833-D9.

134. Zhou Y, Zhou B, Pache L, Chang M, Khodabakhshi AH, Tanaseichuk O, et al. Metascape provides a biologist-oriented resource for the analysis of systems-level datasets. *Nat Commun.* 2019;10(1):1523.

135. Winterbourn CC, and Kettle AJ. Redox reactions and microbial killing in the neutrophil phagosome. *Antioxid Redox Signal.* 2013;18(6):642-60.

136. Minetti M, Mallozzi C, Scorza G, Scott MD, Kuypers FA, and Lubin BH. Role of oxygen and carbon radicals in hemoglobin oxidation. *Arch Biochem Biophys.* 1993;302(1):233-44.

137. Takei H, Araki A, Watanabe H, Ichinose A, and Sendo F. Rapid killing of human neutrophils by the potent activator phorbol 12-myristate 13-acetate (PMA) accompanied by changes different from typical apoptosis or necrosis. *J Leukoc Biol.* 1996;59(2):229-40.

138. Rodriguez-Espinosa O, Rojas-Espinosa O, Moreno-Altamirano MM, Lopez-Villegas EO, and Sanchez-Garcia FJ. Metabolic requirements for neutrophil extracellular traps formation. *Immunology.* 2015;145(2):213-24.

139. Domer D, Walther T, Moller S, Behnen M, and Laskay T. Neutrophil Extracellular Traps Activate Proinflammatory Functions of Human Neutrophils. *Front Immunol.* 2021;12:636954.

140. Wang B, Su X, Zhang B, and Pan S. GSK484, an inhibitor of peptidyl arginine deiminase 4, increases the radiosensitivity of colorectal cancer and inhibits neutrophil extracellular traps. *J Gene Med.* 2023;25(9):e3530.

141. Wei L, Wang X, Luo M, Wang H, Chen H, and Huang C. The PAD4 inhibitor GSK484 enhances the radiosensitivity of triple-negative breast cancer. *Hum Exp Toxicol.* 2021;40(7):1074-83.

142. Davis CA, 3rd, Pearce WH, Haines GK, Shah M, and Koch AE. Increased ICAM-1 expression in aortic disease. *J Vasc Surg.* 1993;18(5):875-80.

143. Stather PW, Sidloff DA, Dattani N, Gokani VJ, Choke E, Sayers RD, et al. Meta-analysis and meta-regression analysis of biomarkers for abdominal aortic aneurysm. *Br J Surg.* 2014;101(11):1358-72.

144. Johnston WF, Salmon M, Pope NH, Meher A, Su G, Stone ML, et al. Inhibition of interleukin-1beta decreases aneurysm formation and progression in a novel model of thoracic aortic aneurysms. *Circulation.* 2014;130(11 Suppl 1):S51-9.

145. Millar J, Nasser E, Ailawadi G, and Salmon M. IL-1 in Abdominal Aortic Aneurysms. *J Cell Immunol.* 2023;5(2):22-31.

146. Nyakundi BB, Erdei J, Toth A, Balogh E, Nagy A, Nagy B, Jr., et al. Formation and Detection of Highly Oxidized Hemoglobin Forms in Biological Fluids during Hemolytic Conditions. *Oxid Med Cell Longev.* 2020;2020:8929020.

147. Ludlow JT, Wilkerson RG, and Nappe TM. *StatPearls*. Treasure Island (FL); 2025.

148. Barbarino F, Waschenbach L, Cavalho-Lemos V, Dillenberger M, Becker K, Gohlke H, et al. Targeting spectrin redox switches to regulate the mechanoproperties of red blood cells. *Biol Chem.* 2021;402(3):317-31.

Acknowledgments

Words fail to fully express the depth of my gratitude to my supervisor, Professor József Balla, MD, PhD, DSc, MHAS, from the Department of Internal Medicine, Faculty of Medicine, University of Debrecen. His profound academic insights, patient mentorship, and consistent moral encouragement have been the cornerstone of my entire research journey.

I owe a sincere debt of gratitude to Professor Dr. György Balla whose invaluable guidance and steadfast backing have sustained me throughout the research process. My heartfelt thanks also go to the Chairman of the Defense Committee for taking on this crucial responsibility with dedication, as well as to the distinguished panel members of the evaluation committee for generously sharing their professional expertise and committing their precious time to the assessment of my thesis. I extend my deepest appreciation to Department of Vascular Surgery and Endovascular Surgery, Semmelweis University. Their perceptive advice and constructive feedback have greatly refined my work, while the provision of human aortic aneurysm and serum samples, materials absolutely essential to my studies, has laid the foundation for the successful completion of my research. Furthermore, I wish to recognize the significant contributions of all research assistants, laboratory technicians, and co-authors; their diligent efforts and fruitful collaboration have not only enriched the quality of my work but also inspired me with new perspectives along the way. Above all, my most profound thanks are reserved for my family, whose unwavering trust and endless support have

served as a constant wellspring of courage and motivation throughout this challenging yet rewarding endeavor.

Last but not least, I wish to acknowledge the indispensable financial support that has made this research feasible. Project 2025-1.2.1-HU-RIZONT-2025-00080 has been implemented with the support provided by the Ministry of Culture and Innovation of Hungary from the National Research, Development and Innovation Fund, financed under the 2025-1.2.1-HU-RIZONT funding scheme. This work was funded by HUN-REN-DE (11003) and NKFIH ADVANCED 149734 (J.B.), the European Union and the European Social Fund under the project EFOP-3.6.2-16-2017-00006 LIVE LONGER, as well as the Ministry of Innovation and Technology of Hungary via the National Research, Development and Innovation Fund under grant number TKP2021-EGA-18. I am also sincerely grateful for the financial assistance provided by the EKÖP-24-4 (Y.D.) University Research Scholarship Program of the Ministry for Culture and Innovation, the Chinese Government Scholarship (Y.D.), and the Tempus Public Foundation (STIPENDIUM HUNGARICUM SCHOLARSHIP, Y.D.). These funding sources have played a pivotal role in supporting both my research pursuits and daily life during this period.

List of Publications

UNIVERSITY of DEBRECEN

UNIVERSITY AND NATIONAL LIBRARY
UNIVERSITY OF DEBRECEN
H-4002 Egyetem tér 1, Debrecen
Phone: +3652/410-443, email: publikaciok@lib.unideb.hu

Registry number: DEENK/38/2026.PL
Subject: PhD Publication List

Candidate: Yuchao Ding
Doctoral School: Kálmán Laki Doctoral School

List of publications related to the dissertation

1. **Ding, Y.**, Potor, L., Sótonyi, P., Szappanos, Á., Gyurok, G. P., Póliska, S., Patsalos, A., Méhes, G., Beke, L., Sikura, K. É., Zavaczki, E., Gáll, T., Pethő, D., Fintha, A., Nagy, B., Juhász, B., Nagy, L., Balla, G., Balla, J.: Heme as a Pro-Inflammatory Stimulus in Abdominal Aortic Aneurysm.
   Antioxidants. 15 (2), 1-21, 2026.
   DOI: http://dx.doi.org/10.3390/antiox15020155
   IF: 6.6 (2024)
2. **Ding, Y.**, Potor, L., Katona, É., Sótonyi, P., Szappanos, Á., Gyurok, G. P., Méhes, G., Hendrik, Z., Fintha, A., Gergely, P., Benyó, Z., Combi, Z., Sikura, K. É., Beke, L., Németh, N., Szabó, B., Fürtös, I., Kalló, G., Csősz, É., Póliska, S., Patsalos, A., Debus, E. S., Nagy, L., Balla, G., Balla, J.: Oxidation of hemoglobin to ferryl hemoglobin contributes to remodeling of the artery wall in abdominal aortic aneurysm.
   Redox Biol. 88, 1-19, 2025.
   DOI: http://dx.doi.org/10.1016/j.redox.2025.103908
   IF: 11.9 (2024)

List of other publications

3. Combi, Z., Potor, L., Nagy, P., Sikura, K. É., Ditrói, T., Jurányi, E. P., Galambos, K., Szerafin, T., Gergely, P., Whiteman, M., Torregrossa, R., **Ding, Y.**, Beke, L., Hendrik, Z., Méhes, G., Balla, G., Balla, J.: Hydrogen sulfide as an anti-calcification stratagem in human aortic valve: altered biogenesis and mitochondrial metabolism of H2S lead to H2S deficiency in calcific aortic valve disease.
   Redox Biol. 60, 1-19, 2023.
   DOI: http://dx.doi.org/10.1016/j.redox.2023.102629
   IF: 10.7

UNIVERSITY of DEBRECEN

UNIVERSITY AND NATIONAL LIBRARY
UNIVERSITY OF DEBRECEN
H-4002 Egyetem tér 1, Debrecen
Phone: +3652/410-443, email: publikaciok@lib.unideb.hu

4. Zhai, Z., Zhang, X., **Ding, Y.**, Huang, Z., Li, Q., Zheng, M., Cho, K., Dong, Z., Fu, W., Chen, Z., Jiang, B.: Eugenol restrains abdominal aortic aneurysm progression with down-regulations on NF-?B and COX-2.
Phytother. Res. 36 (2), 928-937, 2022.
DOI: http://dx.doi.org/10.1002/ptr.7358
IF: 7.2

5. Jiang, B., Zhang, X., **Ding, Y.**, Zhai, Z.: Drug for treating artery-related diseases, and use thereof. 2021
Hatáskör: Európai
Bejelentés ideje: -
Ügyiratszám: P20201792 ()
Szabadalmi szám: EP4043012A1
Szabadalom státusza: Oltalom fennáll - Végleges oltalom alatt áll

6. Jiang, B., Zhang, X., **Ding, Y.**, Zhai, Z.: Medicine for treating artery related diseases and application thereof. 2021
Hatáskör: Kína
Bejelentés ideje: -
Ügyiratszám: CN112569219A ()
Szabadalmi szám: CN112823797A
Szabadalom státusza: Oltalom fennáll - Végleges oltalom alatt áll

7. **Ding, Y.**, Zhang, X., Zhang, J. x., Zhai, Z., Zhang, M. x., Jiang, B.: Progression and Regression of Abdominal Aortic Aneurysms in Mice.
Curr. Med. Sci. 41 (5), 901-908, 2021.
DOI: http://dx.doi.org/10.1007/s11596-021-2425-z
IF: 2.64

Total IF of journals (all publications): 39,04
Total IF of journals (publications related to the dissertation): 18,5

The Candidate's publication data submitted to the Tudóstér have been validated by DEENK on the basis of the Journal Citation Report (Impact Factor) database.

30 January, 2026